Aus der Orthopädischen Universitätsklinik mit Poliklinik Tübingen

Inhibition of the Hedgehog pathway in combination with cytostatics as potential therapeutic option in Ewing Sarcoma

Inaugural-Dissertation
zur Erlangung des Doktorgrades
der Medizin

der Medizinischen Fakultät
der Eberhard Karls Universität
zu Tübingen

vorgelegt von

Keller, Juliane

2020

Dekan:	Professor Dr. I. B. Autenrieth
1. Berichterstatter:	Professor Dr. T. Kluba
2. Berichterstatter:	Professor Dr. R. R. Plentz
Tag der Disputation:	21.04.2017

Content

Abbreviations 5

1 Introduction 9
1.1 Ewing sarcoma 9
1.1.1 Classification and clinical diagnosis of Ewing sarcoma 9
1.1.2 Therapy and prognosis 11
1.2 The mechanism of the Hedgehog pathway 12
1.3 The role of the Hedgehog pathway in tumour genesis and progression 14
1.3.1 Effect of the Hedgehog pathway on proliferation 15
1.3.2 Effect of the Hedgehog pathway on apoptosis 16
1.3.3 The Hedgehog pathway in Ewing sarcoma 17
1.4 Inhibition of the Hedgehog pathway 17
1.4.1 GANT61 18
1.4.2 ATO 19
1.5 Cytostatics in tumour therapy 20
1.5.1 Etoposide 20
1.5.2 Doxorubicin 22

2 Materials and Methods 24
2.1 Methods 24
2.1.1 Cells 24
2.1.2 Cell culture 27
2.1.3 Cytostatics and Inhibitors 28
2.1.4 Equipment 28
2.1.5 Chemicals 32
2.1.6 Kits and enzymes 35
2.1.7 Oligonucleotides 35
2.1.8 Buffers and Solutions 36
2.1.9 Antibodies 37
2.1.10 Software 38
2.2 Methods 39
2.2.1 Cell and molecular biological methods 39
2.2.2 Cell Viability Test (MTS-Assay) 44
2.2.3 Clonogenic Assay 45
2.2.4 Cell Death Assay (“Fluorescence Activated Cell Sorting”, FACS) 46

2.2.5 Western blot 47
2.2.6 3D spheroid cultures 52

3 Results 53
3.1 Identification of Hedgehog pathway component expression profiles in Ewing sarcoma cell lines 53
3.1.1 Quantification of Hh pathway mRNA expression in A673, RD-ES and SK-N-MC cells in comparison to MSC 53
3.1.2 GLI1 and GLI2 protein expression in A673, RD-ES and SK-N-MC in comparison to MSC 54
3.2 Effect of GANT61, ATO, etoposide and doxorubicin on the viability of Ewing sarcoma cell lines 56
3.2.1 Effect of single substance treatment on the viability of A673, RD-ES, SK-N-MC and MSC 57
3.2.3 Effect of inhibitor combinations on the viability A673, RD-ES, SK-N-MC and MSC 61
3.3 Impact of ATO and cytostatics on the colony formation of Ewing sarcoma cell lines 69
3.3.1 Effect of GANT61 and ATO on the colony formation of the Ewing sarcoma cell lines A673, RD-ES and SK-N-MC 70
3.3.2 Effect of etoposide and doxorubicin on the colony formation of the Ewing sarcoma cell lines A673, RD-ES and SK-N-MC 71
3.3.3 Effect of drug combinations on the colony formation of the Ewing sarcoma cell lines A673, RD-ES and SK-N-MC 73
3.3.4 Summary 75
3.4 Impact of GANT61, ATO, etoposide and doxorubicin on 3D spheroid cultures of Ewing sarcoma cell lines 76
3.4.1 Effect of GANT61 and ATO on A673 and SK-N-MC spheroid cultures 76
3.4.2 Effect of etoposide and doxorubicin on A673 and SK-N-MC spheroid cultures 79
3.4.3 Summary 81
3.5 Effect of GANT61, ATO, etoposide and doxorubicin on cell death induction in Ewing sarcoma cell lines 81
3.5.1 Detection of cell death using flow cytometry (FACS-analysis) 81
3.5.2 Detection of apoptosis induction by caspase 3 and PARP cleavage in Ewing sarcoma cell lines 90
3.6 Influence of ATO on GLI1 protein expression in A673, RD-ES and SK-N-MC cells in comparison to MSC 96

4 Discussion 98
4.1 Hh signalling in Ewing sarcoma cell lines 98
4.2 GANT61 and ATO - GLI inhibition in Ewing sarcoma 100
4.2.1 GANT61 100
4.2.2 ATO 102
4.3 Etoposide and doxorubicin sensitivity of Ewing sarcoma cells 104
4.3.1 Etoposide 104
4.3.2 Doxorubicin 106
4.4 Effectiveness of ATO combinations with the cytostatics etoposide and doxorubicin 107
4.5 Conclusion and future outlook 109
5 Abstract 111
6 Zusammenfassung 112
7 List of Figures 114
8 List of Tables 117
9 Literature 118
10 Personal contribution 140
11 Publications 141
12 Acknowledgment 142

Abbreviations

α-ESA	α-eleostearic acid
AIF	Apoptosis-inducing factor
APAF1	Apoptotic protease activating factor 1
APL	Acute promyelocytic leukaemia
APS	Ammonium Persulfate
AQP9	Aquaporin 9
ATO	Arsenic trioxide
BAX	Bcl-2-associated X protein
Bcl-2	B-cell lymphoma
CCND1 or 2	Gene decoding for cyclin D1 or D2
CDK	Cyclin dependent kinase
CK1-α	Casein kinase-1-α
cDNA	Complementary DNA
CNS	Central nervous system
CSC	Cancer stem cell
Ct	Cycle threshold
ΔCt	Ratio of the Ct-value of gene of interest and the Ct-value of TBP
ΔΔCt	Ratio of the ΔCt-value of EWS cell and the ΔCt-value of MSCs
DHH	Desert Hedgehog
DMEM	Dulbecco's modified Eagles's medium
DMSO	Dimethyl sulfoxide
DNA	Deoxyribonucleic acid
DNA-PK	DNA-dependent protein kinase
dNTP	Deoxynucleotide
Doxo	Doxorubicin
DTT	Dithiothreitol
ECL	Enhanced chemiluminescent substrate
ET	Ewing tumour

Eto	Etoposide
EWS	Ewing sarcoma
FACS	Fluorescence activated cell sorting
Fas	First apoptosis signal
FasL	Fas-ligand
FCS	Fetal calf serum
FDA	Food and drug administration
FLI1	Friend leukemia integration 1 transcription factor
FSC	Forward scatter
G1 phase	First gap phase
G2 phase	Second gap phase
GLI	Glioma-associated oncogenes
GSK3-ß	Glycogen synthase kinase-3-ß
Hh	Hedgehog
HPI1-4	Hedgehog pathway inhibitor 1-4
IAP	Proteins that inhibit apoptosis
I-BET151	Inhibitor of the bromodomain and extra terminal domain protein
IC_{50} value	Half maximal inhibitory concentration
IE	Ifosfamide and etoposide
IGF1R	Insulin-like growth factor 1 receptor
IHH	Indian Hedgehog
JNK	c-Jun N-terminal kinase
K252c	Staurosporinone
LDH	Lactate dehydrogenase
MAC	Mitochondrial apoptosis-induced channel
MMP-9	Matrix metalloproteinase 9
M-phase	Mitotic phase
MSC	Mesenchymal stem cell
MTS	3-(4,5-dimethylthiazol2-yl)-5-(3-carboxyphenyl)-2-(4-sulfophenyl)-2H-Tetrazoliumsalt

NADH	Nicotinamide adenine dinucleotide
NADPH	Nicotinamide adenine dinucleotide phosphate
NF-κB	Nuclear factor kappa-light-chain-enhancer of activated B cells
PARP	Poly (ADP-ribose) polymerase
PBS	Phosphate-buffered saline
PCR	Polymerase chain reaction
PKA	Protein kinase A
PML-RAR	Promyelocytic leukaemia retinoic acid receptor
PNET	Peripheral neuroectodermal tumour
P/S	Penicillin/Streptomycin
PTCH	Patched
PVDF	Polyvinyline fluoride
qRT-PCR	quantitative Real-time PCR
RB	Retinoblastoma protein
RNA	Ribonucleic acid
ROS	Reactive oxygen species
RT	Reverse transcriptase
SDS-PAGE	Sodium dodecyl sulfate polyacrylamide gel electrophoresis
SHH	Sonic Hedgehog
SMAC	Second mitochondria-derived activator of caspase
SMO	Smoothened
S-phase	Synthesis phase
SSC	Side scatter
SUFU	Suppressor of fused
TBP	TATA-Box Binding Protein
TBS	Tris-buffered saline
TBS-T	Tris-buffered saline and Tween 20
TEMED	Tetramethylethylenediamine
TGFß	Transforming growth factor beta

TNFR	Tumour necrosis factor receptor
TXNR	Thioredoxin reductase
VAC	Vincristine, actinomycin D and cyclophosphamide
VACA	Vincristine, actinomycin-D, cyclophosphamide and doxorubicin
VDC	Vincristine, doxorubicin and cyclophosphamide
VIDE	Vincristine, ifosfamide, doxorubicin and etoposide

1 Introduction

1.1 Ewing sarcoma

1.1.1 Classification and clinical diagnosis of Ewing sarcoma

Ewing sarcoma (EWS) are mesenchymal tumours, arising from bone but also soft tissue. By now, the names Ewing tumour, Askin's tumour as well as malignant peripheral neuroectodermal tumour (PNET) all come under the term of Ewing sarcoma. EWS are the second most common bone cancer in children and young adults (Karosas, 2010). The most common location is the pelvis, followed by the femur, tibia and fibula, whereas only 15 % are solely located in soft-tissue. The incidence is higher in males compared to females, lying at 1.5:1 (Parkin and Nectoux, 1993). At the time of diagnosis 20 - 30 % of the tumours have metastasised to the lung or other parts of the skeletal system (Delattre et al., 1994; Le Deley et al., 2010; Potratz et al., 2012). However, other authors such as Karosas et al. described that 80 % of the patients have subclinical metastases at the time of presentation (Karosas, 2010). Clinical symptoms include local pain, oedema and reduced functionality in the concerned body part, but are generally very unspecific and often remain undiscovered for a long period of time. In some patients pathological fractures may occur (Kashima et al., 2013).

As EWS are difficultly to distinguish histologically from other small, round blue-cell tumours (Desai and Jambhekar, 2010), diagnosis is confirmed by the characteristic translocations and immune-histochemical results. The EWS gene, a gene decoding an RNA-binding protein is usually fused to the DNA-binding domain of a transcription factor of the ETS family involved in proliferation and tumourigenesis. Two translocations are very common in the Ewing family of tumours, the EWS-FLI1 gene fusion t(11:22)(q24;q12) in 85 - 90 % and the EWS-ERG gene fusion t(21:22)(q22;q12) in 10 % of the EWS cases (Arvand and Denny, 2001; Delattre et al., 1994). Moreover, the most common chimeric gene EWS-FLI1 exists in several different forms. Type 1 results from the fusion of EWS exons 1 - 7 with FLI1 exons 6 - 9 occurs in 65 % of all cases and is suggested to have a better outcome. The second type, a fusion from EWS exons 1 - 7 with FLI1 exons 5 - 9 is only seen in about 25 % of the cases (Lin, 1999). Several other translocations though on a rare basis have been observed, including EWS-E1AF t(17;22),

EWS-ETV t(7:22) and EWS-FEV t(2;22) (Mackall et al., 2002). The chimeric EWS-ETS proteins are important for the maintenance and progression of EWS. *In vitro* EWS cells expressing antisense EWS-ETS transcripts showed decreased tumour growth and a change in their histological appearance (May et al., 1993; Ouchida et al., 1995; Teitell et al., 1999). Several studies suggest EWS-FLI1 working as an aberrant transcription factor modulating the expression of multiple target genes involved in cell signalling pathways such as Hedgehog, Notch-, Wnt-ß-catenin-, TGFß- or IGF1R. Multiple new approaches of regulation and inhibition of these pathways are currently under investigation (Taylor et al., 2011).

The exact cell of EWS origin is not yet fully known. Some studies suggest neuroectodermal cells as the origin of EWS as peripheral neural crest progenitors can be found. Additionally, some EWS cell lines express neuron specific proteins and are able to form dendrite similar extensions (Cavazzana et al., 1987; Morrison et al., 1999). Another more probable origin of Ewing sarcoma are mesenchymal stem cells (MSC) which can differentiate into adipocytes, osteoblasts and chondrocytes (Kolf et al., 2007). Cancer stem cells (CSC) which have MSC plasticity were found in EWS (Riggi et al., 2010) and various studies have shown that suppression or silencing of EWS-FLI1 results in expression profiles similar to MSC (induced expression of CD29, CD44, CD54, CD59 and CD73) (Tirode et al., 2007). The introduction of the EWS-FLI1 fusion protein in MSC leads to expression of Ewing sarcoma characteristic proteins (Castillero-Trejo et al., 2005; Riggi et al., 2005). Furthermore, different EWS cell lines are able to differentiate along the adipogenic and osteogenic lineage upon EWS-FLI1 silencing whereas introduction of the fusion protein into MSC isolated from mice inhibits their ability to proliferate (Tirode et al., 2007; Torchia et al., 2003).

1.1.2 Therapy and prognosis

Without treatment 5-year survival of EWS-patients is only about 5 - 10 % (Rosen et al., 1974). Sex, age, tumour size and location, serum LDH concentration, fever or anaemia are prognostic variables (Balamuth and Womer, 2010). Therefore, EWS is classified into a primarily metastasised and a local type and also the initial tumour size is evaluated for treatment decision (Bacci et al., 2006; Oberlin et al., 2001).

The standard therapy for the local type of EWS currently involves initial chemotherapy followed by surgery and/or radiotherapy and subsequent adjuvant chemotherapy with a 5-year survival rate of over 70 %, whereas therapy of metastasised or relapsed EWS is difficult with survival rates of only up to 20 % (Delattre et al., 1994; Esiashvili et al., 2008; Le Deley et al., 2010). In some cases additional haploidentical stem cell transplantation can be necessary and improves the prognosis in metastasised and relapsed EWS (Burdach et al., 1993; Koscielniak et al., 2005).

Chemotherapy usually consists of a combination of 3 or more substances including alkylating drugs such as ifosfamide or cyclophosphamide, the anthracycline doxorubicin, the topoisomerase inhibitor etoposide or actinomycin D and vincristine (Grier et al., 2003; Le Deley et al., 2014; Womer et al., 2012). In the 1960s vincristine was combined with actinomycin and cyclophosphamide as well as doxorubicin (VAC + doxorubicin) (Jaffe et al., 1976; Rosen et al., 1974). This treatment strategy evolved in North America to an alternating treatment of VDC (vincristine-doxorubicin-cyclophosphamide) and IE (ifosfamide-etoposide) every two weeks. European studies established the regime of VACA (vincristine-doxorubicin-cyclophosphamide-actinomycin) which eventually lead to the currently used chemotherapy of VIDE (vincristine-ifosfamide-doxorubicin-etoposide) (Paulussen et al., 2001; Paulussen et al., 2008). Other studies are adding topotecan-cyclophosphamide to the already used VDC-IE therapy (Hunold et al., 2006; Saylors et al., 2001). After the initial chemotherapy a complete R0 surgical resection is desirable which can be complemented with additional radiotherapy if complete resection is not possible (Haeusler et al., 2010). However, radiotherapy in children has decreased in value in the past decades due to grieve late effects such as second malignancies and growth disturbance (Balamuth and Womer, 2010).

In metastasised and relapsed EWS therapy is difficult. Adding IE to VDC treatment or increasing doses of doxorubicin, cyclophosphamide and ifosfamide have no better outcomes (Grier et al., 2003). Several trials using megatherapy, a therapy combining high dose chemotherapy, body irradiation and autological haematopoietic stem cell transfusion, could not significantly improve patient survival (Burdach et al., 2003; Burdach et al., 2000; Meyers et al., 2001; Oberlin et al., 2006).

1.2 The mechanism of the Hedgehog pathway

In humans, the Hedgehog (Hh) pathway is responsible for various processes in cells. It is important for the development of the embryonic CNS as well as general growth, differentiation and self-renewal of cells (Hooper and Scott, 2005; Katoh and Katoh, 2009; Michaud and Yoder, 2006; Molofsky et al., 2004; Yu et al., 2009).

In 1980 the Hh protein was discovered by Nusslein-Volhard and Wieschaus in Hh-mutant drosophila larvae (*Drosophila melanogaster*) (Nusslein-Volhard and Wieschaus, 1980). Today three Hh ligands, namely Sonic Hedgehog (SHH), Indian Hedgehog (IHH) and Desert Hedgehog (DHH) are known in mammals (Ingham and McMahon, 2001). The Hh pathway is induced by binding of an Hh ligand to its transmembrane receptors Patched 1 and 2 (PTCH1 or PTCH2). These form a complex with the co-receptor proteins “Cell adhesion molecule-related/downregulated by oncogenes” (CDON), the “Brother of Cdo” (BOC) and “Growth arrest-specific 1” (GAS1) (Hanna and Shevde, 2016). Thereupon PTCH1 releases its suppression of Smoothed (SMO), a G-protein-coupled receptor (Carpenter et al., 1998; Teglund and Toftgard, 2010). SMO is localised to the primary cilium, an essential sensory cell organelle whose loss results in disorders of kidneys, liver and pancreas as well as development defects (Eggenschwiler and Anderson, 2007; Michaud and Yoder, 2006). In the primary cilium an intracellular signalling cascade is initiated by SMO that results in the stabilisation of the glioma-associated oncogene (GLI) transcription factors. The GLI1 protein translocates into the nucleus where it induces the transcription of different target genes including Cyclin D1, c-MYC, B-cell lymphoma 2 (Bcl-2) and SNAIL, all involved in the regulation of cellular proliferation and apoptosis resistance (Hooper and Scott, 2005; Riobo and Manning, 2007; Scales and de Sauvage, 2009; Varjosalo and Taipale, 2008). GLI2 and GLI3 can either act as a repressor or as an

activator of the Hh pathway, depending on the PKA activity (Hui and Angers, 2011). In the presence of Hh ligands GLI2 leads to an activation of GLI1 (Hanna and Shevde, 2016), whereas GLI3 acts as a transcriptional repressor of Hh target genes in the absence of Hh ligands (Kasper et al., 2006; Ng and Curran, 2011). Interestingly, GLI1 targets include the genes encoding for PTCH1 and GLI1 itself, leading to a negative feedback of the Hedgehog pathway in case of PTCH1 and a positive feedback in case of GLI1 (Ingham and McMahon, 2001). **Figure 1** shows the mechanism of the Hh pathway in humans.

However, GLI1 signalling is not exclusively regulated by upstream ligand availability. Several other protein mediators are also involved, such as casein kinase-1-α (CK1-α), protein kinase A (PKA), glycogen synthase kinase-3-β (GSK3-β) or the GLI1-inhibitor "suppressor of fused" (SUFU) (Kogerman et al., 1999; Stone et al., 1999).

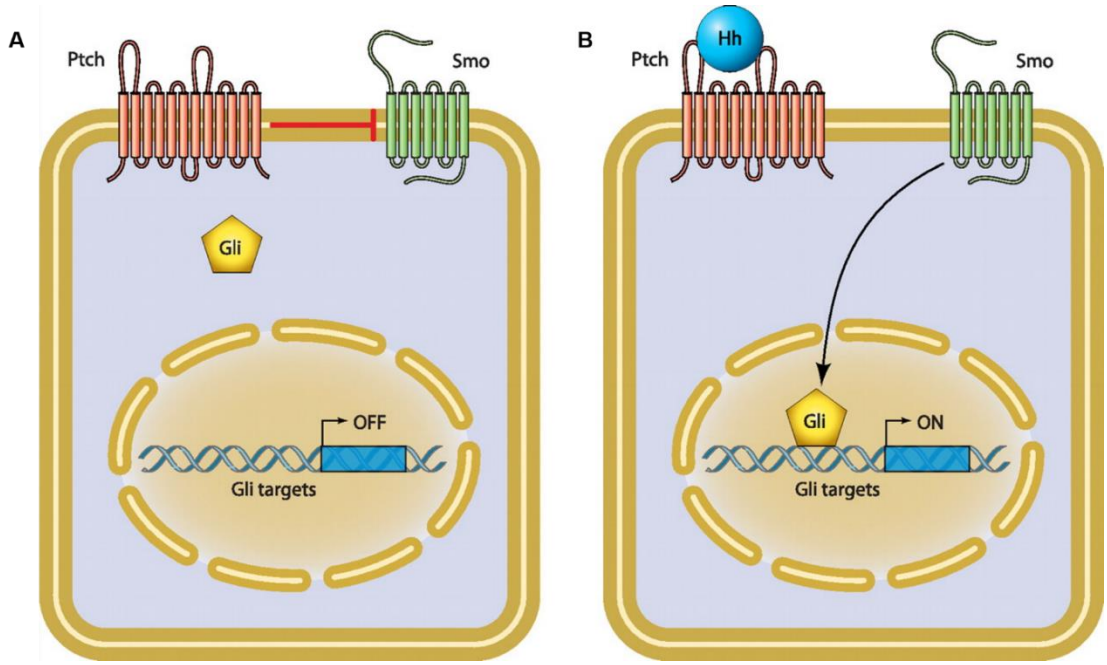

Figure 1: Mechanism of the Hh pathway. *Interaction of the receptors SMO and PTCH regulating GLI activity* ***A:*** *in the absence of Hh ligands and* ***B:*** *with Hh ligands binding to PTCH. (Buller et al., 2012)*

1.3 The role of the Hedgehog pathway in tumour genesis and progression

Hyperactive Hh signalling has been identified in different malignancies such as pancreatic, colon, gastric, lung, breast and prostate cancer, multiple myeloma and different leukaemias. Furthermore, specific mutations in proteins involved in Hh pathway regulation have been found in basal carcinoma and medulloblastoma (McMahon et al., 2003; Scales and de Sauvage, 2009). GLI1 and GLI2 are transcription factors capable of activating their targets. However, GLI2 is the primary mediator of transcriptional activation, initiating GLI1 transcription, which subsequently activates its target genes (Bai et al., 2002; Ikram et al., 2004; Katoh and Katoh, 2009; Thiyagarajan et al., 2007). Both GLI1 and GLI2 are oncogenes, inducing transformation and tumourigenesis (Kasper et al., 2006; Katoh and Katoh, 2009; Kinzler et al., 1987; Zhang et al., 2013). Several studies confirm that an overexpression of Hh ligands (SHH, IHH and DHH) or GLI1 can lead to cancer formation and progression (Pressey et al., 2011). Moreover, decreased PTCH1 activity leads to apoptosis resistance in a murine model (Hahn et al., 1998; Kappler et al., 2003).

In addition to proliferation and inhibition of apoptosis tumour progression is also marked by angiogenesis and the ability to metastasise. Lee et al. found Hh pathway activation to elevate the levels of the angiogenic factors angiopoetin 1 and 2 (Lee et al., 2007). Moreover, in small cell lung cancer Hh signalling has also been found to be a potent regulator of angiogenesis (Velcheti, 2007). Metastasis is regulated through cell adherence on the one hand and mobility on the other hand. The Hh pathway is known to decrease the number of tight junctions and the expression of E-cadherin, a transmembrane protein forming adherence junctions and increasing levels of Snail Family Zinc Finger 1 (SNAI1), which leads to a repression of E-cadherin (Davidson and Sukumar, 2005; Li et al., 2006). SHH and GLI1 can also promote invasion by activating matrix metalloproteinase 9 (MMP-9) expression in oral squamous cell carcinoma (Fan et al., 2014) and gastric cancer (Yoo et al., 2011). MMP-9 is a protein important for the degradation of extracellular matrix (Ohnishi et al., 1998).

1.3.1 Effect of the Hedgehog pathway on proliferation

Proliferation of cells is regulated by a complex cell cycle consisting of the mitotic phase (M-phase) and the interphase. During the M-phase the cytoplasm and DNA is divided, whereas during the interphase the cell is prepared for the next division and DNA is replicated. Proliferation is initiated by external stimulating signals and begins with a gap phase (G1) where cells grow and synthesise proteins. This is followed by the S-phase where DNA is replicated. Before entering the next phase a control point ensures that the cell is ready for DNA replication during the S-phase. After replication the cell is prepared for division during a second gap phase (G2), ending with another control point where eventual mistakes or damages during replication can be repaired (Elledge, 1996). Vital for the correct regulation of the cell cycle are cyclins and cyclin dependent kinases (CDK) both forming active complexes which can regulate cell cycle progression and are specific for each phase (Gillett and Barnes, 1998; Nigg, 1995).

If components of the cell cycle are dysregulated this may lead to uncontrollable proliferation and tumour formation. Besides, cyclins and CDKs, typical cell cycle inhibitors such as the retinoblastoma protein (RB) or p53 can be mutated (Champeris Tsaniras et al., 2014). Furthermore, the dysregulation of other cellular pathways can also lead to an aberrant progression of the cell cycle. One of these is the Hh pathway as several studies suggest. Recently, Sun et al. described that inhibition of GLI1 in chondrosarcoma results in a G2/M arrest of the tumour cells (Sun et al., 2014). Another study found the genes CCND1 and CCND2, encoding for cyclin D1 and D2, respectively to be regulated by GLI1 (Katoh and Katoh, 2009). Cyclin D1 and D2 form cyclin-CDK complexes with CDK4 and CDK6 initiating the entry into S-phase (Sherr and Roberts, 1999). An interaction between the Hh pathway and the tumour suppressor p53 has been suggested but still needs further investigation (Malek et al., 2011). However, Lu et al. found SHH to initiate regeneration in cochlear hair cells through downregulation of Retinoblastoma protein (RB) (Lu et al., 2013).

1.3.2 Effect of the Hedgehog pathway on apoptosis

In contrast to uncontrolled cell disruption during necrosis, apoptosis is the programmed cell death producing cell fragments so called apoptotic bodies that are completely removed by phagocytic cells without causing inflammation (Kurosaka and Kobayashi, 2003; Savill and Fadok, 2000). Apoptotic signals such as e.g. heat, radiation, nutrient deprivation, hypoxia, membrane damage or infection cause regulatory proteins to initiate the apoptotic cascade ultimately leading to caspases activation and cell death (Norbury and Hickson, 2001). Two main forms of apoptosis induction are currently distinguished, the intrinsic and the extrinsic pathway. However, both pathways are linked and influence each other (Igney and Krammer, 2002). Intrinsic apoptosis, also known as the mitochondrial mediated form, is induced by mitochondrial membrane permeabilisation releasing second mitochondria-derived activator of caspase (SMAC) and cytochrome c. SMACs deactivate proteins that inhibit apoptosis (IAP) and thereby induce an effector caspase cascade (Elmore, 2007). Cytochrome c forms a complex with the apoptotic protease activating factor 1 (APAF1) activating caspase 9 thus also inducing an effector caspase cascade (Elmore, 2007; Fesik and Shi, 2001; Tsujimoto, 1998). The extrinsic apoptotic pathway is mediated through receptors of the tumour necrosis factor receptor (TNFR) family. Binding of the cytokine TNF-α to TNFR1 or the transmembrane protein FasL (Fas ligand) to the Fas (First apoptosis signal) receptor results in cleavage of procaspase 8 to the active caspase 8 leading to the induction of an effector caspase cascade (Ramaswamy et al., 2009; Wajant, 2002). The effector caspases 3, 6 and 7 ultimately induce cell shrinkage, chromatin condensation, nuclear DNA fragmentation, cell organelle degradation and vesicle formation (Green, 2011).

Several studies have found the Hh pathway to be involved in apoptosis inhibition. Both GLI1 and GLI2 seem to induce high levels of the anti-apoptotic protein Bcl2 inhibiting the formation of a mitochondrial apoptosis-induced channel (MAC) through which cytochrome c is released (Dejean et al., 2006; Katoh and Katoh, 2009). Athar et al. also found GLI proteins to lead to a decrease of pro-apoptotic proteins such as Fas (Athar et al., 2004) and in ameloblastoma the therapeutic approach of neutralising SHH with antibodies resulted in a decrease of Bcl2 and an increase of Bcl2-associated X protein (BAX) which is implicated in MAC formation (Kanda et al., 2013).

1.3.3 The Hedgehog pathway in Ewing sarcoma

The fusion protein EWS-FLI1 is essential for EWS and has influence on various signalling pathways involved in apoptosis and proliferation. A direct transcriptional target of EWS-FLI1 is GLI1 as experimental modulation of EWS-FLI1 expression and analysis of the interaction between EWS-FLI1 and GLI1 promoter by ChIP assay showed (Beauchamp et al., 2009). The upstream protein PTCH1 is also upregulated by EWS-FLI1, whereas GLI2, GLI3 and the GLI1 inhibitor SUFU are not altered in any way (Zwerner et al., 2008). The increased activity of GLI1 appears to be independent of upstream stimulation mediated by the Hh pathway as SHH and IHH are hardly upregulated and the inhibition of SMO has no measurable effect on GLI1 activation in EWS (Joo et al., 2009; Zwerner et al., 2008).

1.4 Inhibition of the Hedgehog pathway

Different components of the Hh pathway can be targeted by drugs depending on the cause of the abnormal Hh pathway activation. In medulloblastoma (McCall et al., 2007) as well as pancreas and prostate carcinoma (Farooqi et al., 2011; Mo et al., 2011) inhibition of the Hh pathway leads to lower levels of Bcl-2 and therefore a higher rate of apoptosis. One of the targets most focused on in the last years is SMO. Several SMO inhibitors including sonidegib (LDE225) are in different phases of clinical development (Burness, 2015; Rodon et al., 2014) or the already approved for treatment like vismodegib of metastatic basal cell carcinoma (Rudin, 2012).

Downstream of SMO the GLI transcription factors can be targeted by several natural compounds such as staurosporinone (K252c), zerumbone, arcriaflavin C and physalin B and F (Hosoya et al., 2008) as well as the synthetic products HPI1-4, GANT58, GANT61, Arsenic trioxide (ATO), GlaB, JQ1 and I-BET151 (Beauchamp et al., 2011; Gonnissen et al., 2015). As the fusion protein EWS-FLI1 directly leads to an activation of GLI in EWS, two different GLI inhibitors, GANT61 and ATO were used in this work.

1.4.1 GANT61

GANT61 is a small molecule that was first identified in a cell-based screen for inhibitors of GLI1 and GLI2-mediated transcription in human prostate cancer xenografts where it was described to inhibit both the GLI1 and GLI2 dependent transcription as well as binding of GLI1 to the DNA resulting in lower levels of GLI protein expression (Lauth et al., 2007). GANT61 directly binds GLI1 in a groove between zinc fingers 2 and 3 (Agyeman et al., 2014). Through inhibition of GLI1-DNA binding and therefore inhibition of Hh target gene expression, GANT61 leads to a cell cycle arrest, increased apoptosis and inhibition of DNA damage repair as well as cell migration (Gonnissen et al., 2015). Recently Lim et al. found GANT61-induced apoptosis to be dependent on mitochondrial release of reactive oxygen species (ROS), which means that GANT61 also acts through the induction of oxidative stress (Lim et al., 2015).

Since its discovery in 2007 GANT61 has been tested in several *in vitro* and *in vivo* studies. A significant decrease of tumour growth in animal studies has been shown for prostate (Lauth et al., 2007), pancreatic (Fu et al., 2013), hepatocellular (Wang et al., 2013), colon (Mazumdar et al., 2011) and lung cancer (Huang et al., 2014) as well as neuroblastoma (Wickström et al., 2013) and rhabdomyosarcoma (Srivastava et al., 2014). Therefore, GANT61 is currently in preclinical studies for therapy of rhabdomyosarcoma, neuroblastoma, leukaemia, colon, pancreatic and prostate cancer (Agyeman et al., 2014).

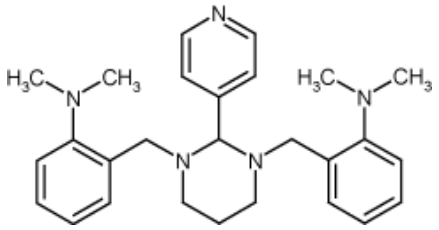

Figure 2: Molecular structure of GANT61 *(Reagents Direct, 2010).*

1.4.2 ATO

An effect of ATO in acute promyelocytic leukaemia (APL) was found in the early 1970s and is today FDA-approved for patients with APL as second line therapy after all-trans retinoic acid thereby often inducing remission with survival rates of about 90 % (Hu et al., 2009; Niu et al., 1999).

Different mechanisms of ATO induced tumour inhibition have been found. In APL the degradation of the promyelocytic leukaemia retinoic acid receptor α (PML-RARα) fusion protein by ATO leads to tumour growth inhibition. Here, ATO binds to cysteine residues of the zinc fingers (Nasr et al., 2008). As GLI proteins also belong to the zinc finger group of proteins a similar mechanism of inhibition has been postulated (Kinzler et al., 1988). Direct GLI2 inhibition by ATO was demonstrated (Kim et al., 2010). ATO inhibits the translocation of GLI2 in and out of the primary cilium, subsequently leading to gradation of GLI2. Beauchamp et al. on the other hand described inhibition of GLI1 transactivation in EWS cell lines after ATO treatment (Beauchamp et al., 2011). Furthermore, cell lines with high levels of GLI1 are more sensitive to ATO (Beauchamp et al., 2011). Additional targets of ATO in other tumour types are Nuclear factor kappa-light-chain-enhancer of activated B cells (NF-κB), thioredoxin reductase (TXNR) and c-Jun N-Terminal Kinase (JNK) (Cavigelli et al., 1996; Hayashi et al., 2002; Kapahi et al., 2000; Lu et al., 2007; Mann et al., 2006). However, NF-κB and JNK do not seem to be targets of ATO in EWS (Beauchamp et al., 2011; White and Burchill, 2008).

In vitro tests have already shown ATO cytotoxicity against EWS cell lines leading to inhibition of migration and invasion (Zhang et al., 2012). An *in vivo* testing of ATO in EWS xenograft models and medulloblastoma allograft models also demonstrated its efficacy (Beauchamp et al., 2011; Kim et al., 2010). However, in another *in vivo* study by Smith et al. using EWS xenografts ATO showed no significant effect (Smith et al., 2012).

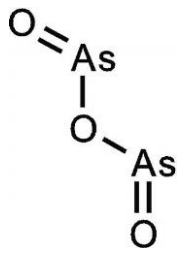

Figure 3: Molecular structure of Arsenic trioxide *(Fisher Scientific, 2015).*

1.5 Cytostatics in tumour therapy

Chemotherapy in EWS consists mostly of a combination of three or more cytostatics such as alkylating substances (ifosfamide or cyclophosphamide), the anthracycline doxorubicin, the topoisomerase inhibitor etoposide, actinomycin D and vincristine (Grier et al., 2003; Le Deley et al., 2014; Womer et al., 2012).

1.5.1 Etoposide

Etoposide was first introduced in 1971 and is now part of the first-line treatment against testicular cancer (Loehrer, 1991; Nichols, 1992), small cell lung cancer (Johnson et al., 1991) as well as Kaposi's sarcoma (Schwartsmann et al., 1997). It also shows established activity in various lymphoma, neuroblastoma, sarcoma and ovarian cancer (Aisner and Lee, 1991). For EWS etoposide was recommended for first-line treatment in 2003 (Grier et al., 2003).

Its origin lies in a plant-based toxin, the podophyllotoxin, which can be obtained from the roots and rhizomes of the *Podophyllum emodi* growing in the Himalaya region, and *Podophyllum peltatum* native to North America (Imbert, 1998; Kelly and Hartwell, 1954). Podophyllotoxin was first synthesised in 1966 (Gensler and Gatsonis, 1966) and showed promising antimitotic and cytotoxic effects in clinical studies due to the inhibition of tubulin to assemble to microtubules during the metaphase (Sackett, 1993). However, the anticancer properties were accompanied by severe gastrointestinal side effects and other toxicities (Imbert, 1998; Kelly and Hartwell, 1954; Stahelin and von Wartburg, 1989). Derivates with less toxic effect were synthesised so that in 1968 a semisynthetic podophyllotoxin glycoside (etoposide) was found by Kuhn and van Wartburg (Kuhn and von Wartburg, 1968). In clinical trials beginning in 1971, the anti-tumour activity of etoposide was proven accompanied by overall modest side effects (Jensen et al., 1990; Muggia et al., 1971; Nissen et al., 1972). **Figure 4** shows the molecular structure of etoposide.

In contrast to podophyllotoxin, etoposide leads to a cell cycle arrest in the G2-phase (Loike and Horwitz, 1976b; Stahelin, 1973). This difference is also reflected in studies to chemo-resistance where cells resistant to tubulin polymerization inhibitors (like podophyllotoxin) were still sensitive to etoposide (Gupta, 1983). The cytotoxic

mechanism of etoposide is based on an accumulation of DNA double strand breaks in the nucleus which leads to a high activity of the DNA-dependent protein kinase (DNA-PK). DNA-PK activates p53, a protein responsible for cell cycle arrest and apoptosis induction (Karpinich et al., 2002). In its activated form p53 upregulates pro-apoptotic proteins, resulting in cytochrome c release from the mitochondria and subsequent intrinsic apoptosis (Karpinich et al., 2002; Siliciano et al., 1997).

Permanent cleavage of DNA double strands is based on an interaction of etoposide with topoisomerase II, which is important for the unwinding and overwinding of DNA during transcription and replication. Usually, topoisomerase II cleaves and reseals DNA double strands (Watt and Hickson, 1994). When interacting with etoposide the re-ligation of these DNA breaks is inhibited leading to apoptosis and ROS as well as trapped topoisomerase I-DNA complexes (Sordet et al., 2006). The application of etoposide as an anti-cancer drug relies on a higher amount of topoisomerase II in proliferating cells compared to quiescent cells and therefore a more distinct cytotoxic effect of etoposide in neoplastic tissue (Hasegawa et al., 1993; Kimura et al., 1994; Sinha, 1995).

Though initially efficient, etoposide resistance has been observed in cancer cells due to alterations in the topoisomerase II enzyme or multidrug resistances (Matsumoto et al., 1999). Furthermore, some side-effects like myelosuppression, leukopenia, thrombopenia or secondary leukaemia can occur (Kobayashi and Ratain, 1994; Kumar, 1993).

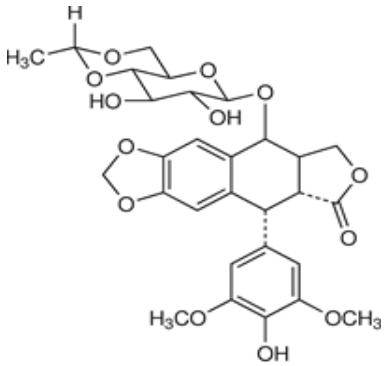

Figure 4: Molecular structure of etoposide *(Medicines Complete, 2016).*

1.5.2 Doxorubicin

Doxorubicin was originally isolated from the microorganism *Streptomyces peucetius var. caesius* after mutagenic treatment in 1968 (Arcamone et al., 1969). It is a class I DNA-binding anthracycline which inhibits nuclear DNA replication and RNA synthesis (Potmesil et al., 1984). Di Marco et al. (1969) were the first to show its highly potent tumour growth inhibition in ascites carcinoma, lymphoma, myeloma and sarcoma. The effect of doxorubicin was stronger compared to the previously discovered daunorubicin in the early 1960s (Casazza et al., 1971). Clinical trials ensued where the anti-tumour properties were confirmed especially in Ewing sarcoma and neuroblastoma. In addition, Wilms' tumours, soft tissue sarcomas and lymphomas were highly sensitive to doxorubicin (Bonadonna et al., 1969; Bonadonna et al., 1970). However, cardiotoxic side-effects ranging from well manageable cardiomyopathy to life-threatening heart failure but also alopecia, stomatitis, myelosuppression and gastroenteritis, limit the application of doxorubicin (Lown, 1993; Minow and Gottlieb, 1975). Therefore, clinical administration favours a combination therapy, rather than treatment with doxorubicin alone to achieve greater response rates at lower concentrations leading to less severe adverse effects (Benjamin et al., 1977; Bonadonna et al., 1977). Today doxorubicin is part of the first-line therapy of various tumours including Ewing sarcoma (Weiss, 1992).

The most probable mechanism of doxorubicin induced cell death is similar to etoposide. The DNA intercalation leads to inhibition of topoisomerase II which results in double strand DNA breaks and as described in chapter 1.5.1 Etoposide for etoposide this ultimately induces apoptosis (Minotti et al., 2004; Tewey et al., 1984). An additional mode of action has been described by Cullinane and Phillips. Instead of intercalating in DNA, doxorubicin can also form drug-DNA adducts, acting as inter-strand crosslinks in the DNA duplex (Cullinane and Phillips, 1990). Doxorubicin-DNA adduct formation is dependent on the addition of formaldehyde which has been shown to enhance cytotoxicity of doxorubicin. Thus, a combination treatment with doxorubicin and formaldehyde releasing drugs might be promising in future tumour therapy (Cutts et al., 2001; Cutts et al., 2015; Swift et al., 2006; Taatjes et al., 1996).

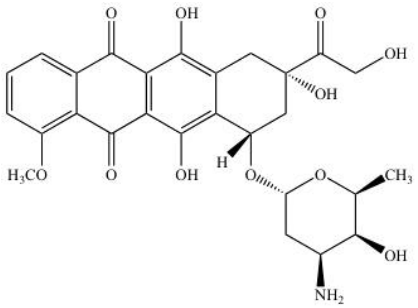

***Figure 5: Molecular structure of doxorubicin**. (Department of Chemistry & Biochemistry UCLA, 2015)*

2 Materials and Methods

2.1 Methods

2.1.1 Cells

All experiments were performed with the three EWS cell lines A673, RD-ES and SK-N-MC. As a control bone marrow derived mesenchymal stem cells (MSC-2014-7) from a healthy donor were used.

A673

A673 were obtained from CLS Cell Lines Service GmbH (Eppelheim, Germany) and were cultivated in Dulbecco's modified Eagles's medium (DMEM) with GlutaMAX 4.5 g/l D-glucose (Gibco, Life Technologies, Darmstadt, Germany). The medium was supplemented with 10 % fetal calf serum (FCS) and 1 % Penicillin/Streptomycin (P/S). A673 cells were diluted between 1:10 and 1:25 and detached from flasks with 1 % trypsin. The cell line was established from a 15 year old female with a soft tissue sarcoma and shows specific characteristics of EWS which lead to its characterization as Ewing tumour (ET). Both the typical t(11;22) translocation and the EWS-FLI1 fusion protein type I were found (Giard et al., 1973; Martinez-Ramirez et al., 2003). Moreover, the cells have a non-functional p53 and express neither p16 nor p14 (May et al., 2013). The adherent cells show a polygonal growth (**Figure 6**).

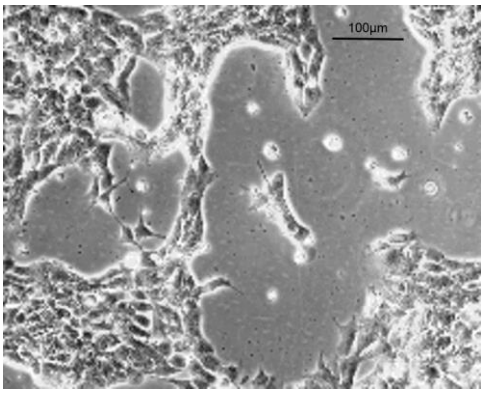

Figure 6: Light micrographs of A673 cells during routine cell culture.

RD-ES

The cell line RD-ES was obtained from CLS Cell Lines Service GmbH (Eppelheim, Germany) and was cultivated in RPMI 1640 with L-glutamine (Gibco, Life Technologies, Darmstadt, Germany). The medium was supplemented with 15 % FCS and 1 % P/S. Cells were detached with 1 % trypsin and diluted between 1:8 and 1:20 during culture. The cell line was established by G. Marshall and M. Kirchen from a 19 year old Caucasian male with primary osseous EWS located in the humerus (CLS, 2016). RD-ES cells are 20 - 25 µm in diameter and grow in small loosely attached clusters (**Figure 7**). Expression of a EWS-FLI1 fusion protein of the type II has been established (Lin et al., 1999).

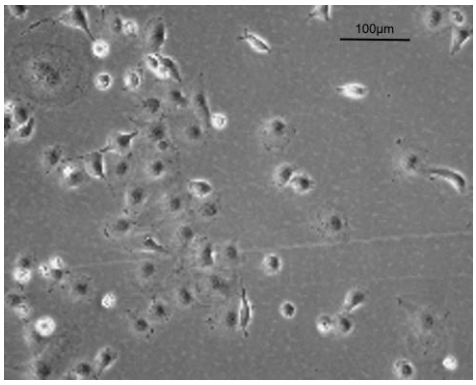

Figure 7: Light micrographs of RD-ES cells during routine cell culture.

SK-N-MC

SK-N-MC were obtained from ATCC (Manaddas, VA, USA) and were maintained in RPMI 1640 with L-glutamine (Gibco, Life Technologies, Darmstadt, Germany). Medium was supplemented with 15 % FCS and 1 % P/S. For cell culture SK-N-MCs were diluted between 1:8 and 1:15 and detached with 1 % trypsin. The cell line was established by J. L. Biedler from a 12 year old Caucasian female with the initial diagnosis of neuroepithelioma (Biedler et al., 1973). Today, it is approved that this cell line was established from the retroorbital metastasis of an Askin's tumour, a peripheral PNET. Before isolation of the cell line the patient received chemotherapy including vincristine, cyclophosphamide, doxorubicin and actinomycin D. The cells express a EWS-FLI1 fusion protein I and have a non-functional p53 (May et al., 2013). SK-N-MCs grow adherent and appear as loosely attached monolayers (**Figure 8**).

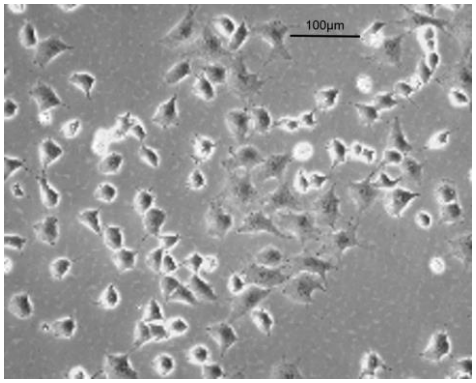

Figure 8: Light micrographs of SK-N-MC cells during routine cell culture.

Control cells (MSC-2014-7)

Mesenchymal stem cells (MSC) are the most probable origin of EWS (Kolf et al., 2007). MSC were isolated and propagated as described by Battula and Treml from a healthy donor (Battula et al., 2009). To confirm their origin they were differentiated towards chondrocytes, adipocytes and osteocytes. MSC were cultivated in DMEM low Glucose (1 g/l), supplemented with 25 ml fresh frozen plasma, 25 ml thrombocyte concentrate, 1ml heparin sodiumsalt (2 IE), 5 ml L-glutamine (2 mM) and 5 ml P/S per 500 ml. Fresh frozen plasma and thrombocyte concentrate were stored at -70 °C. After thawing, both were centrifuged at 3000 rcf for 30 min and the supernatants were added to the medium. Cells were split 1:1 or 1:2 upon reaching 90 % confluency for up to six serial passages using accutase (**Figure 9**).

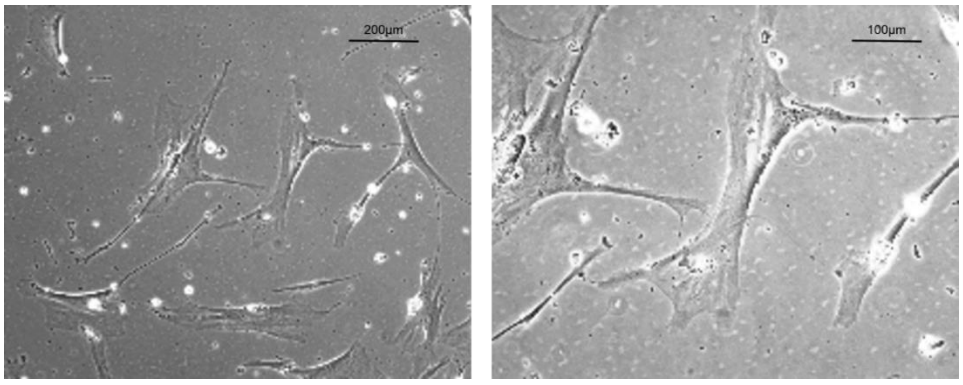

Figure 9: Light micrographs of MSC-2014-7 cells during routine cell culture.

2.1.2 Cell culture

Table 1: Cell culture

Name	Material Number	Manufacturer
Accutase	A6964	Sigma-Aldrich, St. Louis, Missouri, USA
DMEM high glucose (4.5 g/l) + GlutaMax-I	31966-021	Gibco, Life Technologies, Darmstadt, Germany
DMEM + low Glucose (1 g/l), no glutamine	11880-028	Gibco, Life Technologies, Darmstadt, Germany
RPMI 1640	21875-091	Gibco, Life Technologies, Darmstadt, Germany
DPBS	14190-094	Gibco, Life Technologies, Darmstadt, Germany
Fetal Calf Serum (FCS)	S0615	Biochrom, Berlin, Germany
Fresh Frozen Plasma	15900014	Blood bank from University Hospital, Tübingen, Germany
Heparin sodium salt	A3004	AppliChem GmbH, Darmstadt, Germany
L-Glutamine	G7513-100ML	Sigma-Aldrich, St. Louis, Missouri, USA
Penicillin/Streptomycin	P4333	Sigma-Aldrich, St. Louis, Missouri, USA
Platelet concentrate	15900011	Blood bank from University Hospital, Tübingen, Germany
Trypsin-EDTA	T4174m	Sigma-Aldrich, St. Louis, Missouri, USA

2.1.3 Cytostatics and Inhibitors

Table 2: Cytostatics and Inhibitors

Name	Material Number / Description	Manufacturer
ATO	Trisenox	Pharmacy of University Hospital, Tübingen
Doxorubicin	S1208	Selleckchem, Houston, Texas, USA
Etoposide	E1383/ VP-16-213	Sigma-Aldrich, St. Louis, Missouri, USA
GANT61	Ab120904	Abcam, Cambridge, UK

Table 3: Stock solutions

Inhibitor	Solvent	Concentration of stock solution
ATO	H_2O (ultrapure, autoclaved)	0.1 mM
Doxorubicin	DMSO	5 mM
Etoposide	DMSO	5 mM
GANT61	DMSO	5 mM

2.1.4 Equipment

Table 4: Devices

Name	Material Number / Description	Manufacturer
Balance (0.5 – 4100 g)	6J4100-2M	Kern, Balingen, Germany
Balance (10 mg – 220 g)	ABJ220_4M	Kern, Balingen, Germany
Benchtop centrifuge	Centrifuge 5424 R	Eppendorf, Hamburg, Germany
Centrifuge	5804 R	Eppendorf, Hamburg, Germany

Electric pipette	Pipetus akku	Hirschmann Laborgeräte, Eberstadt, Germany
Electrophoresis chamber	Mini PROTEAN® Tetra Cell	Bio-Rad Laboratories GmbH, Munich, Germany
Flow cytometer	LSR II	Becton Dickinson, Franklin Lakes, New Jersey, USA
Freezer (-20 °C)		Liebherr, Bulle, Switzerland
Freezer (-70 °C)		GFL, Burgwedel, Germany
Fridge (4 °C)	30 GT/N1201V	Haier, Qingdao, China
Gel casting station	Mini PROTEAN® Tetra Handcast system	Bio-Rad Laboratories GmbH, Munich, Germany
Horizontal shaker	MTS 4	IKA, Staufen, Germany
Incubator	CB 150	Binder, Tuttlingen, Germany
Magnetic stirrer	MAG RCT	IKA, Staufen, Germany
Microplate reader	EL 800	Bio-Tek, Winooski, Vermont, USA
Microscope	Fluovert FS	Leica, Wetzlar, Germany
Microscope	DM IRBE	Leica, Wetzlar, Germany
Multichannel pipette	Xplorer plus	Eppendorf, Hamburg, Germany
Multidispenser	Handy Step	Bran, Wertheim, Germany
Neubauer counting chamber	T=0.1 mm; 0.0025 mm^2	Karl Hecht GmbH & Co KG, Sondheim, Germany
pH-meter	Five easy FE 20	Mettler-Toledo, Greifensee, Switzerland
Power Supply	PowerPac™ Basic, 164-5050	Bio-Rad Laboratories GmbH, Munich, Germany

Photometer	NanoDrop 3300	Thermo Scientific, Waltham, Massachusetts, USA
qRT-PCR machine	CFX96 Real-time system, C1000 Thermal Cycler	Biorad, Hercules, California, USA
Single channel pipette	Research Plus	Eppendorf, Hamburg, Germany
Sterile workbench		BDK, Sonnenbühl-Genkingen, Germany
Thermomixer	Thermomixer Comfort 5355	Eppendorf, Hamburg, Germany
Ultrasonic bath	Transsonic 450	Ela Schmidbauer GmbH, Singen, Germany
Vortex mixer	REAXtop	Heidolph, Schwabach, Germany
Waterbath	WB 22	Memmert, Schwabach, Germany
Westernblot developing machine	Curix 60 Processor	Agfa-Gevaert N. V., Mortsel, Belgium

Table 5: Disposables

Name	**Material Number**	**Manufacturer**
<u>Culture plates</u> **6-well plates** **12-well plates**	 657160 665102	 Greiner Bio-One, Frickenhausen, Germany
96-well plates, F-bottom	655180	Greiner Bio-One, Frickenhausen, Germany
96-well plates, U-bottom	650101	Greiner Bio-One, Frickenhausen, Germany
96-well plates, U-bottom, non-binding	650901	Greiner Bio-One, Frickenhausen, Germany

Amersham Hyperfilm™ELC	28-9068-37	GE Healthcare Bio-Sciences, Pittburgh, USA
Cell culture flasks **T75** **T175**	 658175 660175	Greiner Bio-One, Frickenhausen, Germany
Centrifugation tubes **15ml** **50ml**	 188261 210261	Greiner Bio-One, Frickenhausen, Germany
Combitips advanced®, 5.0 ml	0030089456	Eppendorf, Hamburg, Germany
Cryo-tubes, 1.5 ml	72379004	Sarstedt, Nümbrecht, Germany
Nitrile gloves (Reha soft Nitrile)	942206	Hartmann, Heidenheim, Germany
PCR-plates (96-wells)	Multiplate PCR plates / ML 9651	Biorad, Hercules, California, USA
Pasteur pipettes		WU, Mainz, Germany
Pipette tips **10 µl** **100 µl** **200 µl** **1250 µl**	 692150 692066 692069 790058	Biozym, Hessisch Oldendorf, Germany
Reaction tubes **0.5 ml** **1.5 ml** **2.0 ml**	 0030124537 0030120086 0030120094	Eppendorf, Hamburg, Germany
Serological pipettes **5 ml** **10 ml** **25 ml**	 357543 357551 357525	Falcon, Franklin Lakes, NJ, USA

Syringes	B-D Discardit II syringe (1100 x 2 ml)	Becton, Dickinson and Company, Heidelberg, Germany
Transfer membrane Immobilon™-p	IPVH00010	Merck KGaA, Darmstadt, Germany
Drain tubes	18 / 72379004	Becton, Dickinson and Company, Heidelberg, Germany

2.1.5 Chemicals

Table 6: Chemicals

Name	Material Number	Manufacturer
Acrylamide/bisacrylamide mixture, 30 % (Rotiphorese® Gel 30)	3029.1	Carl Roth GmbH & Co. KG, Karlsruhe, Germany
Acryl Aqua Clean	0330111	WAK Chemie Medical GmbH, Steinbach, Germany
Bio-Rad Protein Assay Dye Reagent concentrate	500-0006	Bio-Rad Laboratories GmbH, Munich, Germany
Bovine serum albumin (albumin fraction V, pH 7.0)	A1391,0050	AppliChem GmbH, Darmstadt, Germany
CellTiter 96 Aqueous One Solution Cell Proliferation Assay (MTS-Assay)	G3580	Promega, Fitchburg, Wiisconsin, USA
Crystal violet	T123.1	Carl Roth GmbH & Co. KG, Karlsruhe, Germany

Descosept AF (surface desinfection)	00-311-010	Dr. Schuhmacher, Malsfeld, Germany
Dimethylsulfoxide (DMSO)	C6295-50ml	Sigma-Aldrich, St. Louis, Missouri, USA
dNTP-Mix	20-2010	PEQLAB Biotechnologie GmbH, Erlangen, Germany
ECL substrate (Thermo Scientific™ Pierce™ ECL Western Blotting Substrate)	PI-32109	Thermo Scientific, Waltham, Massachusetts, USA
EDTA	8040.3	Carl Roth GmbH & Co.KG, Karlsruhe, Germany
Ethanol absolute	1.00983.2511	Merck, Darmstadt, Germany
Fixable Viability Dye eFluor® 450	65-0863	eBioscience, San Diego, California, USA
Formaldehyde	4235.2	Carl Roth GmbH & Co.KG, Karlsruhe, Germany
Glycerol	1040921000	Merck, Darmstadt, Germany
Glycine	0079	Carl Roth GmbH & Co.KG, Karlsruhe, Germany
Halt Protease Inhibitor Cocktail EDTA free (100x)	87785	Thermo Scientific, Waltham, Massachusetts, USA
Methanol AnulaR Normapur	20847.307	VWR, Fontenay-Sous-Bois, France

Powdered milk, blotting grade, low fat	T145.2	Carl Roth GmbH & Co.KG, Karlsruhe, Germany
Sodium dodecyl sulfate	20760	SERVA Electrophoresis GmbH, Heidelberg, Germany
Sodium chloride	1.06404.1000	Merck, Darmstadt, Germany
Sodium hydroxide	71690	Fluka, Buchs, Switzerland
Tris ultrapure	A1086	AppliChem GmbH, Darmstadt, Germany
Triton X-100	T9284	Sigma-Alderich, St. Louis, Missouri, USA
Trypan blue	T8154	Sigma-Aldrich, St. Louis, Missouri, USA
Tween® 20	9127.1	Carl Roth GmbH & Co.KG, Karlsruhe, Germany

2.1.6 Kits and enzymes

Table 7: Kits and enzymes

Name	Material Number	Manufacturer
Random Primer Mix	S 1330 S	New England Biolabs, Ipswich, Massachusetts, USA
RNeasy Mini-Kit	74104	Qiagen, Venlo, Netherlands
RQ1 RNase-free DNase	M6101	Promega, Fitchburg, Wisconsin, USA
RT-PCR-Kit (10x RT-buffer, 100 mM DTT, Reverse transcriptase)	845-RT-5000	Analytik Jena, Jena, Germany
SYBR Select Master Mix for CFX	4472937	Life Technologies, Austin, Texas, USA

2.1.7 Oligonucleotides

Table 8: Oligonucleotides

Name	Sequence (5'→3')	Tm in °C
Gli1 forward	CCA ACT CCA CAG GCA TAC AGG AT	62.4
Gli1 reverse	CAC AGA TTC AGG CTC ACG CTT C	62.1
Gli2 forward	AAG TCA CTC AAG GAT TCC TGC TCA	61.0
Gli2 reverse	GTT TTC CAG GAT GGA GCC ACT T	60.3
Gli3 forward	CGC GAC TGA ACC CCA TTC TAC	61.8
Gli3 reverse	GTG TTG TTG GAC TGT GTG CCA TT	60.6
PTCH 1 forward	CCC CTG TAG GAA GTG GAC ACT CTC	66.1
PTCH 1 reverse	AAG GAA GAT CAC CAC TAC CTT GGC T	63.0

SMO forward	GCT ACT TCC TCA TCC GAG GAG TCA	64.4
SMO reverse	GGC GCA GCA TGG TCT CTT	61.0
TBP forward	TGC ACA GGA GCC AAG AGT GAA	59.8
TBP reverse	CAC ATC ACA GCT CCC CAC CA	61.4

The oligonucleotides were synthesised by Eurofins MWG Operon, Ebersberg, Germany.

2.1.8 Buffers and Solutions

Electrode buffer (10x)	250 mM Tris/HCL, pH 8.6; 2 M Glycine
Running buffer	1:10 electrode buffer; 0.1 % (m/V) SDS
Blotting buffer	1:10 electrode buffer; 20 % methanol
Sample loading buffer (2x)	125 mM Tris/HCL, pH 6.8; 4 % (m/V) SDS 20 % (V/V) Glycerol 10 % (V/V) ß-mercaptoethanol Bromphenol blue
TBS-T	10 mM Tris/HCL, pH 7.5; 150 mM NaCl 0.1 % Tween
Protein lysis buffer	40 mM Tris/HCl, pH 7.4; 300 mM NaCl; 2 mM EDTA; 20 % Glycerol; 2 % Triton X100
FACS buffer	2 % FCS; 2 mM EDTA (Diluted in PBS)
Crystal violet stock solution (10x)	1 % Crystal violet (diluted in 20 % ethanol)
Crystal violet working solution	1:10 Crystal violet stock solution (diluted in 20 % ethanol)

2.1.9 Antibodies

Table 9: Antibodies

Name	Material Number	Manufacturer
ß-Tubulin (9FS) Rabbit mAb	2128	Cell Signaling Technology, Danvers, Massachusetts, USA
Cleaved Caspase 3 (Asp175) (5A1E) Rabbit mAb	9664	Cell Signaling Technology, Danvers, Massachusetts, USA
Cleaved PARP (Asp214) (D64E10) XP® Rabbit mAb	5625	Cell Signaling Technology, Danvers, Massachusetts, USA
Gli1 Rabbit mAb	2553	Cell Signaling Technology, Danvers, Massachusetts, USA
Gli2 (H-300) Rabbit pAb	SC-28674	Santa Cruz, Dallas, Texas, USA
Peroxidase AffiniPure Goat Anti-Rabbit IgG (H+L)	111-035-003	Jacksson ImmunoResearch, West Grove, Pennsylvania, USA

Thermo Scientific PageRuler Prestained Protein Ladder (#26616)

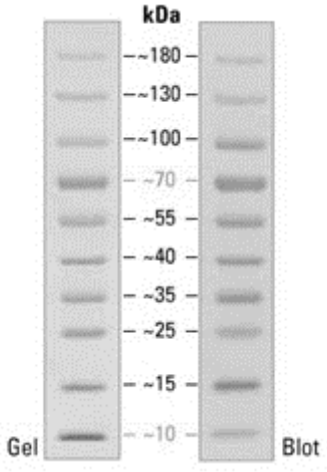

***Figure 10: SDS-PAGE band profile of the PageRuler Prestained Protein Ladder**. Images are from a 4 - 20 % Tris-glycine gel (SDS-PAGE) and subsequent transfer to membrane (Thermo Fisher Scientific, 2015).*

2.1.10 Software

Table 10: Software

Name	Use	Developers
CFX-Manager™	Analysis of qTR-PCR data	Biorad, Hercules, California, USA
FACSDiva	Acquisition of flow cytometry data	Becton Dickinson, Franklin Lakes, New Jersey, USA
FlowJo 4.6.2.	Analysis of flow cytometry data	Tree Star, Ashland, Oregon, USA
Microsoft Office Paket	Analysis of data, diagrams	Microsoft Corporation, Redmond, USA
Prism5	Calculation of IC_{50}-values	GraphPad Software, La Jolla, California, USA

2.2 Methods

2.2.1 Cell and molecular biological methods

Cell culture

Cells were cultured in T75 or T175 cell-culture flasks at 37 °C, 5 % CO_2 and were passaged at 80 - 90 % confluency. For passaging, medium was removed, cells were washed with 5 ml PBS (10 ml for T175 flasks) and then enzymatically detached with 2 ml (4 ml for T175 flasks) 1 x trypsin-EDTA (A673, RD-ES and SK-N-MC) or accutase (MSC-2014-7). The reaction was stopped after 5 min incubation at 37 °C, 5 % CO_2 by adding medium containing fetal calf serum.

Determination of cell number

The cell suspension was centrifuged at 7 °C and 1500 rpm for 7 min. The supernatant was aspirated and the cell pellet diluted in 1 ml medium. 10 µl of a 1:10 diluted cell suspension were added to 90 µl trypan blue and pipetted between cover glass and Neubauer counting chamber. Living cells (not stained) in the four big squares were counted under the microscope and the number of cells per ml was calculated as follows:

$$Number\ of\ cells\ \left(\frac{cells}{ml}\right) = X \div 4 \times 10^4 \times 10 \qquad \text{Equation 1}$$

X = cells counted in all four big squares

4 = quotient for four squares

10^4 = chamber factor

10 = 10 time dilution

Freezing and thawing of cells

For freezing of cells, cells were counted as described above and the cell suspension with 1 x 10^6 cells was centrifuged at 7 °C and 1500 rpm for 7 min. The supernatant was aspirated and the cell pellet re-suspended in 1 ml of freezing-medium (10 % DMSO and 90 % FCS). Cells in freezing-medium were transferred into a cryo-tube, which was kept at -20 °C for 1 h, then transferred into a -70 °C freezer overnight and kept in liquid nitrogen at -196 °C for long-time storage.

For thawing of cells, a cryo-tube was taken from liquid nitrogen and warmed up until the ice chunk had separated from edge of the tube. 5 ml culture medium were added to quickly inhibit the cytotoxic effect of DMSO and the suspension was transferred into a 15 ml centrifugation tube. Cells were centrifuged at 7 °C and 1500 rpm for 7 min, the supernatant was aspirated and the cell-pellet was re-suspended in 10 ml cell line specific medium. The cell suspension was transferred into a cell-culture flask (T75) which was filled up with the respective medium to 15 ml final volume. Medium was changed at the next day to remove cells that had not attached.

Extraction of RNA from cell-lysate

The innuPREP RNA Mini Kit from Analytik Jena was used for RNA extraction. 10^6 cells were harvested in a 1.5 ml Eppendorf tube and 350 µl of RLT buffer were added to the cell pellet. Subsequently, the cell pellet was re-suspended with help of an insulin syringe and either frozen at -20 °C or directly used for RNA extraction.

Therefore, the lysate was transferred into a Spin Filter D and centrifuged at 10,000 g for 2 min so that the lysate was completely filtrated into the 2.0 ml receiver tube. The filtrate was kept and mixed with 350 µl of 70 % ethanol. The sample was transferred into the Spin Filter R and centrifuged again at 10,000 g for 2 min. The receiver tube was replaced and 500 µl of washing solution HS were added to the Spin Filter which was centrifuged at 10,000 g for 1 min. This step was repeated with 700 µl of washing solution LS and the Spin Filter was centrifuged at 10,000 g once for 1 min and then for 3 min. Finally, the Spin Filter R was placed into a 1.5 ml Eppendorf tube and the sample was incubated with 40 µl RNase-free water for 1 min at RT before centrifugation at 6,000 g for 1 min. The filtrate containing the RNA was either frozen at -20 °C or DNase digestion was carried out immediately.

DNAse digestion

To eliminate any contamination with DNA, DNAse digestion was performed. Using the RQ1 RNase free DNase from Promega (Promega, Madison, Wisconsin, USA) each RNA-sample was treated as follows:

16 µl	RNA-sample
2 µl	10x DNase buffer
2 µl	RQ1 DNase

The mixture was incubated in a 1.5 ml Eppendorf tube at 37 °C for 30 min before adding 2 µl stopping reagent for another 10 min at 65 °C.

Following the DNase digestion, the RNA content and purity of each sample was measured using the NanoDrop (Thermo Scientific, Waltham, Massachusetts). Absorption of 1 µl of each sample was determined photometrically at 260 nm and 280 nm. 260 nm correspond to the maximum absorption of nucleic acids, whereas 280 nm correspond to that of proteins. 1 µl RNase-free water was used as a blank-value. Thus, a contamination of the RNA samples with DNA or proteins can be assumed when the quotient of 260 nm and 280 nm is below 1.9. Pure RNA should have a value between 1.9 and 2.1. In addition the quotient of 260 nm and 230 nm, which should not come below 1.7 was determined to rule out any other aromatic contaminations.

The RNA-concentration (C) was calculated as follows:

$$c(RNA) = A_{260} \times C \qquad \text{Equation 2}$$

A_{260} = Value of absorption at 260 nm

C = nucleic acid specific coefficient for RNA of 0.04 µg/µl

The samples were then either stored at -20 °C or reverse transcription to cDNA was performed.

Reverse transcription

For the transcription of RNA to complementary DNA (cDNA) a reverse transcriptase (RT) and short "random primer" were used. 1 µg of RNA were mixed with 2 µl of 60 µM "random primer" mix (New England Biolabs, Ipswich, Massachusetts, USA) in a 0.5 ml Eppendorf tube. To attain a final volume of 14.2 µl RNase-free-water was added, mixed slightly followed by incubation at 65 °C for 5 min. The samples were left at room-temperature for another 10 min before addition of 5.8 µl of Master-Mix to each Eppendorf tube.

Master-Mix:	2 µl	10x RT-Buffer
	0.64 µl	25 mM dNTP mix
	2 µl	100 mM DTT
	1 µl	RT-Enzyme

The entire Master-Mix was prepared for all samples.

The samples were put into the PCR-machine and polymerase chain reaction (PCR) was started overnight:

10 min	25 °C
5 min	42 °C
60 min	55 °C
15 min	70 °C
Break	8 °C

The cDNA was either kept at -20°C or used directly for a quantitative real-time PCR (qRT-PCR).

Quantitative Real-Time PCR

To quantify the abundance of GLI1, GLI2, GLI3, PTCH1 and SMO mRNA, qRT-PCR was used. The qRT-PCR method detects the amount of cDNA after each amplification cycle by a fluorescent double-strand DNA intercalating dye (Rajeevan et al., 2001; Schmittgen et al., 2000). The reaction mixture consists of the SYBR Select Master Mix for CFX (Life Technologies, Austin, Texas, USA), both "forward" and "reverse" primers for the target genes GLI1, GLI2, GLI3, PTCH1, SMO or the control gene "TATA-Box Binding Protein" (TBP) (Eurofins MWG Operon, Ebersberg, Germany) and RNase free water.

Reaction mixture: 5 µl SYBR Select Master Mix for CFX
1 µl forward Primer (10 µM)
1 µl reverse Primer (10 µM)
1 µl RNase free water

To the 9 µl reaction mixture 1 µl cDNA (50 ng) or H_20 as a negative control was pipetted. The 96 well plate was closed with foil and centrifuged at 7 °C and 1500 rpm for 7 min. All samples were prepared as duplicates and tested in four independent tests. The CFX96 real-time System (Biorad, Hercules, USA) was used for the detection of the amplification products. **Table 11** shows an overview of the qRT-PCR program.

Table 11: qRT-PCR program.

Temperature in °C	Duration	Number of cycles
50	2 min	1
95	2 min	1
95 **60**	15 sec 1 min	45
Melt curve from 75 °C to 95 °C: Increase of 0.2 °C in 1 sec		
25	2 min	1

During the PCR-reaction the wanted cDNA segment is amplified by binding of the specific oligonucleotides and the Taq-polymerase. Due to the intercalation of SYBR-Green in the new synthesized DNA, the fluorescence increases proportionally to the amount of DNA-product. The cycle threshold (Ct) marks the cycle where the specific fluorescence significantly increases above the background fluorescence. For the efficiency-corrected relative quantification (ΔΔCt) the "housekeeping" gene TBP was used as reference gene. The ratio (ΔCt) between the Ct-value of the gene of interest and the Ct-value of TBP was calculated:

$$\Delta Ct = Ct(gene\ of\ interest) - Ct(TBP) \qquad \text{Equation 3}$$

As the basal expression of genes in EWS cells in comparison to the basal expression in the control cells MSC-2014-7 was of interest, the ΔCt-values of both the EWS cell line and MSC-2014-7 were compared (ΔΔCt):

$$\Delta\Delta Ct = \Delta Ct(EWS\ cells) - Ct(MSC) \qquad \text{Equation 4}$$

The quantitative expression of the gene of interest could then be calculated as follows:

$$E = 2^{-\Delta\Delta Ct} \qquad \text{Equation 5}$$

2.2.2 Cell Viability Test (MTS-Assay)

To determine the effect of different substances on the viability of cells MTS assays were performed, where the reduction of the yellow 3-(4,5-dimethylthiazol2-yl)-5-(3-carboxyphenyl)-2-(4-sulfophenyl)-2H-Tetrazoliumsalt (MTS) to a violet formazan is measured. This reaction is accomplished by the reduction equivalents NADPH and NADH and can be photometrically determined at 490 nm with the amount of measured colouring agent equal to the rate of glycolysis of the cells (Mosmann, 1983).

For the MTS-assay cells were seeded into 96-well-plates using 0.5 x 10^4 cells/well (RD-ES, SK-N-MC and MSC-2014-7) or 1.0 x 10^4 cells/well (A673) in 100 µl (A673, RD-ES and MSC-2014-7) or 250 µl (SK-N-MC) of medium. Cells were incubated at 37 °C, 5 % CO_2 for 24 h and then treated with different concentrations of the inhibitors by exchanging the medium. A control using the inhibitors solvent in accordance with the highest inhibitor concentration applied was also prepared. After 96 h incubation 15 µl

(A673 and RD-ES) or 20 µl (SK-N-MC) of MTS reagent (CellTiter 96 Aqueous One Solution Cell Proliferation Assay, Promega, Fitchburg, Wisconsin, USA) were added to each well and plates were incubated for another 90 min at 37 °C and 5 % CO_2. The absorbance was measured at 490 nm and a reference wavelength of 630 nm using an EL 800 reader (BioTek, Winooski, Vermont, USA).

The negative control absorbance was set to 100 % and viability of treated cells calculated accordingly. Triplicates were prepared from each concentration and four independent experiments were performed.

2.2.3 Clonogenic Assay

To analyse the effect of the agents on the ability to proliferate and form colonies from single cells, a clonogenic assay was performed, which was first established with Hela cells in 1955 (Puck and Marcus, 1955). For this purpose very low densities of cells were evenly sown into 6-well-plates (A673 with 1000 cells/well; RD-ES and SK-N-MC with 500 cells/well) by diluting the required cells in 2 ml medium and spreading them evenly onto the bottom of one well. Cells were allowed to attach for 24 h at 37 °C and 5 % CO_2 and then treated with different concentrations of inhibitors for another 72 h. The supernatant was aspirated and replaced with fresh medium without inhibitor every 2 - 3 days for 9 - 15 days until colonies in negative controls were grown. Each 6-well plate included two negative controls treated with the inhibitors solvent. Colonies were stained with crystal violet.

Stock solution: 1 % crystal violet in 20 % ethanol (v/v)

Working solution: stock solution 1:10 in 20 % ethanol (v/v)

For this the medium was aspirated and cells were washed with 1 ml/well PBS. After aspiration of PBS cells were incubated for 10 min at room temperature with 500 µl/well ice-cold methanol, remaining methanol was transferred into special waste and 500 µl of crystal violet working solution were added to each well. Plates were incubated for 30 min at room temperature on a horizontal shaker and then washed out with dH_2O.

Plates were dried upside down on cellulose paper and could be photographed the next day.

2.2.4 Cell Death Assay ("Fluorescence Activated Cell Sorting", FACS)

Flow cytometry can assess several parameters of a cell population at the same time and evaluates large cell populations. The size of cells can be determined with the forward scatter (FSC) and the granularity with the side scatter (SSC). Furthermore, the expression of intracellular proteins and specific surface markers as well as the amount of DNA in the cells can be quantified. For the verification of cell death induction "Fixable viability dye Fluor - eFluor® 450" (eBioscience, San Diego, California, USA), a DNA-intercalating dye that only stains cells lacking an intact cell membrane was used. As the integrity of cell membranes is lost in dying cells eFluor® 450 uptake can serve as a marker (Fulwyler, 1965; Julius et al., 1972).

For the assay 2.5 x 10^5 MSC-2015-7 or A673, 1.5 x 10^5 RD-ES or 1 x 10^5 SK-N-MC cells were seeded in 2 ml corresponding medium into 6-well plates and incubated at 37 °C, 5 % CO_2 for 24 h. The medium was exchanged with 2 ml fresh medium containing single and combined concentrations of cytostatics and/or GLI1-inhibitors and plates were incubated for another 72 h at 37 °C, 5 % CO_2. Each condition was assessed threefold including a negative control without inhibitor.

For staining of the cells using "Fixable viability dye Fluor - eFluor® 450" medium was transferred into 2 ml Eppendorf tubes and the adherent cells were detached by incubating plates for 5 min at 37 °C, 5 % CO_2 with 500 µl trypsin-EDTA (EWS cell lines) or accutase (MSC-2014-7). The detached cells were transferred into the respective Eppendorf tube containing the medium supernatant of the well and the tube was centrifuged for 5 min at 5,000 g. The supernatant was removed carefully, cell pellets were re-suspended in 200 µl PBS and placed into the cavity of a round-bottom 96-well-plate. The plate was centrifuged for 5 min at 5,000 g. PBS was discarded and cells were washed once more with 200 µl PBS. The staining dye was prepared diluting "Fixable viability dye Fluor - eFluor® 450" 1:1000 in PBS. Cells were incubated for 30 min at 4 °C in the dark using 100 µl of diluted dye per well. Following the incubation cells were centrifuged and washed once again with 200 µl PBS. After centrifugation cells were fixed with 100 µl/well 0.5 % formaldehyde at 4 °C in the dark. After 30 min of incubation the plate was centrifuged, cells washed with 200 µl PBS, centrifuged again and then pellets were re-suspended in 100 µl FACS-buffer. Plates could be stored at 4 °C for seven days until

analysis. Before measurement additional 100 µl FACS-buffer were added to each sample and cells were transferred into 5 ml FACS-vials. Kept on ice and protected from light, samples were analysed subsequently with an LSRII flow cytometer at 450 nm (BD Bioscience, Heidelberg, Germany). The results were calculated using the FlowJo Software (Tree Star Inc., Ashland, USA).

2.2.5 Western blot

To detect the abundance of specific proteins such as GLI1, GLI2 as well as the apoptotic cleavage of Poly (ADP-ribose) polymerase (PARP) and caspase 3 the method of the western blot was used. For this proteins were isolated and quantified, separated using gel electrophoresis, transferred onto a membrane and incubated with the corresponding antibodies. The method was first developed by Harry Towbin and shortly after refined by W. Neal Burnette (Burnette, 1981; Towbin et al., 1979).

Preparation of protein samples

1.5×10^5 cells were sown into 12-well plates containing 1 ml of medium per well and incubated at 37 °C and 5 % CO_2. After 24 h cells were treated with different concentrations of inhibitors for 48 h. For a negative control cells were left in 1 ml of medium containing the inhibitor solvent for 2 days.

The isolation of proteins was carried out on ice. Medium was transferred into a 2 ml Eppendorf tube, centrifuged at 5,000 rcf for 5 min and the cells were detached with 500 µl of trypsin-EDTA (A673, RD-ES and SK-N-MC) or accutase (MSC-2014-7) in the meantime. 500 µl of the centrifuged supernatant were aspirated and the rest used to take up the detached cells. Once more, the samples were centrifuged at 5,000 rcf for 5 min and the supernatant was aspirated. To lyse the cells, 200 µl of lysis-buffer containing 1:100 diluted proteinase-inhibitor were added to each Eppendorf tube. The lysates were sonificated 4 times for 20 s putting the samples on ice for 30 s between each sonification step. Samples were centrifuged at 13,800 rcf for 10 min and 200 µl of the supernatant transferred into a new Eppendorf tube. Proteins were kept at -20 °C.

Bradford Assay for quantification of protein concentration in samples

Protein concentrations were quantified photometrically by adding Coomassie Brilliant Blue and performing a Bradford Assay. Coomassie Brilliant Blue is a triphenylmethane dye that appears red in its unbound form and blue in its protein bound form, which leads to a shift in the absorbance. Triphenylmethane can form complexes with cationic and non-polar side chains of proteins under acidic conditions. For the statistically correct evaluation, triplets of each protein sample and samples of a BSA dilution series were used. Protein samples were thawed and diluted 1:100 in dH_2O (3 µl protein sample + 297 µl dH_2O). For the dilution series a standard concentration stock with 1.41 mg/ml BSA was used.

Dilution series:
a) 100 µg/ml - 21.3 µl stock + 278.7 µl dH_2O
b) 80 µg/ml - 17.0 µl stock + 283.0 µl dH_2O
c) 60 µg/ml - 12.8 µl stock + 287.2 µl dH_2O
d) 40 µg/ml - 8.5 µl stock + 292.5 µl dH_2O
e) 20 µg/ml - 4.3 µl stock + 295.7 µl dH_2O
f) 10 µg/ml - 2.13 µl stock + 297.87 µl dH_2O
g) 5 µg/ml - 1.06 µl stock + 198.94 µl dH_2O
h) blank - 300 µl dH_2O

Each 80 µl/well of the samples were pipetted into a 96-well-plate. 20 µl of staining reagent (Bio-Rad Protein Assay Dye Reagent Concentrate) were added to each well and mixed. The plate was incubated for 5 min and the absorbance was measured at 620 nm on the microplate reader (BioTek, Winooski, Vermont, USA) making sure no air bubbles were in the wells.

SDS Page

For separation of proteins based on their molecular weight and size the sodium dodecyl sulfate polyacrylamide gel electrophoresis (SDS-PAGE) was used. SDS denatures proteins and masks their original charge by a strong negative charge. Therefore, due to their molecular weight, smaller molecules migrate faster through the acrylamide matrix to the anode (positively charged electrode) finding themselves nearer to the bottom of the gel. By comparison to a marker containing proteins with specific known molecular

weights, the molecular weight of the separated proteins can be estimated (Raymond and Weintraub, 1959; Shapiro et al., 1967).

For the SDS-PAGE, polyacrylamide gels consisting of a stacking gel (5 %) and a separating gel (10 %) were casted. Glass panels and combs from the Bio-Rad gel casting device were first cleaned with dH_2O and 70 % ethanol. The station for the gels was set up, the glass panels put together and inserted into the holding device. 10 % separating gel and 5 % stacking gel were prepared in two 50 ml tubes. **Table 12** shows the composition of the solutions sufficient for four gels.

Table 12: Composition of SDS gels (sufficient for 4 gels).

	Separating gel 10 %	**Stacking gel 5 %**
Destilled water (ddH_2O)	15.8 ml	11 ml
30 % Acrylamide	13.4 ml	2.6 ml
1.5 M Tris/HCl pH 8.8 (separating buffer)	10 ml	-
1 M Tris/HCl pH 6.8 (stacking buffer)	-	2 ml
20 % SDS	200 µl	80 µl
10 % APS	400 µl	160 µl
TEMED	16 µl	16 µl

The separating gel was prepared and poured between glass panels leaving about 3 cm space at the top and covered with a 2 mm layer of isopropanol (approximately 300 µl per gel). After the separating gel had polymerised, isopropanol was removed and the gel was left for 5 min until all of the remaining isopropanol had vaporised. Then APS and TEMED were added to the stacking gel and the gel was poured on top of separating gel. Combs were inserted taking care that no air bubbles were enclosed and the gel was left until it had completely polymerised. Gels were used immediately or wrapped in damp paper and foil and stored at 4 °C for up to 3 days.

Proteins were thawed in 1.5 ml Eppendorf tubes on ice, mixed with the same volume of sample buffer, incubated on the thermomixer at 95 °C for 5 min and stored on ice until loading on the gel. Gels were transferred into the electrophoresis chamber (Bio-Rad

Laboratories GmbH, Munich, Germany) and the chamber was filled with running buffer up to the markings. Combs were drawn carefully and the slots were rinsed with running buffer to remove any existing gel residual. 1 - 2 slots per gel were filled with each 5 µl of marker (Thermo Scientific PageRuler Prestained Protein Ladder (#26616)) and the proteins were pipetted carefully into the remaining slots making sure that no slot overflows (max 60 µl/slot). SDS-PAGE was run at 17 mA per gel (4 gels = 68 mA) until the blue running front nearly reached the end of gel (1.5 - 2 h). Gels were then immediately used for the western blot.

Blotting

For detection of apoptotic caspase 3 and PARP cleavage as well as GLI1 and GLI2, the western blot method was used.

To transfer the proteins from the gel onto a PVDF membrane, sponges and whatman paper were soaked in blotting buffer, a PVDF membrane was put in 100 % methanol for 10 s before it was transferred into blotting buffer. The stacking gel had to be detached from separating gel and the blotting sandwich was assembled in a tub filled with blotting buffer to avoid any air getting enclosed. The blotting chamber was filled with blotting buffer up to marking and the blot was run at 20 V overnight for 16 - 18 h.

Assembly of the blotting sandwich:

- White side of support grid
- 1 Sponge
- 1 Whatman paper
- PVDF membrane
- Gel
- 1 Whatman paper
- 1 Sponge
- Black side of support grid

After proteins were blotted onto the PVDF membrane, the membranes were removed from the blot sandwich and stained with 1 % black ink (#17, Pelikan, Hannover, Germany) diluted in TBS-T (4 membranes need 30 ml) on horizontal shaker for 15 min. Ink was drained and membranes were washed with TBS-T for 5 min. For blocking, 5 %

milk powder in 20 ml TBS-T was prepared and membranes were incubated therein for 30 min. For detection of the cleaved forms of caspase 3 (17 - 20 kDa) and PARP (89 kDa) as well as the loading control ß-tubulin (55 kDa) on the same membrane, membranes had to be cut into segments. For detection of GLI1 or GLI2, the entire membrane was incubated with the first antibody in 50 ml tubes at 4 °C overnight on a roller mixer.

Dilution of first antibodies:

anti-cleaved Caspase 3 (5A1E):	diluted 1:500 in 5 % milk powder in 20 ml TBS-T
ß-Tubulin (9F3) rabbit mAb:	diluted 1:2,000 in 5 % BSA in TBS-T
anti-cleaved PARP (DE64E10):	diluted 1:500 in 5 % BSA in TBS-T
GLI1 Rabbit mAb:	diluted 1:10,000 in 5 % BSA in TBS-T
GLI2 (H-300):	diluted 1:200 in 5 % BSA in TBS-T

After the first antibody incubation membranes were washed 3-times with TBS-T for each 15 min. The membranes were incubated for 2 h with the secondary, horseradish peroxidase conjugated antibody diluted 1:10,000 in 40 ml 5 % milk powder in TBS-T. After three washing steps using TBS-T for each 15 min, membranes were covered with 4 ml of “enhanced chemiluminescent substrate” (ECL-solution) for two minutes. The remaining liquid was discarded and membranes were wrapped in plastic foil. For development, the wrapped membranes were placed into a film cassette and a film was exposed to the membrane for a period of time depending on the detected protein (Caspase 3 and PARP: 45 min; ß-tubulin: 2 - 5 min; Gli1: 25 - 30 min; Gli2: 10 sec). The film was developed with an automatic developing machine (Agfa-Gevaert N. V., Mortsel, Belgium).

2.2.6 3D spheroid cultures

To analyse the effect agents have on cells growing in a 3D culture, substances were tested on cells grown as spheroids as described in a paper by Vinci et al. (Vinci et al., 2012). Only the cell lines A673 and SK-N-MC were able to form spheroids, therefore, RD-ES had to be excluded from this experiment.

Cells were sown out in non-adherent round-bottom 96-well-plates (A673: 0.5×10^4 cells/well in 150 µl medium; SK-N-MC: 0.25×10^4 cells/well in 200 µl medium) and the plate was centrifuged for 7 min at 1500 rpm. As SK-N-MCs did not yet stick together, the plate was centrifuged for another 7 min at 1500 rpm the next day. After 4 days spheroids were photographed at the microscope (Leica, Wetzlar, Germany) (day 0) and thereafter treated with different concentrations of inhibitors in a final volume of 250 µl for another 4 days until a second micrograph was taken (day 4). For each condition four spheroids were analysed and medium with solvent was added to the 4 negative controls.

3 Results

3.1 Identification of Hedgehog pathway component expression profiles in Ewing sarcoma cell lines

The EWS-FLI1 fusion protein typical for Ewing sarcoma is known to modulate the expression of genes involved in multiple signalling pathways including the Hh pathway (Taylor et al., 2011). Previous studies have identified the GLI1 protein as a direct transcriptional target of EWS-FLI1 (Beauchamp et al., 2009). As GLI1 is involved in tumourigenesis and can be targeted by different inhibitors, the expression of GLI1 was of special interest in this work. Basal expression of both activating transcription factors GLI1 and GLI2 was analysed at mRNA and protein level. Moreover, the mRNA expression of additional pathway components like GLI3, SMO and PTCH was examined. Finally, the influence of the GLI inhibitor ATO on levels of GLI1 protein in EWS cell lines was investigated.

3.1.1 Quantification of Hh pathway mRNA expression in A673, RD-ES and SK-N-MC cells in comparison to MSC

As a basis of this work, the expression of GLI1, GLI2, GLI3, SMO and PTCH1 mRNA in the three EWS cell lines A673, RD-ES and SK-N-MC in comparison to healthy MSC was analysed by qRT-PCR.

In **figure 11** the results of the mRNA expression analysis are presented. The mRNA expression in MSC-2014-7 was set to 100 %. The results show an overexpression of GLI1-mRNA only in the cell lines A673 (803 ± 40 %) and RD-ES (193 ± 44 %). SK-N-MC cells expressed lower levels of GLI1 (35 ± 1 %) than MSC. However, only in A673 cells GLI1-mRNA abundance was significantly higher than in MSC. An overexpression of GLI2-mRNA could only be proved in A673 cells (185 ± 41 %). Both RD-ES and SK-N-MC cells showed GLI2-mRNA expression levels similar to MSC. GLI3 was slightly overexpressed in A673 cells (155 ± 44 %) but underexpressed in both RD-ES (13 ± 6 %) and SK-N-MC (26 ± 2 %) cells. In contrary to A673 and SK-N-MC, the RD-ES cell line was the only cell line showing reduced SMO-mRNA compared to MSC. Interestingly, all three EWS cell lines presented an overexpression of PTCH1-mRNA (A673: 314 ± 35 %; RD-ES: 131 ± 11 %; SK-N-MC: 159 ± 24 %) which was especially significant in A673 cells.

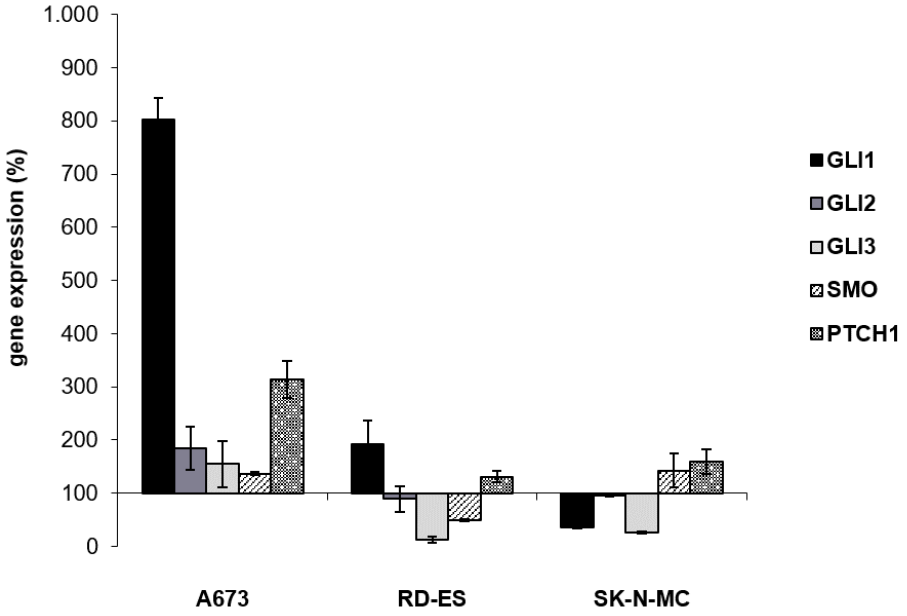

Figure 11: Relative expression of Hedgehog pathway genes in EWS cell lines A673, RD-ES and SK-N-MC in comparison to MSC-2014-7. *Each 1 x 10^6 cells of A673, RD-ES, SK-N-MC and MSC were lysed, the mRNA cleaned and transcribed into cDNA. 50 ng of cDNA were analysed by qRT-PCR. Ct-values of the genes GLI1, GLI2, GLI3, SMO and PTCH1 were determined. For calculation of the ΔCt-values of all analysed genes the expression of the reference gene TBP was also determined. The ΔΔCt-values were determined by comparison of gene expression in control cells MSC-2014-7 with gene expression in EWS cell lines. Gene expression is given in percent, expression in MSC-2014-7 was set to 100 %. Mean values were plotted from four independent replicates. Standard deviations are represented by black error bars. Data presented in this figure was also published (Boehme et al., 2016 (1)).*

3.1.2 GLI1 and GLI2 protein expression in A673, RD-ES and SK-N-MC in comparison to MSC

To determine the GLI1 and GLI2 protein levels of A673, RD-ES and SK-N-MC in comparison to MSC western blot analysis was performed. **Figure 12** shows the 100 kDa GLI1 isoform and also higher molecular weight bands in all three EWS cell lines. Moreover, MSC also present a slight band at 100 kDa with a very faint ß-tubulin band compared to the EWS cell lines. However, having set the GLI1 protein levels in MSC to 100 %, the quantified data suggests that all three EWS cell lines hold comparable levels of GLI1 protein, which are lower than in MSC (A673: 63 %; RD-ES: 57 % and SK-N-MC: 67 %). Furthermore, GLI1 protein in A673 cells is not higher expressed than in RD-ES and SK-N-MC which would have been expected based on GLI1-mRNA levels of A673. Interestingly, smaller bands are found in all cell lines, including a very dominant band running at 45 - 55 kDa in the MSC-2014-7 lane.

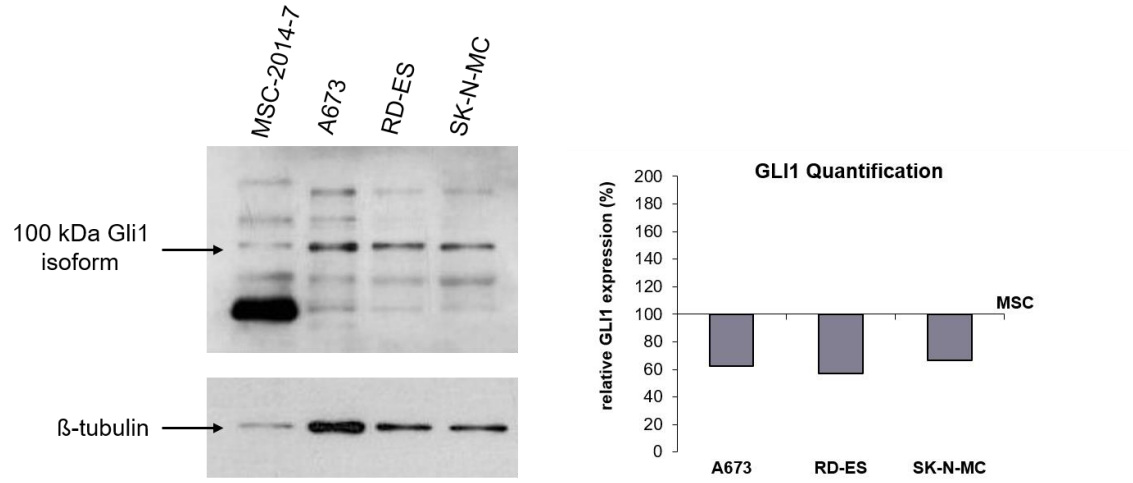

Figure 12: Expression of GLI1 protein in the EWS cell lines A673, RD-ES and SK-N-MC as well as MSC-2014-7. *1.5 x 10^4 cells/well of A673, RD-ES, SK-N-MC or MSC-2014-7 were sown into a 12-well plate. After 72h proteins were isolated and their concentration was measured with Bradford assay. For the western blot protein samples were loaded as follows: lane 1: MSC-2014-7; lane 2: A673; lane 3: RD-ES and lane 4: SK-N-MC. Proteins were separated by SDS-PAGE and blotted onto a PVDF membrane. Membranes were incubated with the primary antibodies GLI1 rabbit Ab or tubulin rabbit mAb overnight. A horseradish peroxidase-conjugated anti-rabbit pAb was used as secondary antibody. ECL substrate was added to the membrane and chemiluminescence signals were recorded on a film. ImageJ was utilised for western blot quantification. Data presented in this figure was also published (Boehme et al., 2016 (1)).*

Figure 13 shows the expression of the full length and repressor form of GLI2 protein. In MSC-2014-7 with the GLI2 antibody significant running at 80 kDa and 170 kDa were detected. In the EWS cell lines the upper band had a size of about 130 kDa, whereas the 80 kDa band was detected as well. As ß-tubulin expression varied strongly, the expression of both full length and repressor form of GLI2 was set in relation to the equivalent ß-tubulin expression. Therefore, the quantified data showed decreased expression of both GLI2 forms in all EWS cell lines, compared to MSC whose GLI2 levels were set to 100 %. GLI2 full length expression of the EWS cell lines in comparison to MSC was slightly higher (GLI2 full length in A673: 13 %; RD-ES: 17 % and SK-N-MC: 27 %) than the repressor form (GLI2 repressor form in A673: 6 %; RD-ES: 12 % and SK-N-MC: 18 %).

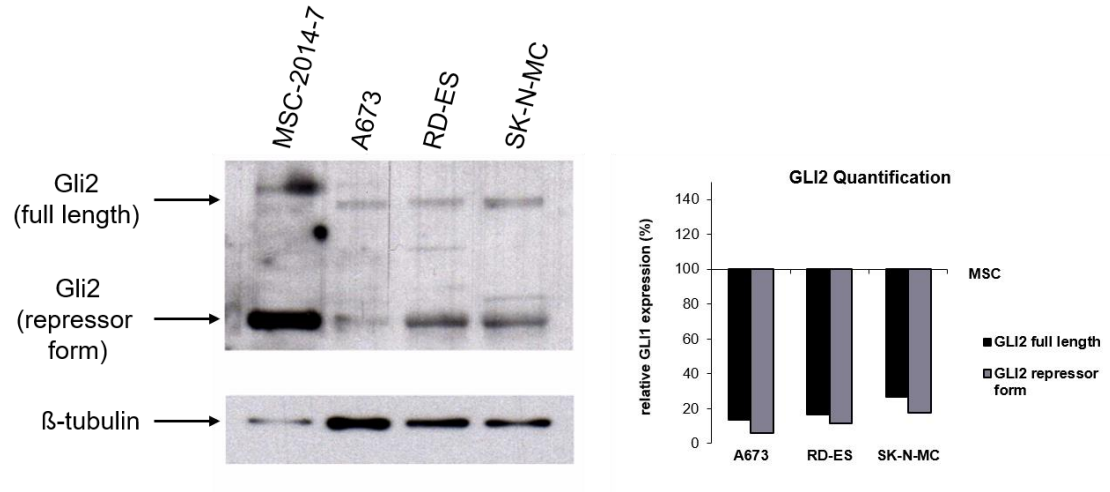

Figure 13: Expression of GLI2 protein in the EWS cell lines A673, RD-ES and SK-N-MC as well as MSC-2014-7. *1.5 x 10^4 cells/well of A673, RD-ES, SK-N-MC or MSC-2014-7 were sown into a 12-well plate. After 72h proteins were isolated and their concentration was measured with Bradford assay. For the western blot protein samples were loaded as follows: lane 1: MSC-2014-7; lane 2: A673; lane 3: RD-ES and lane 4: SK-N-MC. Proteins were separated by SDS-PAGE and blotted onto a PVDF membrane. Membranes were incubated with the primary antibodies GLI2 rabbit pAb or tubulin rabbit mAb overnight. A horseradish peroxidase-conjugated anti-rabbit pAb was used as secondary antibody. ECL substrate was added to the membrane and chemiluminescence signals were recorded on a film. ImageJ was utilised for western blot quantification. Data presented in this figure was also published (Boehme et al., 2016 (1)).*

3.2 Effect of GANT61, ATO, etoposide and doxorubicin on the viability of Ewing sarcoma cell lines

Inhibition of the Hh pathway in different types of cancer has proven efficiency in several studies (Agyeman et al., 2014; Hu et al., 2009; Rudin, 2012). As described in chapter 1.3.3, EWS-FLI1 interacts with the Hh pathway downstream of SMO and PTCH1. Therefore, the effect of the GLI1 inhibitors GANT61 and ATO as well as the cytostatics etoposide and doxorubicin, already used in EWS therapy (chapter 1.5), on the viability of EWS cells in comparison to healthy MSC was analysed by MTS assay.

3.2.1 Effect of single substance treatment on the viability of A673, RD-ES, SK-N-MC and MSC

GANT61

Figure 14 shows that the EWS cell line A673 has the highest sensitivity to GANT61. A significant drop in viability was already achieved using 15 µM GANT61 (35 ± 7 %) whereas 50 µM reduced viability to 14 ± 2 % of the mock treated control. Both RD-ES and SK-N-MC cells showed no significant decrease in viability using concentrations up to 25 µM GANT61 (RD-ES: 106 ± 4 % and SK-N-MC: 100 ± 5 %). 50 µM GANT61 reduced the viability to 49 ± 12 % in RD-ES 73 ± 10 % in SK-N-MC. Unfortunately, the healthy control cells MSC-2014-7 showed a similar sensitivity as A673 cells. The viability of MSC started to decrease at a dose of 10 µM GANT61 (79 ± 4 %) and reached a plateau at 25 µM (7 ± 0 %), being the lowest viability attained in all cells examined.

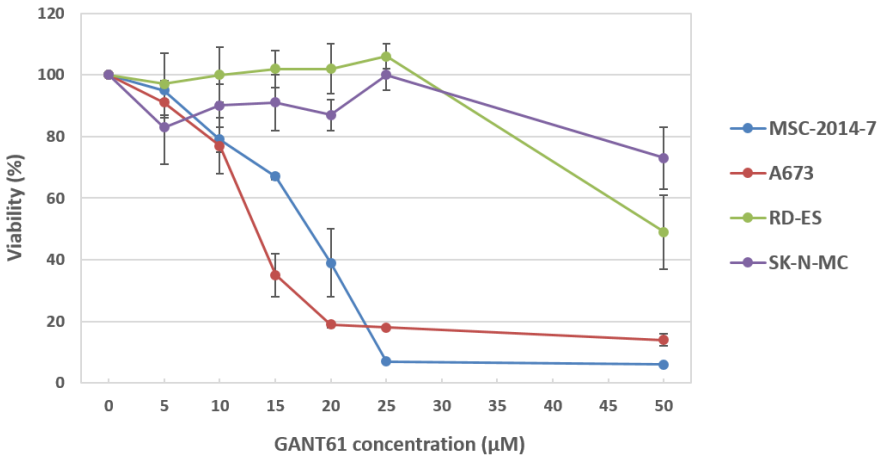

Figure 14: Effect of GANT61 on the viability of the EWS cell lines A673, RD-ES and SK-N-MC in comparison to MSC. *0.5 x 10^4 cells/well RD-ES, SK-N-MC and MSC-2014-7 or 1 x 10^4 cells/well A673 were sown into 96-well plates. After 24 h cells were treated with different concentrations of GANT61 or the inhibitors solvent in case of the negative controls for 96 h. For analysis cells were incubated with MTS reagent and absorbance was measured at 490 nm. Negative controls were set to 100 % viability and the relative viability was calculated. Mean values were plotted from four independent experiments. Standard deviations are represented by black error bars.*

Arsenic trioxide

Figure 15 shows that A673 cells also exhibited the highest ATO sensitivity of all EWS cell lines, with 0.5 µM ATO reducing viability to 43 ± 5 % and reaching even lower values at 2 µM ATO (24 ± 3 %) and 5 µM ATO (23 ± 2 %). RD-ES and SK-N-MC were less sensitive, retaining 31 ± 4 % (RD-ES), respectively 47 ± 4 % (SK-N-MC) viable cells at 5 µM ATO. Moreover, viability of RD-ES did not drop before 2 µM (53 ± 7 %) and 93 ± 10 % of SK-N-MC cells were viable at 3 µM ATO. Interestingly, the MSC showed an increase of viability upon treatment with ATO concentrations up to 5 µM (130 ± 14 %), whereas 10 µM reduced viability to 82 ± 6 %.

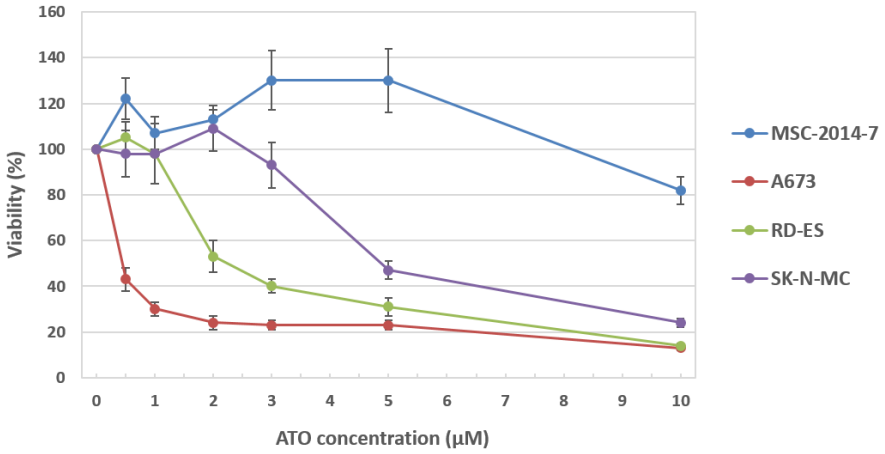

Figure 15: Effect of ATO on the viability of the EWS cell lines A673, RD-ES and SK-N-MC in comparison to MSC*. 0.5 x 10^4 cells/well RD-ES, SK-N-MC and MSC-2014-7 or 1 x 10^4 cells/well A673 were sown into 96-well plates. After 24 h cells were treated with different concentrations of ATO or the inhibitors solvent in case of the negative controls for 96 h. For analysis cells were incubated with MTS reagent and absorbance was measured at 490 nm. Negative controls were set to 100 % viability and the relative viability was calculated. Mean values were plotted from four independent experiments. Standard deviations are represented by black error bars.*

Etoposide

Figure 16 shows that all three EWS cell-lines have a similar sensitivity to etoposide with a significantly decreased viability after addition of 1 µM etoposide (A673: 63 ± 5 %; RD-ES: 58 ± 4 % and SK-N-MC: 67 ± 13 %). Moreover, 5 µM etoposide reduced the viability to 34 ± 3 % in A673 cells, 39 ± 1 % in SK-N-MC cells or even 18 ± 3 % in RD-ES cells. The control cells MSC-2014-7 seemed to be completely resistant to all etoposide concentrations applied with viability not falling below 96 ± 9 % at 10 µM etoposide, which reduced the viability of A673 to 19 ± 1 %, RD-ES to 13 ± 2 % and SK-N-MC to 30 ± 2 %, respectively.

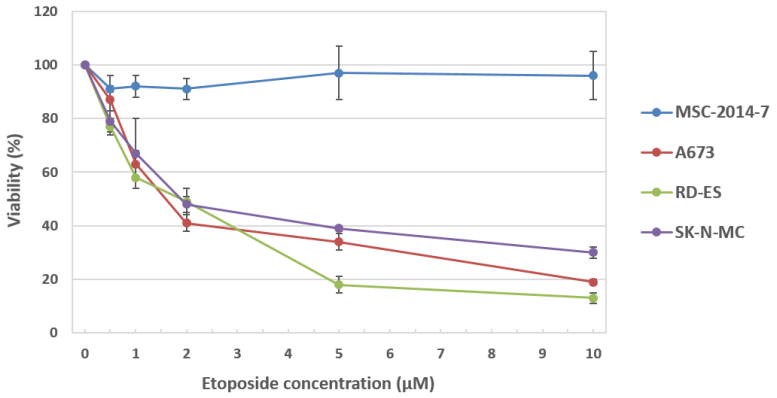

Figure 16: Effect of etoposide on the viability of the EWS cell lines A673, RD-ES and SK-N-MC in comparison to MSC*. 0.5 x 10^4 cells/well RD-ES, SK-N-MC and MSC-2014-7 or 1 x 10^4 cells/well A673 were sown into 96-well plates. After 24 h cells were treated with different concentrations of etoposide or the inhibitors solvent in case of the negative controls for 96 h. For analysis cells were incubated with MTS reagent and absorbance was measured at 490 nm. Negative controls were set to 100 % viability and the relative viability was calculated. Mean values were plotted from four independent experiments. Standard deviations are represented by black error bars.*

Doxorubicin

Figure 17 shows that the lowest viability obtained by incubation with 100 nM doxorubicin was 41 ± 1 % in A673 cells, 49 ± 2 % in RD-ES cells and 43 ± 4 % in SK-N-MC cells, while viability of MSC did not drop under 61 ± 4 % using the same concentration. Furthermore, applying 50 nM doxorubicin 81 ± 3 % of MSC were viable compared to 39 ± 3 % (A673), 61 ± 3 % (RD-ES) and 57 ± 3 % (SK-N-MC) in the EWS cell lines.

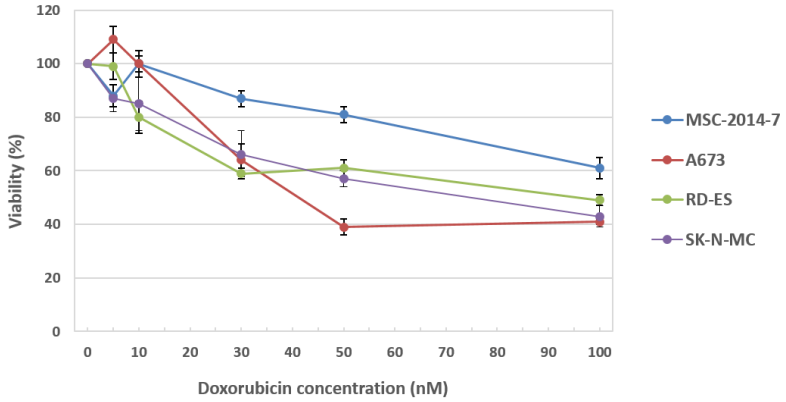

Figure 17: Effect of doxorubicin on the viability of the EWS cell lines A673, RD-ES and SK-N-MC in comparison to MSC*. 0.5 x 10^4 cells/well RD-ES, SK-N-MC and MSC-2014-7 or 1 x 10^4 cells/well A673 were sown into 96-well plates. After 24 h cells were treated with different concentrations of doxorubicin or the inhibitors solvent in case of the negative controls for 96 h. For analysis cells were incubated with MTS reagent and absorbance was measured at 490 nm. Negative controls were set to 100 % viability and the relative viability was calculated. Mean values were plotted from four independent experiments. Standard deviations are represented by black error bars.*

IC_{50} values

For the administration in patients a significantly more distinct effect of the substances on cancer cells compared to normal, healthy cells is required. As shown in **Table 13** upon treatment with ATO, etoposide and doxorubicin the EWS cell lines A673, RD-ES and SK-N-MC were significantly more sensitive compared to MSC, indicating high selectivity of these drugs. Only GANT61 reduced the viability of the control cells MSC-2014-7 sufficiently to determine an IC_{50} value. Moreover, MSC exhibited a lower GANT61 IC_{50} value than the EWS cell lines RD-ES and SK-N-MC.

Table 13: IC_{50} values of the EWS cell lines A673, RD-ES and SK-N-MC compared to the control cells MSC-2014-7 after treatment with ATO, GANT61, etoposide or doxorubicin. *MTS-Assays were performed four days after treatment with ATO, GANT61, etoposide or doxorubicin in the three EWS cell lines and MSC-2014-7 in quadruplicate. Mock treated control was set to 100 % viability. IC_{50} values were determined by non-linear regression of the MTS results using GraphPad Prism. Data presented in this table was also published (Boehme et al., 2016 (1)).*

Cell line	IC_{50} – ATO	IC_{50} – GANT61	IC_{50} – etoposide	IC_{50} – doxorubicin
A673	0.23 µM	12.01 µM	0.88 µM	27.18 nM
RD-ES	1.91 µM	35.37 µM	1.06 µM	115 nM
SK-N-MC	4.42 µM	59.56 µM	1.11 µM	75.15 nM
MSC-2014-7	**10 µM ATO 82.4 % viable**	**16.05 µM**	**35 µM etoposide 85.6 % viable**	**150 nM doxorubicin 58.6 % viable**

Summary

Viability of the EWS cell lines could be reduced by all four inhibitors applied. MSC seemed to be largely resistant to the ATO and etoposide doses applied. Although treatment with 150 nM doxorubicin reduced the viability of MSC-2014-7 down to 60 %, all EWS cell lines appeared to be more sensitive. Only GANT61 was not selective between MSC and the EWS cell lines tested. Therefore, it was excluded from combination experiments.

3.2.3 Effect of inhibitor combinations on the viability A673, RD-ES, SK-N-MC and MSC

Etoposide and Arsenic trioxide

Figure 18 demonstrates the effect of combined etoposide and ATO treatment of the EWS cell lines in comparison to MSC. In A673 cells (**Figure 18A**) a clear dependency of the viability on the etoposide dose is visible, whereas an increase of the ATO dose was less critical for the combined effect. Using 0.5 µM etoposide viability was reduced to 87 ± 9 %. Increasing ATO concentrations from 0.1 µM to 0.3 µM reduced the viability from 104 ± 13 % to 51 ± 5 %. However, applying combinations of ATO and etoposide viability stagnated between 67 % and 70 %, which was, in case of treatment with 0.2 µM and 0.3 µM ATO, still higher compared to single treatment with ATO. This effect could be repeated using 0.75 µM etoposide (viability after single treatment: 72 ± 7 %) combined with 0.1 µM to 0.3 µM ATO, where combined treatment led to a viability of 54 ± 7 % to 52 ± 5 %. Only using an etoposide concentration of 1 µM (viability after single treatment: 63 ± 5 %), the viability of cells treated with the drug combinations was clearly reduced below that of ATO treated cells to about 40 % for the combination with 0.1 µM and 0.2 µM ATO, respectively. This combined effect was intensified applying 0.3 µM ATO and 1 µM etoposide (viability of 30 ± 2 %).

In RD-ES cells viability after combined treatment was more dependent on the increase of the ATO dose (**Figure 18B**). Treatment with 0.5 µM etoposide (viability after single treatment: 77 ± 3 %) and 1 µM ATO (viability after single treatment: 83 ± 15 %) already resulted in a very significant drop of viability upon combination (47 ± 8 %). Viability was reduced further to 32 ± 4 % in cells treated with 0.5 µM etoposide and 1.5 µM ATO (viability after single treatment with 1.5 µM ATO: 72 ± 5 %) or even to 25 ± 2 % after application of 0.5 µM etoposide and 2 µM ATO (viability after single treatment with 2 µM ATO: 53 ± 7 %). Combinations using increasing concentrations of 0.75 µM etoposide (viability after single treatment: 69 ± 3 %) or 1 µM etoposide (viability after single treatment: 58 ± 4 %) led to no further reduction of the viability of RD-ES cells compared to using 0.5 µM etoposide.

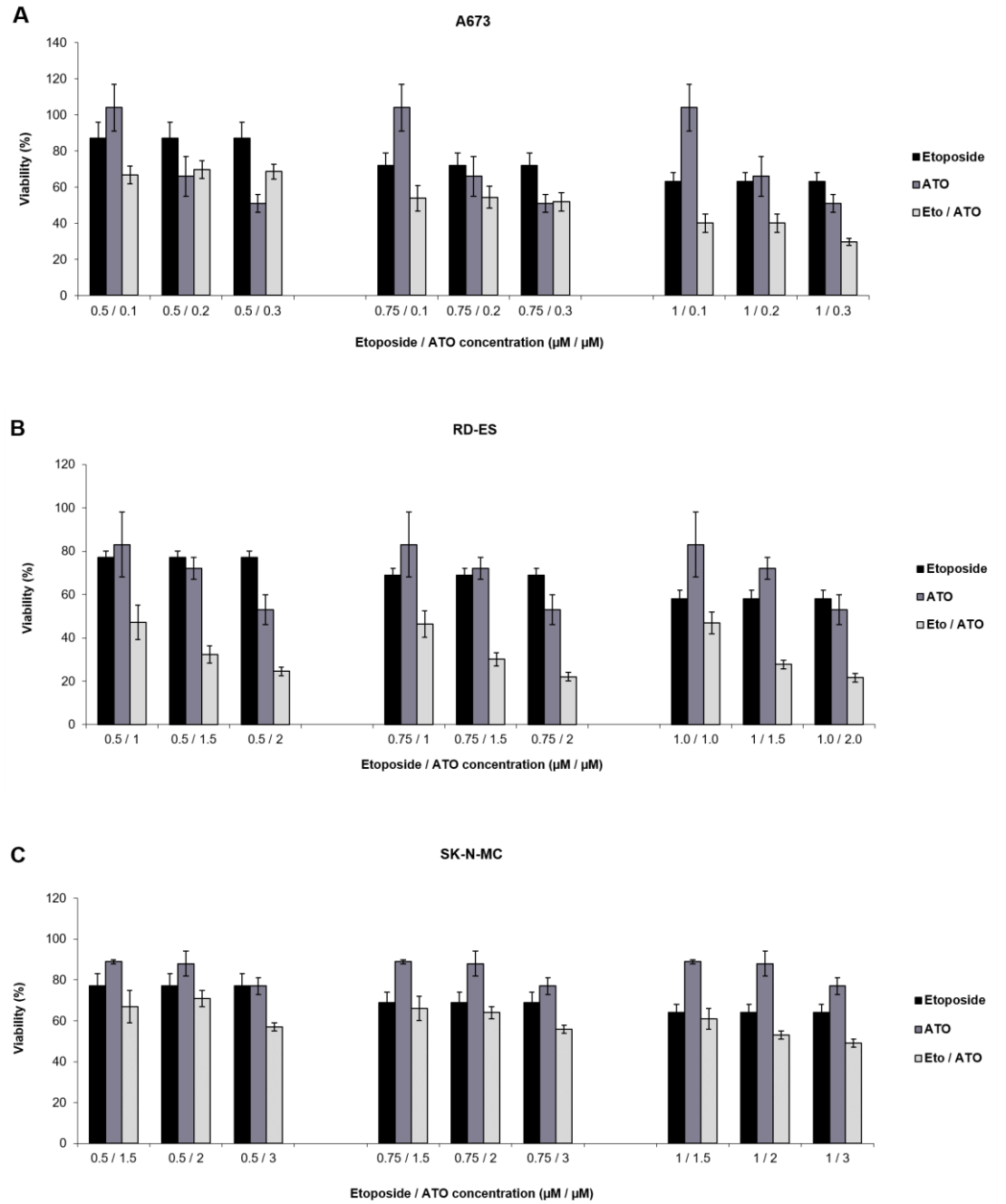

Figure 18: Effect of combined etoposide and ATO treatment on the viability of the EWS cell lines A673, RD-ES and SK-N-MC. A: *1 x 10^4 cells/well A673,* ***B:*** *0.5 x 10^4 cells/well RD-ES and* ***C:*** *0.5 x 10^4 cells/well SK-N-MC were sown into 96-well plates. After 24 h cells were treated with single concentrations and combinations of etoposide (Eto) and ATO as well as the inhibitors solvents in case of the negative controls for 96 h. For analysis cells were incubated with MTS-reagent and absorbance was measured at 490 nm. Negative controls were set to 100 % viability and the relative viability was calculated. Mean values were plotted from four independent experiments. Standard deviations are represented by black error bars. Data presented in this figure was also published (Boehme et al., 2016 (1)).*

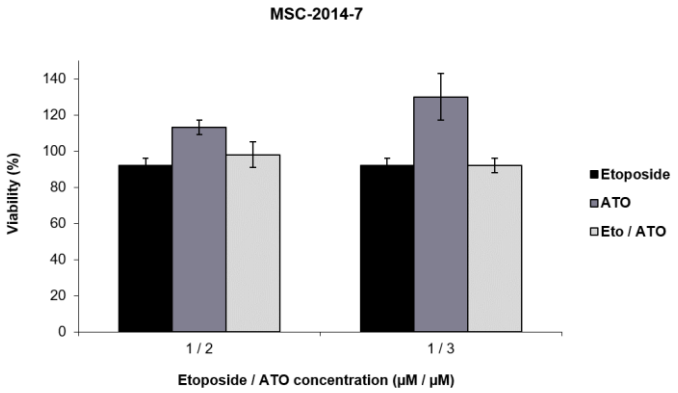

Figure 19: Effect of combined etoposide and ATO treatment on the viability of MSC-2014-7 control cells. *0.5 x 10^4 cells/well MSC-2014-7 were sown into 96-well plates. After 24 h cells were treated with single concentrations and two combinations of etoposide (Eto) and ATO as well as the inhibitors solvents in case of the negative controls for 96 h. For analysis cells were incubated with MTS-reagent and absorbance was measured at 490 nm. Negative controls were set to 100 % viability and the relative viability was calculated. Mean values were plotted from four independent experiments. Standard deviations are represented by black error bars. Data presented in this figure was also published (Boehme et al., 2016 (1)).*

SK-N-MC cells (**Figure 18C**) were least sensitive to treatment using etoposide or ATO. Upon combination of the highest drug doses applied, 1 µM etoposide and 3 µM ATO, 49 ± 2 % of cells were still viable, whereas single doses of etoposide or ATO reduced viability to 64 ± 4 % or 77 ± 4 %, respectively. All other combined treatments were less efficient: 57 ± 2 % (0.5 µM etoposide / 3 µM ATO) and 56 ± 2 % (0.75 µM etoposide / 3 µM ATO) with decreased etoposide or ATO doses having even reduced impact on viability upon single treatment.

Figure 19 shows the reaction of MSC-2014-7 cells to combined treatment using the highest doses of 1 µM etoposide and 2 or 3 µM ATO applied to the EWS cell lines A673, RD-ES and SK-N-MC. Viability only dropped to 92 ± 4 % upon application of 1 µM etoposide and 92 ± 4 % upon treatment with the combination of 1 µM etoposide with 3 µM ATO. Interestingly, single application of 3 µM ATO increased viability of MSC to 130 ± 13 %.

Doxorubicin and Arsenic trioxide

Figure 20A shows a strong dependence of A673 cell viability on the ATO doses applied. Combined treatment with 5 nM doxorubicin (viability after single treatment: 97 ± 9 %) and 0.2 µM ATO (viability after single treatment: 72 ± 4 %) already resulted in a very significant drop of viability to 47 ± 8 %. Viability was reduced further to 28 ± 3 % in cells treated with 5 nM doxorubicin and 0.3 µM of ATO (viability after single treatment: 51 ± 2 %). Increasing the concentrations of doxorubicin to 10 nM (viability after single treatment: 96 ± 9 %) and 30 nM (viability after single treatment: 85 ± 9 %) led to no further combined reduction of the viability of A673 cells (27 ± 1 % for 10 nM doxorubicin / 0.3 µM ATO; 27 ± 1 % for 30 nM doxorubicin / 0.3 µM ATO). Using a low dose of 0.1 µM ATO (viability after single treatment: 99 ± 8 %) in combination with 5 nM, 10 nM or 30 nM doxorubicin did not result in a significant loss of viable cells in comparison to doxorubicin single treatment except for the combination of 10 nM doxorubicin with 0.1 µM ATO where viability decreased to 73 ± 4 %.

In RD-ES cells (**Figure 20B**) both increasing ATO and doxorubicin doses affected the combined outcome. Treatment of cells with 5 nM doxorubicin and increasing ATO concentrations only resulted in a significant intensification of viability loss when the highest ATO concentration of 2 µM had been used (5 nM doxorubicin: viability 99 ± 5 %; 2 µM ATO: viability 53 ± 7 %; combination: viability 30 ± 2 %). When doubling the dose of doxorubicin to 10 nM (viability after single treatment: 80 ± 6 %) a significant effect was achieved in combination with 1.5 µM ATO (viability after single treatment: 72 ± 5 %; combined: viability 41 ± 6 %), whereas a combination with 2 µM ATO led to an even lower viability (10 nM doxorubicin / 2 µM ATO: 27 ± 1 %) of RD-ES cells. The smallest number of viable cells was obtained with 30 nM doxorubicin (viability after single treatment: 59 ± 2 %) combined with 1.5 µM ATO (26 ± 2 %) or combined with 2 µM ATO (21 ± 1 %).

Quite contrary to the cell lines A673 or RD-ES, combination treatment of SK-N-MC cells (**Figure 20C**) was only favourable using 30 nM doxorubicin (viability after single treatment: 56 ± 1 %) in combination with 1.5 µM ATO (viability after single treatment: 95 ± 5 %) reducing viability to 45 ± 3 %, which was even slightly improved by increasing ATO doses to 2 µM (combination: viability 43 ± 3 %) or 3 µM (combination: viability 36 ± 3 %). Whereas upon treatment with 3 µM ATO alone 78 ± 13 % of cells were still viable.

The highest concentrations of 30 nM doxorubicin and 2 µM or 3 µM ATO applied in EWS were not sufficient to reduce viability in MSC-2014-7 cells below 87 ± 3 % obtained with 30 nM doxorubicin single treatment as shown in **Figure 21**.

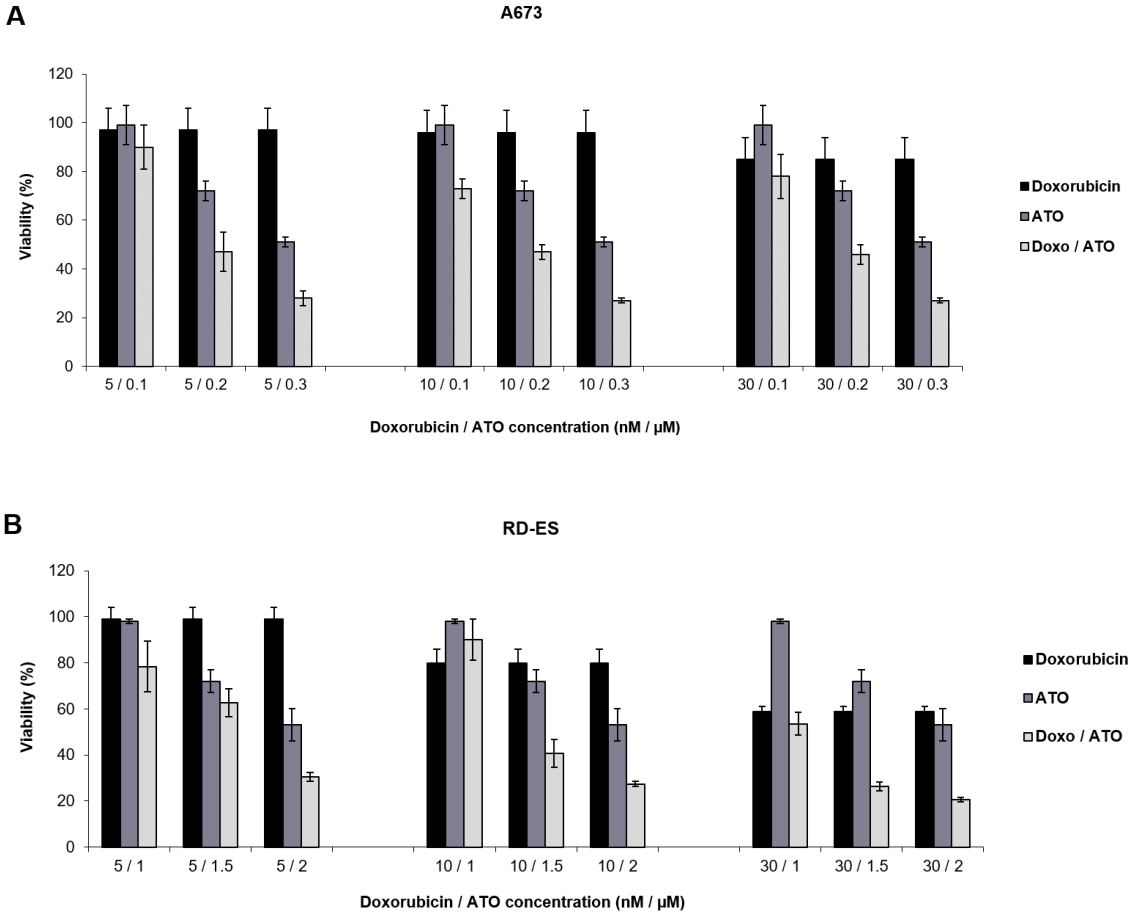

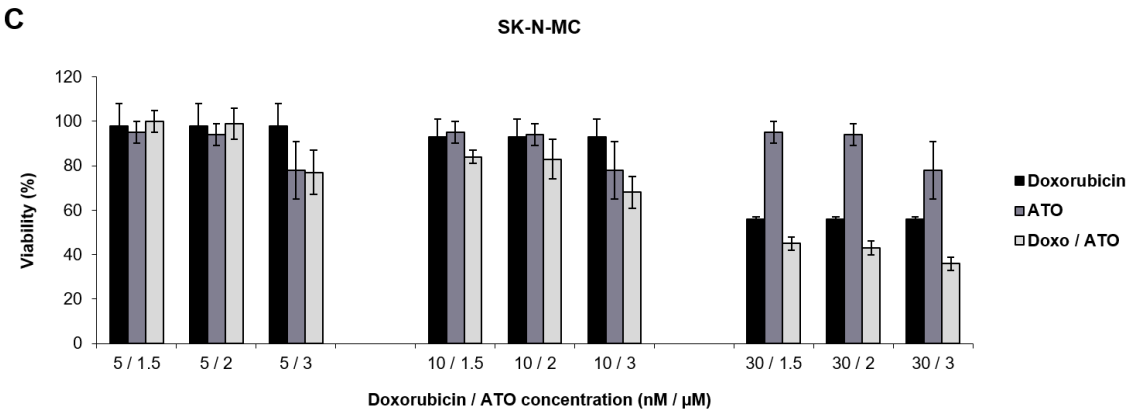

Figure 20: Effect of combined doxorubicin and ATO treatment on the viability of the EWS cell lines A673, RD-ES and SK-N-MC. ***A:*** *1 x 10^4 cells/well A673,* ***B:*** *0.5 x 10^4 cells/well RD-ES and* ***C:*** *0.5 x 10^4 cells/well SK-N-MC were sown into 96-well plates. After 24 h cells were treated with single concentrations and combinations of doxorubicin (Doxo) and ATO as well as the inhibitors solvents in case of the negative controls for 96 h. For analysis cells were incubated with MTS-reagent and absorbance was measured at 490 nm. Negative controls were set to 100 % viability and the relative viability was calculated. Mean values were plotted from four independent experiments. Standard deviations are represented by black error bars. Data presented in this figure was also published (Boehme et al., 2016 (1)).*

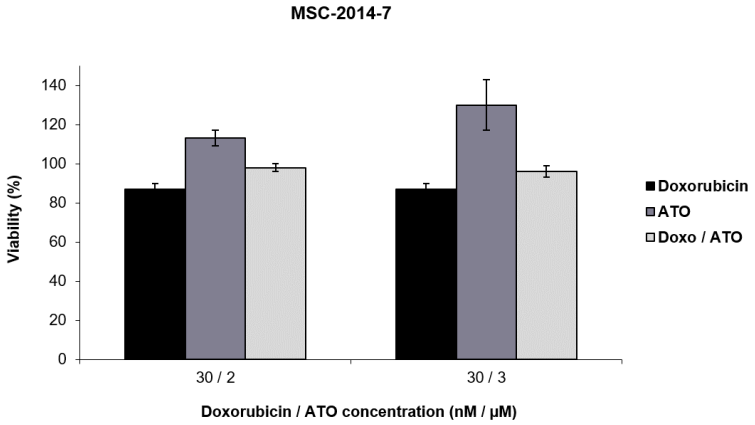

Figure 21: Effect of combined doxorubicin and ATO treatment on the viability of MSC-2014-7 control cells. *0.5 x 10^4 cells/well MSC-2014-7 were sown into 96-well plates. After 24 h cells were treated with single concentrations and two combinations of doxorubicin (Doxo) and ATO as well as the inhibitors solvents in case of the negative controls for 96 h. For analysis cells were incubated with MTS-reagent and absorbance was measured at 490 nm. Negative controls were set to 100 % viability and the relative viability was calculated. Mean values were plotted from four independent experiments. Standard deviations are represented by black error bars. Data presented in this figure was also published (Boehme et al., 2016 (1)).*

Etoposide, doxorubicin and Arsenic trioxide

For further evaluation of the effect of cytostatics and ATO on the viability of EWS cell lines, cells were treated with two triple combinations of etoposide, doxorubicin and ATO. Concentrations for triple treatment were selected on the basis of the previous viability assay results.

In A673 cells (**Figure 22A**) a combination of 1 µM etoposide (viability after single treatment: 63 ± 5 %), 5 nM doxorubicin (viability after single treatment: 109 ± 5 %) and 0.1 µM ATO (viability after single treatment: 99 ± 5 %) was sufficient to drastically reduce viability to 33 ± 1 %. This was also an improvement compared to the respective double applications (0.1 µM ATO / 1 µM etoposide: 40 ± 5 % and 0.1 µM ATO / 5 nM doxorubicin: 90 ± 9 %). Additional loss of viability was not obtained using 0.3 µM ATO together with 5 nM doxorubicin and 1 µM etoposide (37 ± 1 %). Indeed, viability was higher compared to both double treatments (0.3 µM ATO / 5 nM doxorubicin: 28 ± 3 % and 0.3 µM ATO / 1 µM etoposide: 30 ± 2 %).

As already described, RD-ES cells (**Figure 22B**) presented a less pronounced drop in viable cells when applying 0.5 µM etoposide (77 ± 3 %), 5 nM doxorubicin (99 ± 5 %) or 1 µM ATO (83 ± 15 %) as single dose. The triple combination led to 51 ± 2 % viable cells, which was equal compared to the double combination of 0.5 µM etoposide and 1 µM ATO (47 ± 8 %). However, with the dose of ATO doubled (2 µM ATO: 53 ± 7 %) viability of the triple approach reached a level as low as 20 ± 1 %, which was superior compared to both double combinations (0.5 µM etoposide / 2 µM ATO: 25 ± 2 % and 5 nM doxorubicin / 2 µM ATO: 30 ± 2 %).

SK-N-MC cells (**Figure 22C**) were requiring higher doses of doxorubicin and ATO. A viability of 39 ± 2 % could be obtained with combined treatment of cells with 0.5 µM etoposide (viability after single treatment: 77 ± 6 %), 30 nM doxorubicin (viability after single treatment: 66 ± 9 %) and 3 µM ATO (viability after single treatment: 77 ± 4 %). However, using the double combination of 30 nM doxorubicin and 3 µM ATO (36 ± 3 %) was more efficient. In SK-N-MC the applied etoposide dose was increased to 1 µM (viability after single treatment: 64 ± 4 %), which showed no further impact on viability after triple application (1 µM etoposide / 30 nM doxorubicin / 3 µM ATO: 37 ± 1 %). Indeed, both double treatments obtained similar results (3 µM ATO / 1 µM etoposide: 49 ± 2 % and 3 µM ATO / 30 nM doxorubicin: 36 ± 3 %).

For control (**Figure 23**) MSC-2014-7 cells were treated with the highest drug doses applied in combination (1 µM etoposide, 30 nM doxorubicin and 3 µM ATO) in the three EWS cell lines. Viability was not reduced below 96 ± 5 % (single application of 30 nM doxorubicin), which shows that even a triple combination had barely any effect on the viability of the control cells.

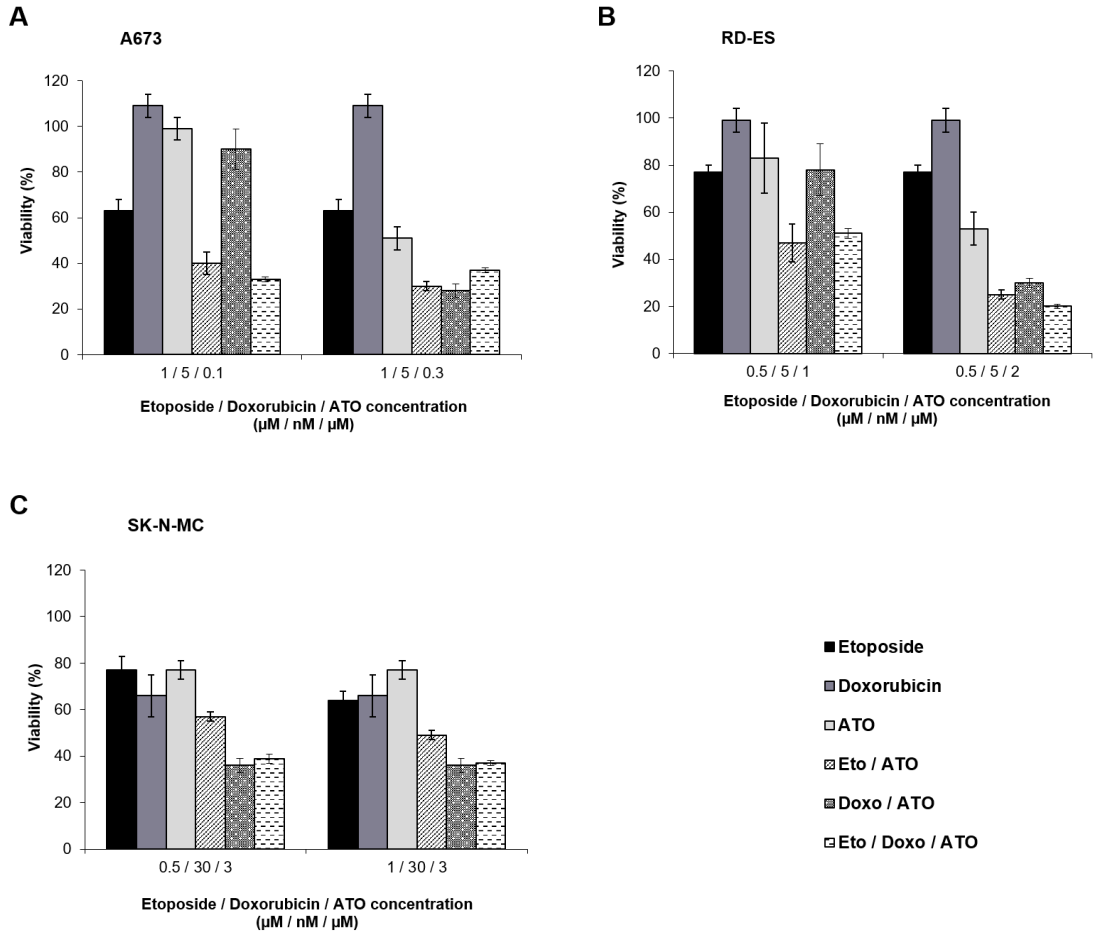

Figure 22: Effect of combined etoposide, doxorubicin and ATO treatment on the viability of the EWS cell lines A673, RD-ES and SK-N-MC. A: *1 x 10^4 cells/well A673,* ***B:*** *0.5 x 10^4 cells/well RD-ES and* ***C:*** *0.5 x 10^4 cells/well SK-N-MC were sown into 96-well plates. After 24 h cells were treated with two triple combinations, the single concentrations and the double combinations of etoposide (Eto) and ATO as well as doxorubicin (Doxo) and ATO or the inhibitors solvents in case of the negative controls for 96 h. For analysis cells were incubated with MTS-reagent and absorbance was measured at 490 nm. Negative controls were set to 100 % viability and relative viability was calculated. Mean values were plotted from four independent experiments. Standard deviations are represented by black error bars (Results for single and double treatments correspond to results depicted in figure 19 and 21). Data presented in this figure was also published (Boehme et al., 2016 (1)).*

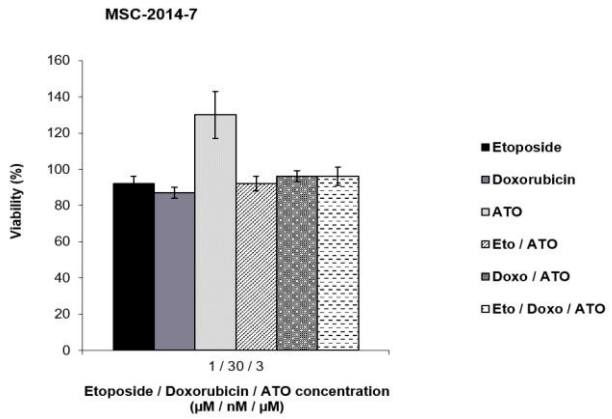

Figure 23: Effect of combined etoposide, doxorubicin and ATO treatment on the viability of MSC-2014-7 control cells. *0.5 x 10^4 cells/well MSC-2014-7 were sown into 96-well plates. After 24 h cells were treated with a triple combination, the single concentrations and the double combinations of etoposide (Eto) and ATO as well as doxorubicin (Doxo) and ATO or the inhibitors solvents in case of the negative controls for 96 h. For analysis cells were incubated with MTS-reagent and absorbance was then measured at 490 nm. Negative controls were set to 100 % viability and the relative viability was calculated. Mean values were plotted from four independent experiments. Standard deviations are represented by black error bars (Results for single and double treatments correspond to results depicted in figure 20 and 22). Data presented in this figure was also published (Boehme et al., 2016 (1)).*

Summary

Combination of etoposide and ATO, doxorubicin and ATO or all three drugs showed additive effects in all three EWS cell lines tested, whereas MSC were barely compromised. However, sensitivity to the individual drugs and combinatorial effects were very different between the cell lines. Moreover, the triple combination was not clearly superior compared to double combinations.

3.3 Impact of ATO and cytostatics on the colony formation of Ewing sarcoma cell lines

In the previous MTS assays a first analysis of the consequences of GANT61, ATO, etoposide and doxorubicin treatment of EWS cell lines was made. Apart from the influence of these inhibitors on the viability of cells, the ability to proliferate and to form colonies from single cells was analysed. As single cells have a lack of cell-cell contacts and soluble factors generated by their neighbour cells this assay simulates the process of metastasis in a very simple manner. The ability of single tumour cells to metastasise is fundamentally dependant on their ability to migrate but also their ability to proliferate again in a new environment. The reduction of colonies was examined in all three EWS cell lines treated with three different concentrations of GANT61, ATO, etoposide and doxorubicin and with a combination of etoposide and ATO as well as a combination of doxorubicin and ATO.

3.3.1 Effect of GANT61 and ATO on the colony formation of the Ewing sarcoma cell lines A673, RD-ES and SK-N-MC

GANT61

Both RD-ES (**Figure 24B**) and SK-N-MC cells (**Figure 24C**) were largely resistant to treatment with GANT61. A significant reduction of colony numbers could only be obtained with a dose of 20 µM GANT61. In A673 cells (**Figure 24A**) a concentration of 10 µM GANT61 was already sufficient to decrease the amount of colonies and with 15 µM only very few, small colonies remained, whereas 20 µM of GANT61 completely suppressed the ability of A673 cells to form colonies.

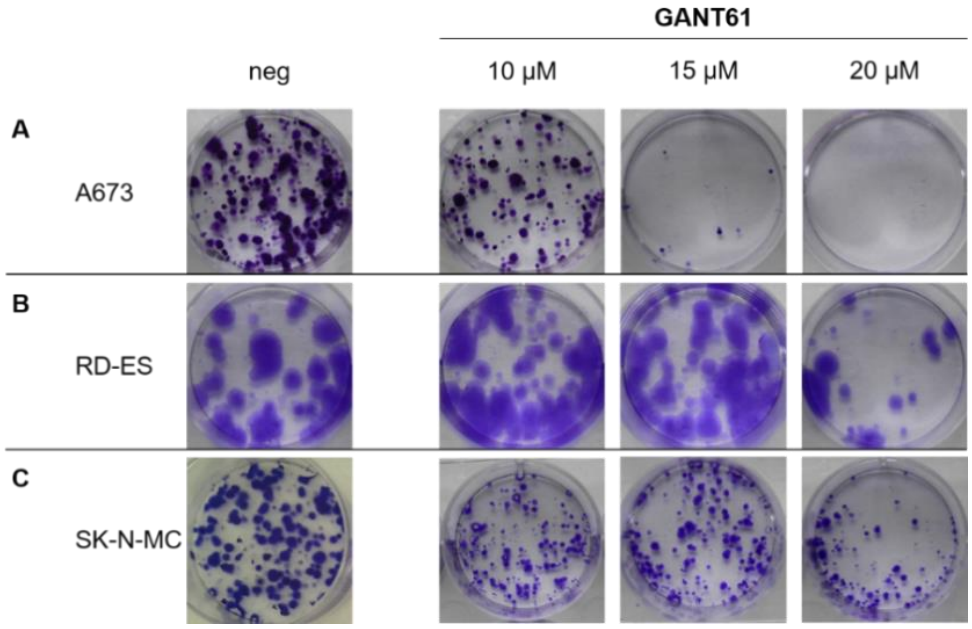

Figure 24: Clonogenic assay of the EWS cell lines A673, RD-ES and SK-N-MC treated with GANT61. ***A:*** *1 x 10^3 cells/well A673,* ***B:*** *0.5 x 10^3 cells/well RD-ES or* ***C:*** *0.5 x 10^3 cells/well SK-N-MC were sown into 6-well plates and treated with solvent only (negative control) or 10 µM, 15 µM or 20 µM GANT61 for 72 h. Subsequently, every 72 h medium was replaced with fresh medium without inhibitor and cells were incubated until negative controls were grown. Colonies were then fixed with methanol and stained with crystal violet. For documentation results were photographed.*

Arsenic trioxide

Figure 25 demonstrates that 0.5 µM ATO did not have a significant impact on the colony formation of any of the cell lines examined. 1 µM ATO reduced both colony number and size in RD-ES (**Figure 25B**) and A673 cells (**Figure 25A**). 3 µM ATO were sufficient to completely abolish colony formation of RD-ES cells and to largely prevent colony formation of A673 cells. Only SK-N-MC cells (**Figure 25C**) still formed a reduced number of colonies after treatment using 3 µM ATO.

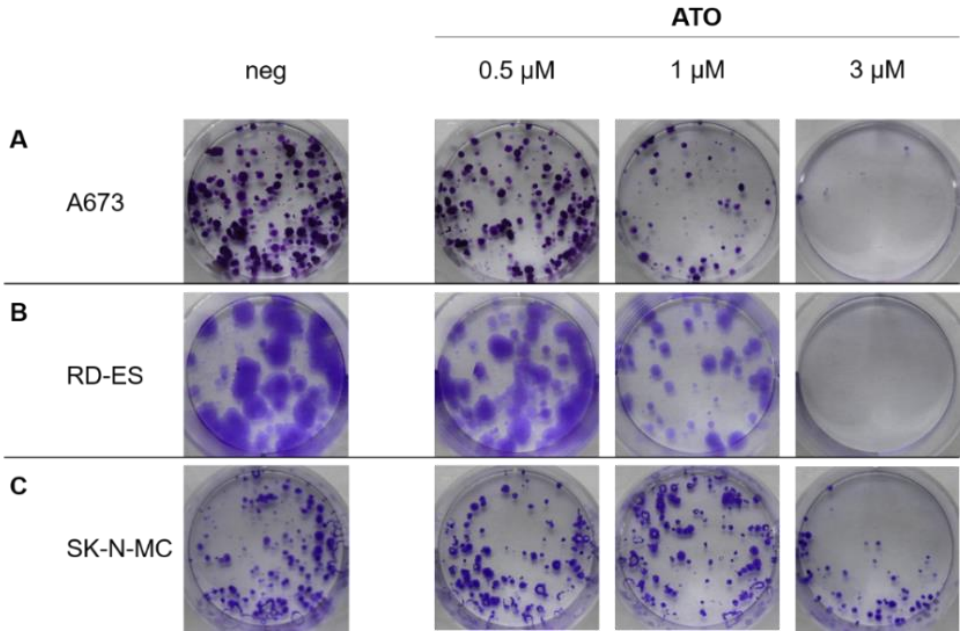

Figure 25: Clonogenic assay of the EWS cell lines A673, RD-ES and SK-N-MC treated with ATO. ***A:*** *1 x 10^3 cells/well A673,* ***B:*** *0.5 x 10^3 cells/well RD-ES or* ***C:*** *0.5 x 10^3 cells/well SK-N-MC were sown into 6-well plates and treated with solvent only (negative control) or 0.5 µM, 1 µM or 3 µM ATO for 72 h. Subsequently, every 72 h medium was replaced with fresh medium without inhibitor and cells were incubated until negative controls were grown. Colonies were then fixed with methanol and stained with crystal violet. For documentation results were photographed. Data presented in this figure was also published (Boehme et al., 2016 (1)).*

3.3.2 Effect of etoposide and doxorubicin on the colony formation of the Ewing sarcoma cell lines A673, RD-ES and SK-N-MC

Etoposide

In comparison to the MTS assay results (chapter 3.2.1) lower concentrations of etoposide were needed for a significant reduction of colony growth. The number of RD-ES and SK-N-MC colonies (**Figure 26B and C**) decreased in a dose dependent manner starting at 0.2 µM etoposide with only few colonies persisting when treated with 0.3 µM etoposide. RD-ES cells formed no colonies under treatment with 0.5 µM etoposide, whereas one small SK-N-MC colony grew under this dose. In contrast, 0.2 µM etoposide had only a minor effect on A673 cells (**Figure 26A**). Though colony growth decreased dose dependently applying a dose of 0.3 µM etoposide and 0.5 µM etoposide, some colonies were still persisting at the highest dose applied.

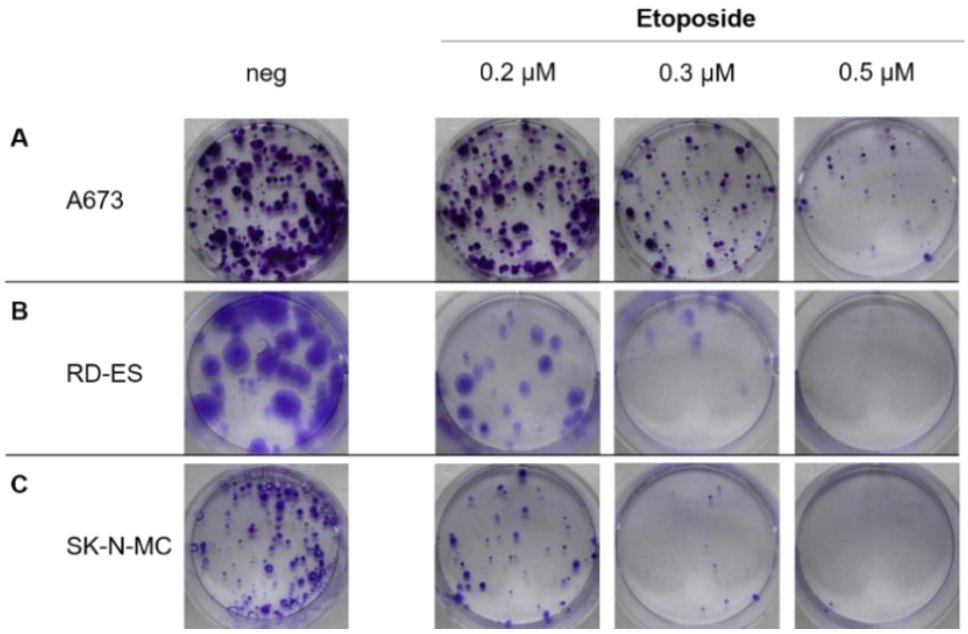

Figure 26: Clonogenic assay of the EWS cell lines A673, RD-ES and SK-N-MC treated with etoposide. ***A:*** *1 x 10^3 cells/well A673,* ***B:*** *0.5 x 10^3 cells/well RD-ES or* ***C:*** *0.5 x 10^3 cells/well SK-N-MC were sown into 6-well plates and treated with solvent only (negative control) or 0.2 µM, 0.3 µM or 0.5 µM etoposide for 72 h. Subsequently, every 72 h medium was replaced with fresh medium without inhibitor and cells were incubated until negative controls were grown. Colonies were then fixed with methanol and stained with crystal violet. For documentation results were photographed. Data presented in this figure was also published (Boehme et al., 2016 (1)).*

Doxorubicin

Figure 27 indicates a similar sensitivity of all three EWS cell lines to treatment with doxorubicin. As for etoposide, cells showed a significantly higher doxorubicin sensitivity in the colony formation assay compared to the MTS assay. Even 10 nM doxorubicin were sufficient for a very significant reduction of colony growth. For A673 and RD-ES cells 15 nM doxorubicin were required for a complete suppression of their ability to form colonies (**Figure 27A and B**). Only SK-N-MC cells still formed some small colonies under treatment with 15 nM doxorubicin (**Figure 27C**).

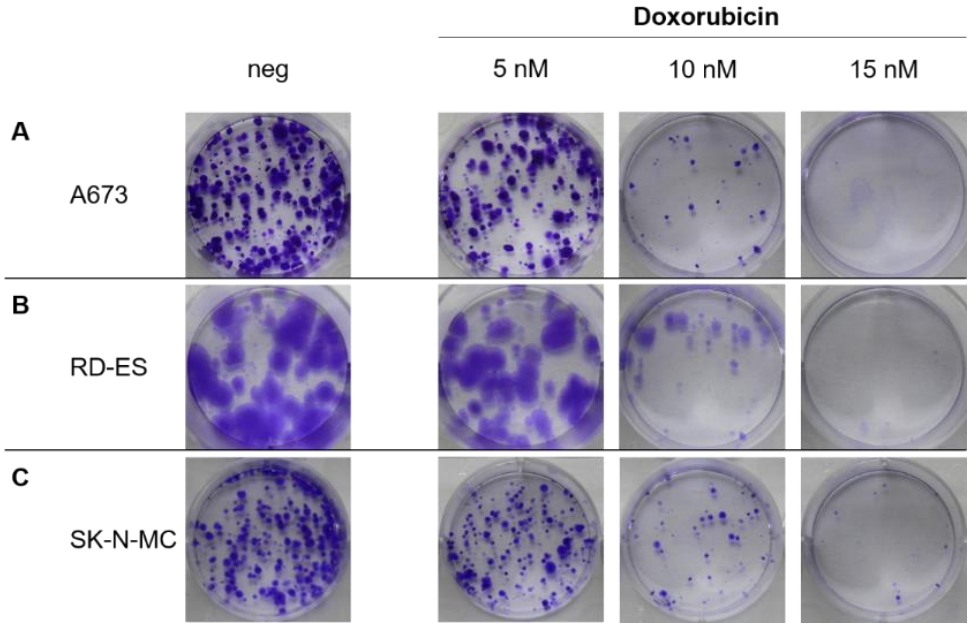

Figure 27: Clonogenic assay of the EWS cell lines A673, RD-ES and SK-N-MC treated with doxorubicin. ***A:*** *1 x 10^3 cells/well A673,* ***B:*** *0.5 x 10^3 cells/well RD-ES or* ***C:*** *0.5 x 10^3 cells/well SK-N-MC were sown into 6-well plates and treated with solvent only (negative control) or 5 nM, 10 nM or 15 nM doxorubicin for 72 h. Subsequently, every 72 h medium was replaced with fresh medium without inhibitor and cells were incubated until negative controls were grown. Colonies were then fixed with methanol and stained with crystal violet. For documentation results were photographed. Data presented in this figure was also published (Boehme et al., 2016 (1)).*

3.3.3 Effect of drug combinations on the colony formation of the Ewing sarcoma cell lines A673, RD-ES and SK-N-MC

To examine any additive effects of the GLI inhibitor ATO and the cytostatics etoposide and doxorubicin four combinations of either etoposide with ATO or doxorubicin with ATO were examined in all three EWS cells lines. In order to ensure a better comparability between the cell lines each 0.5 µM and 1 µM ATO were combined with either 0.1 µM and 0.2 µM etoposide or 5 nM and 10 nM doxorubicin.

Etoposide and Arsenic trioxide

As presented in **Figure 28A** A673 cells showed a reduction of colony number using any of the combinations. Already combining 0.1 µM etoposide and 0.5 µM ATO showed an effect. When doubling the amount of etoposide to 0.2 µM the colony number remained stable, whereas the double amount of 1 µM ATO potentiated the effect. Compared to single treatments shown in **Figure 25A and 26A** inhibitor combinations were significantly more efficient in A673 cells.

In RD-ES (**Figure 28B**) and SK-N-MC cells (**Figure 28C**) treatment with 0.1 µM etoposide and 0.5 µM ATO had a visible impact on colony formation as well. Elevating the ATO or etoposide dose in RD-ES cells enhanced the suppression of colony formation with 0.2 µM etoposide and 1 µM ATO being sufficient for a complete inhibition. For comparison, under both single treatments colonies were persisting (**Figure 25B and 26B**). In SK-N-MC cells elevation of the ATO dose was dominant over etoposide. Again, with the highest doses of 0.2 µM etoposide and 1 µM ATO applied no colony remained, which is once more clearly superior compared to the single treatments (**Figure 25C and 26C**).

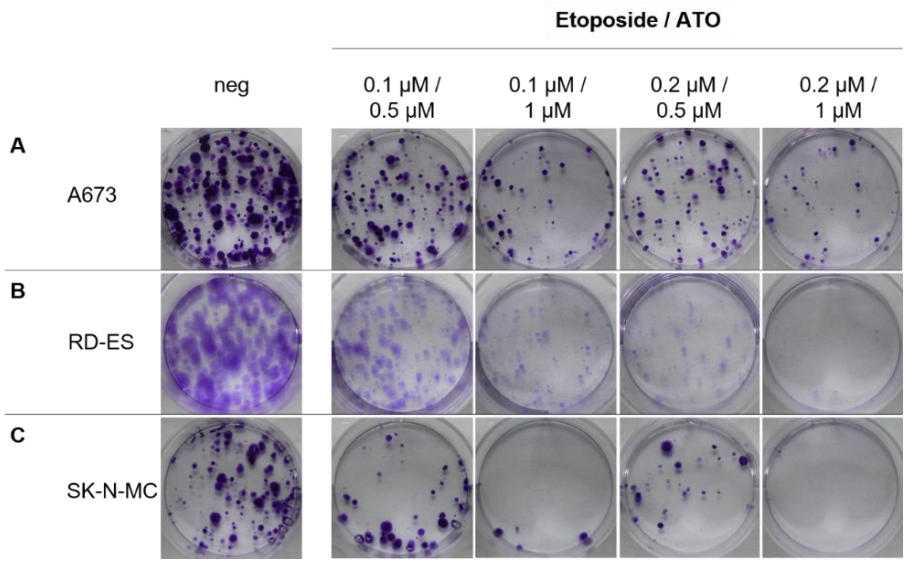

Figure 28: Clonogenic assay of the EWS cell lines A673, RD-ES and SK-N-MC treated with a combination of etoposide and ATO. A: *1 x 10^3 cells/well A673,* ***B:*** *0.5 x 10^3 cells/well RD-ES or* ***C:*** *0.5 x 10^3 cells/well SK-N-MC were sown into 6-well plates and treated with solvent only (negative control) or different inhibitor concentrations for 72 h. Subsequently, every 72 h medium was replaced with fresh medium without inhibitor and cells were incubated until negative controls were grown. Colonies were then fixed with methanol and stained with crystal violet. For documentation results were photographed. Data presented in this figure was also published (Boehme et al., 2016 (1)).*

Doxorubicin and Arsenic trioxide

All three EWS cell lines presented a slight reduction of the number of colonies when treated with a combination of 5 nM doxorubicin and 0.5 µM ATO. The effect was more distinct in RD-ES cells (**Figure 29B**), where also the size of the remaining colonies was reduced. Moreover, in RD-ES 5 nM doxorubicin combined with 1 µM ATO were sufficient for a complete suppression of colony growth, which was clearly superior compared to single treatment **(Figure 25B and 27B)**. The combination of 5 nM

doxorubicin and 0.5 µM ATO used on A673 cells led to a stronger reduction of colony formation compared to single treatment. However, two colonies could still be observed with 10 nM doxorubicin and 1 µM ATO being applied. Yet, also in A673 cells the drug combinations were more efficient compared to single administration **(Figure 25A and 27A)**. SK-N-MC cells (**Figure 29C**) were more sensitive to the combination of doxorubicin and ATO than A673, but a complete suppression of colony formation could only be obtained with a combination of 10 nM doxorubicin and 1 µM ATO. Again, all combinations exceeded the impact of single treatment **(Figure 25C and 27C)**.

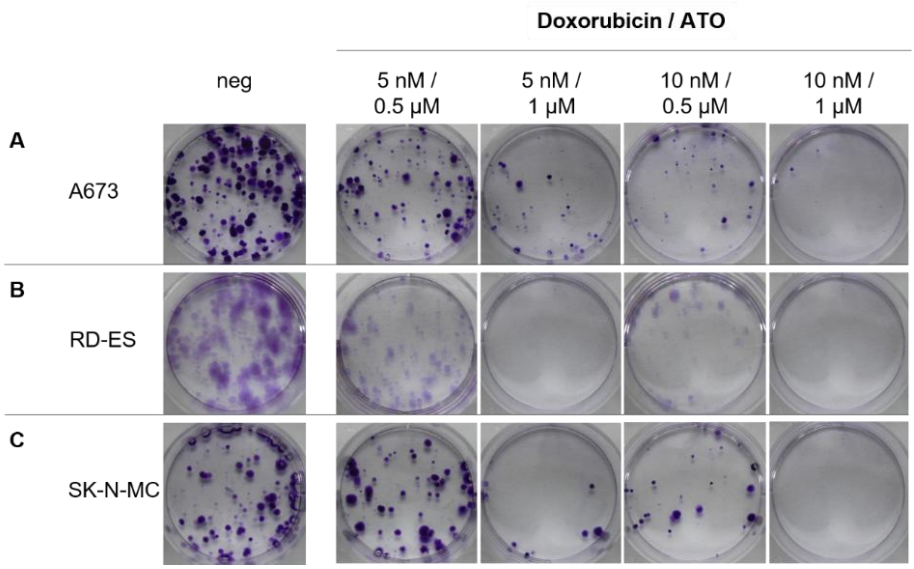

Figure 29: Clonogenic assay of the EWS cell lines A673, RD-ES and SK-N-MC treated with a combination of doxorubicin and ATO. A: *1 x 10^3 cells/well A673,* ***B:*** *0.5 x 10^3 cells/well RD-ES or* ***C:*** *0.5 x 10^3 cells/well SK-N-MC were sown into 6-well plates and treated with solvent only (negative control) or different inhibitor concentrations for 72 h. Subsequently, every 72 h medium was replaced with fresh medium without inhibitor and cells were incubated until negative controls were grown. Colonies were then fixed with methanol and stained with crystal violet. For documentation results were photographed. Data presented in this figure was also published (Boehme et al., 2016 (1)).*

3.3.4 Summary

As in the viability assays, A673 cells showed a greater sensitivity to GANT61 compared to RD-ES and SK-N-MC. The ATO sensitivity of colony formation in A673 and RD-ES cells was comparable. On the other hand, A673 cells were most resistant to etoposide. Only doxorubicin affected growth of all three EWS cell lines to the same extent. The combined treatment of the EWS cell lines using etoposide and ATO but also doxorubicin and ATO potentiated the suppression of colony formation achieved by the single substances.

3.4 Impact of GANT61, ATO, etoposide and doxorubicin on 3D spheroid cultures of Ewing sarcoma cell lines

All previously used methods have only shown the drug effects on cells grown in monolayer. However, tumour cells in the human body grow in 3D structures and therefore have different cellular interactions but also access to oxygen, nutrients and drugs compared to the same cells grown *in vitro* in monolayers. Hence, the effect of GANT61, ATO and cytostatics was tested on cells growing in 3D spheroid cultures simulating conditions occurring in vivo. Using round bottom non-adherent 96-well-plates cells were grown for 4 days to establish spheroids which was photographically documented. Only the EWS cell lines SK-N-MCs and A673 were able to form and sustain spheroids for 10 days, whereas RD-ES loosely concentrated at the bottom of the well and were therefore not used for further experiments (**Figure 30**).

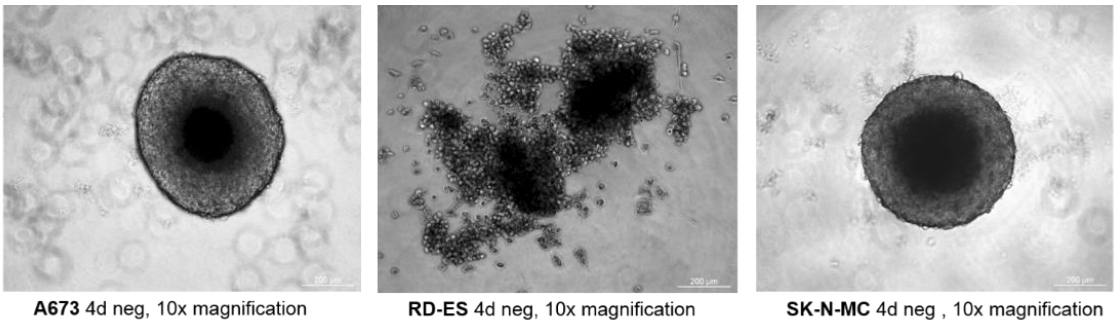

Figure 30: 3D spheroid formation of the EWS cell lines A673, RD-ES and SK-N-MC. *0.5 x 10^4 cells/well (A673 and RD-ES) or 0.25 x 10^4 cells/well (SK-N-MC) were sown into non-adherent-u-bottom 96-well plates. Spheroid formation was documented via light micrographs 4 days after seeding.*

3.4.1 Effect of GANT61 and ATO on A673 and SK-N-MC spheroid cultures

Four days after plating growing spheroids from 0.5 x 10^4 cells/well (A673) or 0.25 x 10^4 cells/well (SK-N-MC) were treated with 10 µM or 15 µM GANT61, respectively 2 µM or 5 µM ATO for another 4 days. The negative controls were treated with the inhibitors solvent.

GANT61

Figure 31 shows spheroids of SK-N-MC and A673 cells increasing in diameter after 4 days irrespectively of GANT61 or solvent addition. Spheroid size was only minimally reduced upon GANT61 treatment. However, 15 µM GANT61 were sufficient to affect spheroid integrity of SK-N-MC cells, which indicates a decline in cellular cohesion. Integrity of A673 spheroids was minimally affected by 15 µM GANT61, showing a slight bulge in the spheroid surface.

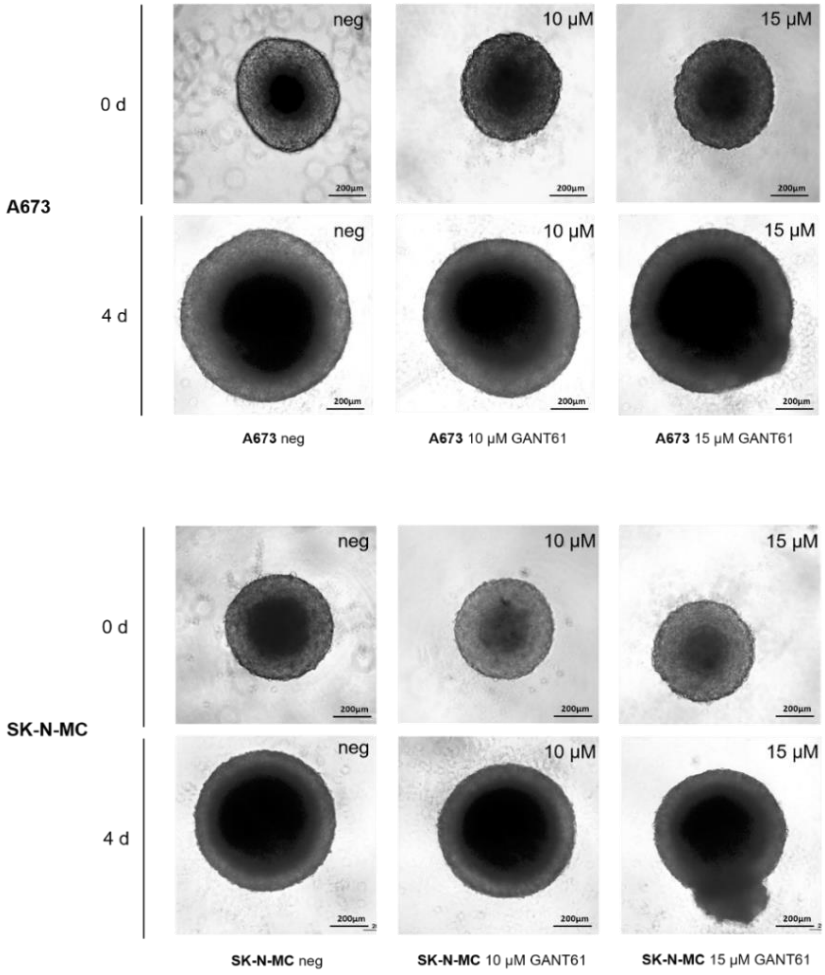

Figure 31: Effect of GANT61 on A673 and SK-N-MC cells growing in 3D spheroid cultures. *0.5 x 10^4 cells/well (A673) or 0.25 x 10^4 cells/well (SK-N-MC) were sown into non-adherent-u-bottom 96-well plates and incubated for 4 days to allow spheroid formation. Spheroids were documented via light micrographs before treatment (0 d) and after four days of treatment (4 d) with the inhibitors solvent (DMSO) as a negative control or with 10 µM or 15 µM GANT61. All treatments were performed in quadruplicates with representative micrographs shown.*

Arsenic trioxide

As indicated in **Figure 32,** SK-N-MC and A673 spheroids treated with 2 µM ATO showed a significant growth suppression compared to the solvent treated control, which was only marginally reinforced applying a higher concentration of 5 µM ATO in SK-N-MC. Furthermore, ATO compromised spheroid integrity, which became particularly obvious in the A673 spheroids, but was also present in the SK-N-MC spheroids.

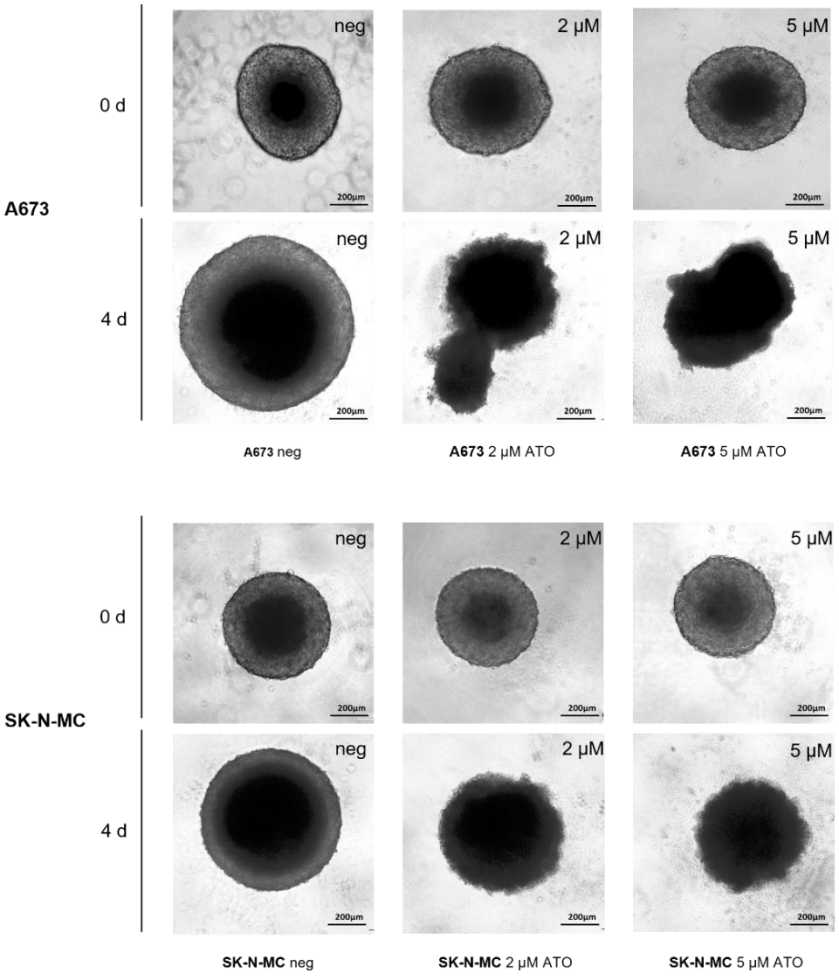

Figure 32: Effect of ATO on A673 and SK-N-MC cells growing in 3D spheroid cultures. *0.5 x 10^4 cells/well (A673) or 0.25 x 10^4 cells/well (SK-N-MC) were sown into non-adherent-u-bottom 96-well plates and incubated for 4 days to allow spheroid formation. Spheroids were documented via light micrographs before treatment (0 d) and after four days of treatment (4 d) with the inhibitors solvent (H_2O) as a negative control or with 2 µM or 5 µM ATO. All treatments were performed in quadruplicates with representative micrographs shown. Data presented in this figure was also published (Boehme et al., 2016 (1)).*

3.4.2 Effect of etoposide and doxorubicin on A673 and SK-N-MC spheroid cultures

Four days after plating growing spheroids from 0.5 x 10^4 cells/well (A673) or 0.25 x 10^4 cells/well (SK-N-MC) were treated with 2 µM or 5 µM etoposide, respectively 30 nM or 50 nM doxorubicin for another 4 days. The negative control spheroids were incubated with the inhibitors solvent.

Etoposide

As presented in **Figure 33,** spheroid growth of both EWS cell lines was completely inhibited by 2 µM etoposide applied for 4 days. Spheroids grown from the cell line SK-N-MC showed a loss of cell surface integrity starting with 2 µM etoposide. With a concentration of 5 µM etoposide applied the spheroid structure was completely lost. Integrity of A673 spheroids was still retained upon etoposide administration, only a slight surface discontinuity could be seen.

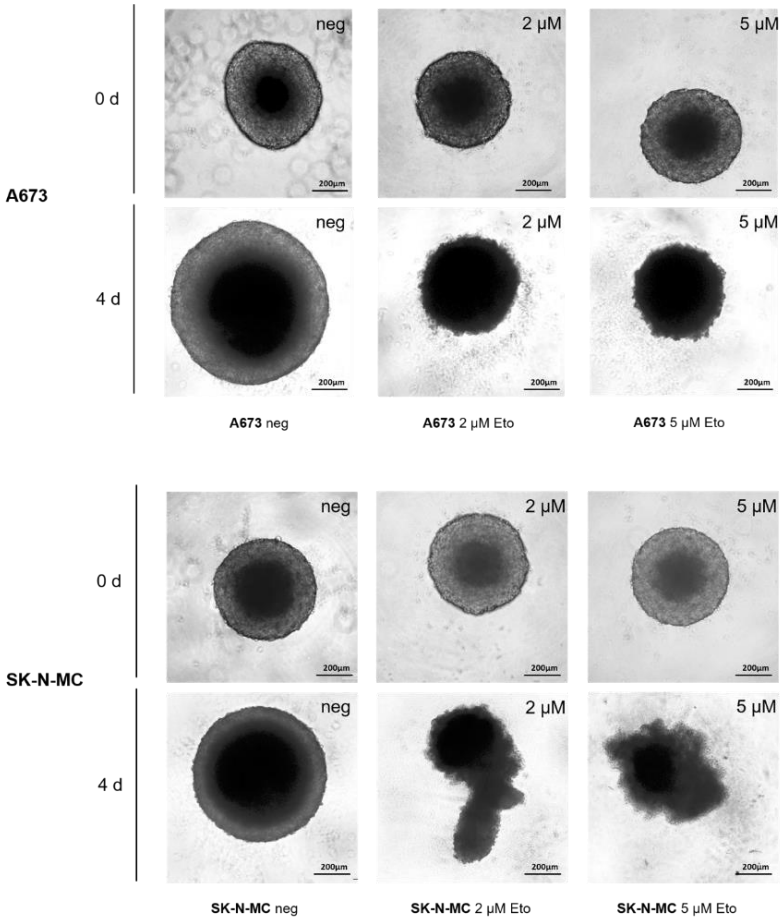

Figure 33: Effect of etoposide on A673 and SK-N-MC cells growing in 3D spheroid cultures. *0.5 x 10^4 cells/well (A673) or 0.25 x 10^4 cells/well (SK-N-MC) were sown into non-adherent-u-bottom 96-well plates and incubated for 4 days to allow spheroid formation. Spheroids were documented via light micrographs before treatment (0 d) and after four days of treatment (4 d) with the inhibitors solvent (DMSO) as a negative control or with 2 µM or 5 µM etoposide. All treatments were performed in quadruplicates with representative micrographs shown. Data presented in this figure was also published (Boehme et al., 2016 (1)).*

Doxorubicin

A dose dependent decrease in spheroid growth as well as a destabilisation of the spheroid surface integrity was observed in the SK-N-MC spheroids treated with 30 nM and 50 nM doxorubicin. Also the size of the A673 spheroids was reduced by doxorubicin treatment, whereas spheroid integrity was barely affected showing detachment of some cells from the spheroids.

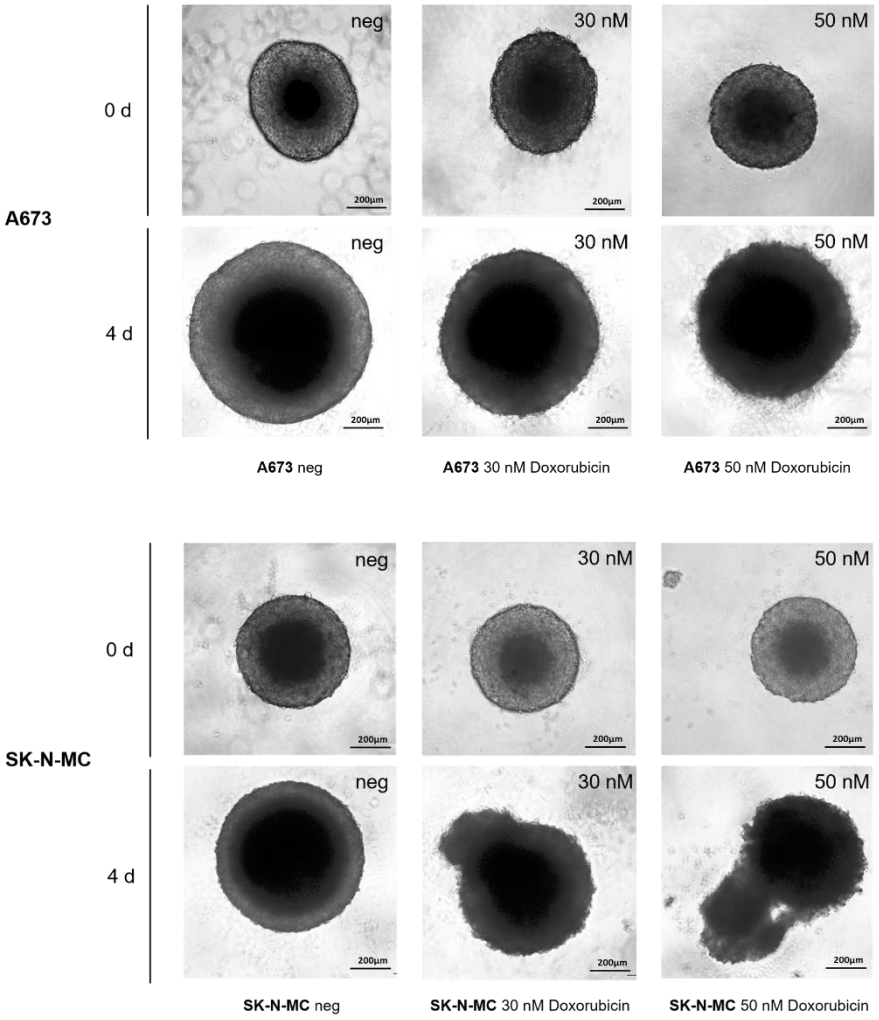

Figure 34: Effect of doxorubicin on A673 and SK-N-MC cells growing in 3D spheroid cultures. *0.5 x 10^4 cells/well (A673) or 0.25 x 10^4 cells/well (SK-N-MC) were sown into non-adherent-u-bottom 96-well plates and incubated for 4 days to allow spheroid formation. Spheroids were documented via light micrographs before treatment (0 d) and after four days of treatment (4 d) with the inhibitors solvent (DMSO) as a negative control or with 30 nM or 50 nM doxorubicin. All treatments were performed in quadruplicates with representative micrographs shown. Data presented in this figure was also published (Boehme et al., 2016 (1)).*

3.4.3 Summary

3D spheroid cultures of both EWS cell lines SK-N-MC and A673 seemed to be largely resistant to treatment with GANT61. Using ATO or etoposide on the other hand, the lower concentration of 2 µM was sufficient to largely inhibit spheroid growth and to affect spheroid integrity in both cell lines. This effect was only slightly reinforced by application of a higher dose of ATO or etoposide. Doxorubicin treatment led to slight suppression of spheroid growth of both cell lines. Spheroid integrity was especially compromised in A673 cells.

3.5 Effect of GANT61, ATO, etoposide and doxorubicin on cell death induction in Ewing sarcoma cell lines

3.5.1 Detection of cell death using flow cytometry (FACS-analysis)

All previously performed tests have demonstrated the impact of GANT61, ATO, etoposide and doxorubicin on the viability and proliferation of EWS cells. To determine whether the substances not only transiently compromise the cellular metabolism and arrest growth but also induce cell death, flow cytometry was performed using the "Fixable Viability Dye - eFluor® 450" for staining of cells. Only dying cells take up eFluor® 450 as the dye cannot pass intact cellular membranes. The ratio between dye-positive and dye-negative cells is therefore considered proportional to the rate of cell death in that cell population.

In the following graphs the rate of cell death is shown for the EWS cell lines and MSC-2014-7 treated with selected concentrations of GANT61, ATO, etoposide, doxorubicin and combinations thereof. The highest concentrations applied were always tested on the control cells MSC-2014-7.

Effect of GLI-Inhibition using GANT61 and ATO on cell death induction of A673, RD-ES, SK-N-MC and MSC

GANT61

All three EWS cell lines as well as MSC-2014-7 were treated with 10 µM and 15 µM GANT61. No significant effect on cell death induction was observed. Only A673 cells showed at least 9 ± 2 % dead cells upon treatment with 15 µM GANT61 (**Figure 35A**). In SK-N-MC cells 5 ± 3 % dead cells were detected with 10 µM GANT61 but there was no further increase upon application of 15 µM (**Figure 35C**). GANT61 did not affect MSC-2014-7 (**Figure 35D**). Surprisingly some more living cells were present when RD-ES cells were treated with GANT61 though rates did not drop lower than -3 % (**Figure 35B**).

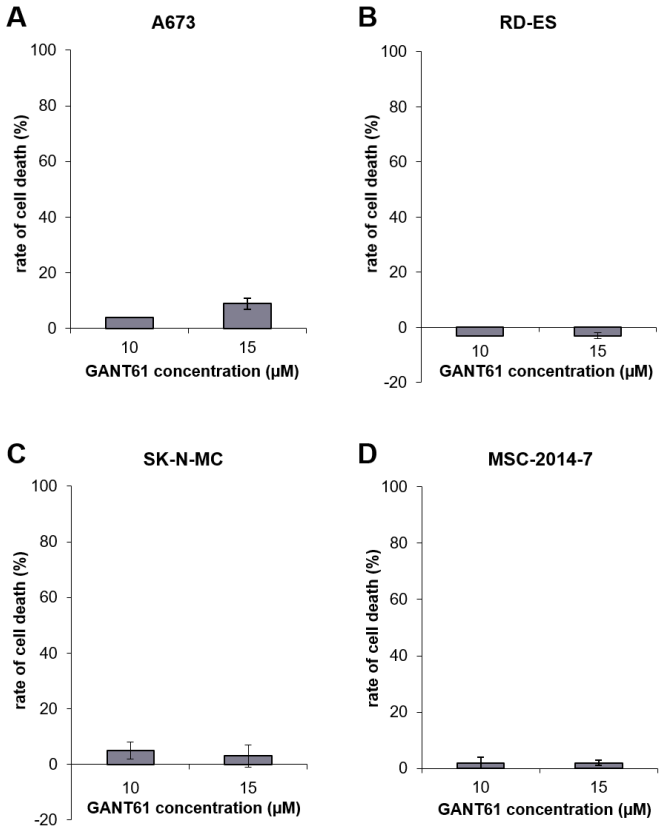

Figure 35: Effect of GANT61 on cell death induction in the EWS cell lines A673, RD-ES and SK-N-MC in comparison to MSC-2014-7. A: *2.5 x 10^5 cells/well A673,* ***B:*** *1.5 x 10^5 cells/well RD-ES,* ***C:*** *1 x 10^5 cells/well SK-N-MC or* ***D:*** *2.5 x 10^5 cells/well MSC-2014-7 were sown out into 6-well plates. After 24 h cells were treated with 10 µM or 15 µM GANT61 or the inhibitor solvent for 72 h. Cells were then stained with eFluor® 450 and analysed by flow cytometry. Negative controls were set to 0 % cell death and the rate of cell death upon treatment using GANT61 calculated. Mean values were plotted from three independent replicates. Standard deviations are represented by black error bars. Data presented in this figure was also published (Boehme et al., 2016 (1)).*

Arsenic trioxide

Figure 36 shows cell death induction after treatment with ATO. All three EWS cell lines presented rates as high as 63 ± 1 % (A673), 41 ± 3 % (RD-ES) or 70 ± 0 % (SK-N-MC) under treatment with 5 µM ATO. Interestingly, concentrations up to 0.5 µM ATO did not raise cell death above 13 ± 2 % in A673 cells (**Figure 36A**). 1 µM ATO however, led to 65 ± 0 % dye positive cells in A673, which could not be further enhanced by increasing ATO doses. RD-ES cells (**Figure 36B**) showed no cell death upon treatment with 1 µM ATO. However, 2 µM ATO were sufficient for 32 ± 5 % death cells, which was further enhanced by 3 µM ATO (44 ± 1 %). As in the MTS assay, SK-N-MC cells (**Figure 36C**) were most resistant with only 9 ± 1 % dead cells upon treatment with 2 µM ATO. SK-N-MC cells showed an increase in dead cells to 21 ± 3 % upon treatment with 3 µM ATO and 70 ± 0 %, the highest value obtained in the EWS cell lines with 5 µM ATO being applied. No significant uptake of eFluor® 450 was observed in MSC-2014-7 (**Figure 36D**), levels of cell death ranging between -2 % and 2 % under treatment with the highest dose of 5 µM ATO.

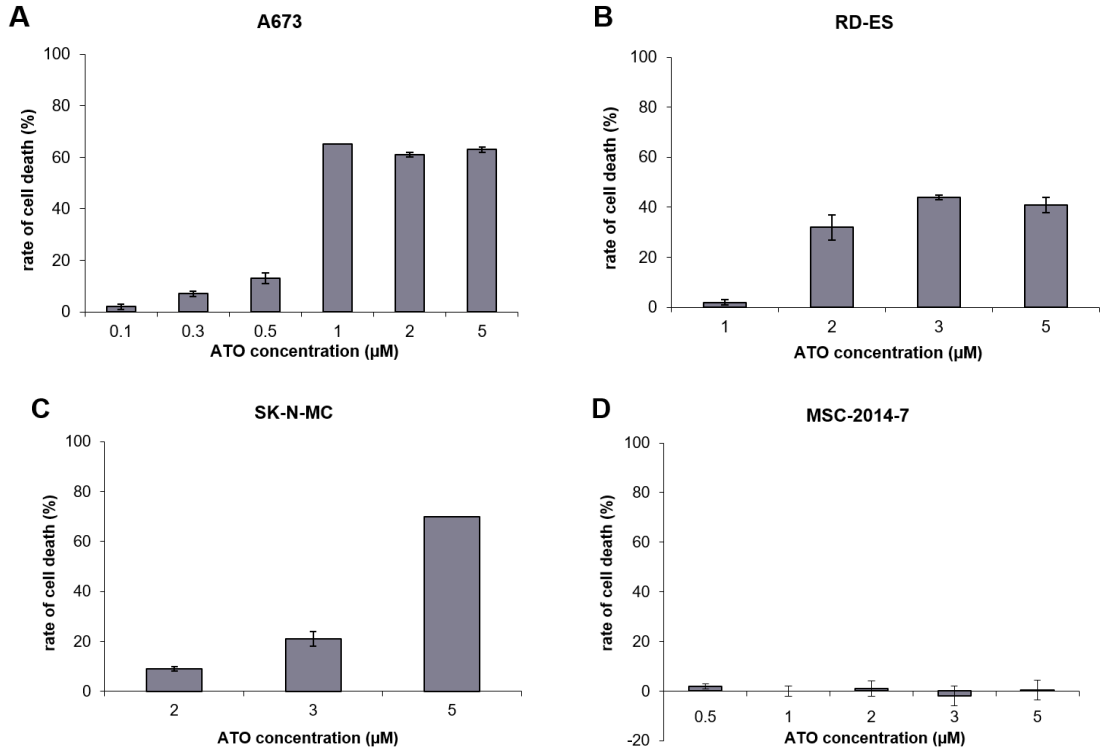

Figure 36: Effect of ATO on cell death induction in the EWS cell lines A673, RD-ES and SK-N-MC in comparison to MSC-2014-7. ***A:*** *2.5 x 10^5 cells/well A673,* ***B:*** *1.5 x 10^5 cells/well RD-ES,* ***C:*** *1 x 10^5 cells/well SK-N-MC or* ***D:*** *2.5 x 10^5 cells/well MSC-2014-7 were sown out into 6-well plates. After 24 h cells were treated with A673: 0.1 µM, 0.3 µM, 0.5 µM, 1 µM, 2 µM or 5 µM ATO; RD-ES: 1 µM, 2 µM, 3 µM or 5 µM ATO; SK-N-MC: 2 µM, 3 µM or 5 µM ATO and MSC-2014-7; 0.5 µM, 1 µM, 2 µM, 3 µM or 5 µM ATO or the inhibitor solvent for 72 h. Cells were then stained with eFluor® 450 and analysed by flow cytometry. Negative controls were set to 0 % cell death and the rate of cell death upon treatment using ATO was calculated. Mean values were plotted from three independent replicates. Standard deviations are represented by black error bars. Data presented in this figure was also published (Boehme et al., 2016 (1)).*

Effect of the cytostatics etoposide and doxorubicin on cell death induction of A673, RD-ES, SK-N-MC and MSC

Etoposide

Etoposide treated A673, RD-ES and SK-N-MC cells showed a dose dependent increase of cell death reaching the highest levels after application of 5 µM etoposide. In A673 cells (**Figure 37A**) 55 ± 2 % already lost their membrane integrity after treatment with 1 µM etoposide which reached up to 71 ± 1 % with 5 µM etoposide. Both RD-ES and SK-N-MC cells were more resistant to etoposide, their ratio of eFluor® 450 positive cells being 21 ± 0 % (RD-ES) or 32 ± 4 % (SK-N-MC) after treatment with 2 µM etoposide. The amount of dead cells increased under 5 µM etoposide, obtaining 40 ± 1 % (RD-ES) and 39 ± 4 % (SK-N-MC). MSC-2014-7 were resistant to all etoposide concentrations applied showing maximal 2 ± 2 % dye positive cells after application of 2 µM etoposide (**Figure 37D**).

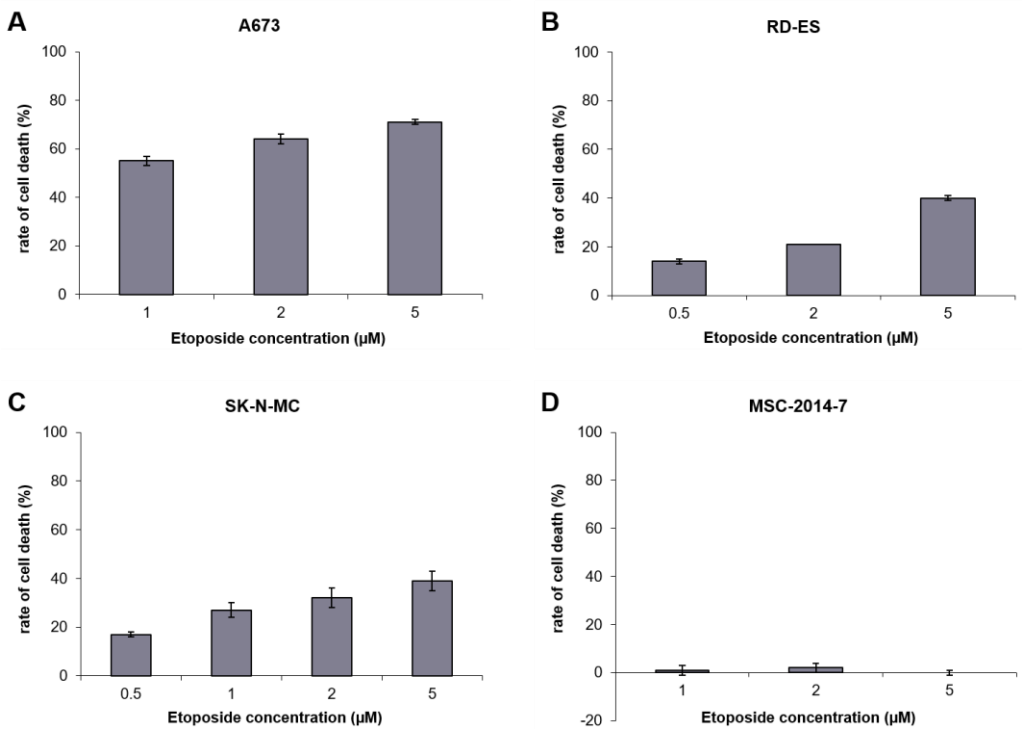

Figure 37: Effect of etoposide on cell death induction in the EWS cell lines A673, RD-ES and SK-N-MC in comparison to MSC-2014-7. ***A:*** *2.5 x 10^5 cells/well A673,* ***B:*** *1.5 x 10^5 cells/well RD-ES,* ***C:*** *1 x 10^5 cells/well SK-N-MC or* ***D:*** *2.5 x 10^5 cells/well MSC-2014-7 were sown out into 6-well plates. After 24 h cells were treated with A673: 1 µM, 2 µM or 5 µM etoposide; RD-ES: 0.5 µM, 2 µM or 5 µM etoposide; SK-N-MC: 0.5 µM, 1 µM, 2 µM or 5 µM etoposide and MSC-2014-7: 1 µM, 2 µM or 5 µM etoposide or the inhibitor solvent for 72 h. Cells were then stained with eFluor® 450 and analysed by flow cytometry. Negative controls were set to 0 % cell death and the rate of cell death upon treatment using etoposide was calculated. Mean values were plotted from three independent replicates. Standard deviations are represented by black error bars. Data presented in this figure was also published (Boehme et al., 2016 (1)).*

Doxorubicin

As presented in **Figure 38A** 30 nM doxorubicin were sufficient for a significant increase of the uptake of eFluor® 450 to 42 ± 3 % in A673 cells, whereas 5 nM had no noticeable effect (2 ± 3 %). A higher concentration of 50 nM doxorubicin led to 55 ± 1 % dead cells. In RD-ES cells a significant leap in eFluor® 450 uptake was achieved with 30 nM doxorubicin as well (26 ± 1 %) (**Figure 38B**), whereas lower concentrations led to poor rates dead cells (5 nM doxorubicin: 2 ± 2 %; 10 nM doxorubicin: 8 ± 1 %). 50 µM doxorubicin induced maximal cell death of 29 ± 2 % obtained for RD-ES cells. The effect of doxorubicin in SK-N-MC cells (**Figure 38C**) was more pronounced than in RD-ES cells. Levels of eFluor® 450 positive cells lay at 32 ± 2 % with 30 nM doxorubicin and increased to 41 ± 1 % upon treatment with 50 nM doxorubicin. Treatment of MSC-2014-7 with 50 nM doxorubicin induced a maximum of 3 ± 3 % cell death (**Figure 38D**).

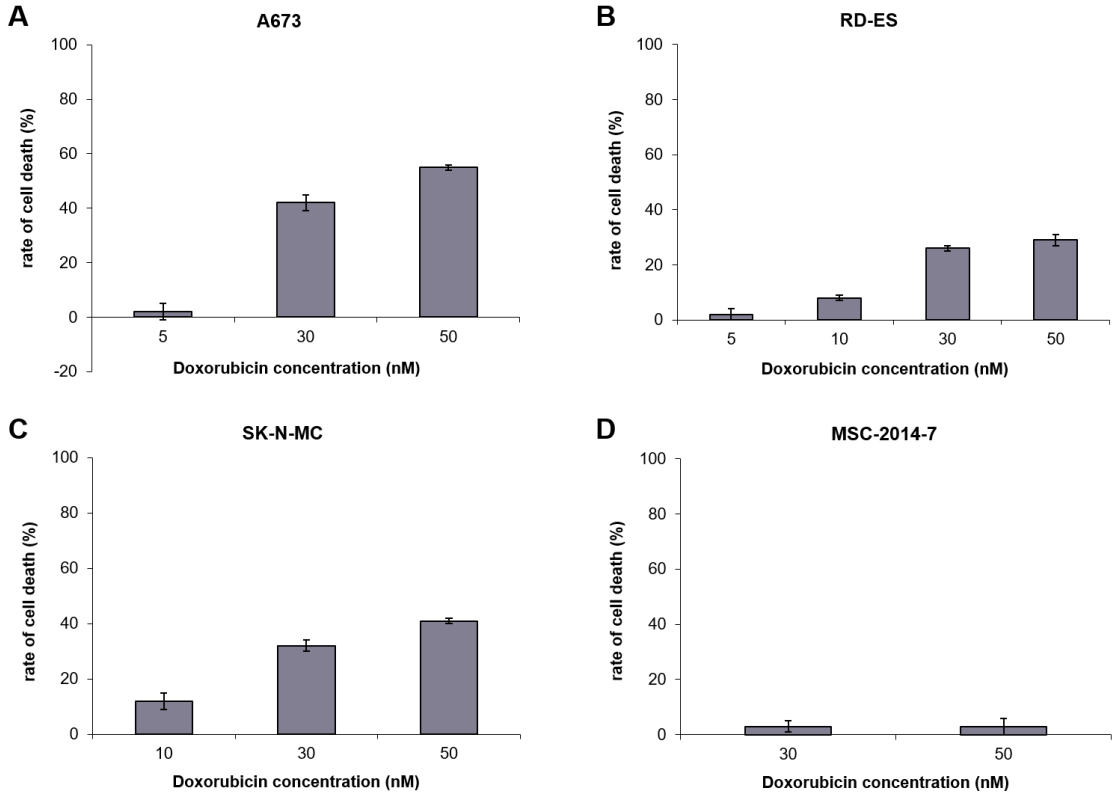

Figure 38: Effect of doxorubicin on cell death induction in the EWS cell lines A673, RD-ES and SK-N-MC in comparison to MSC-2014-7. A: *2.5 x 10^5 cells/well A673,* ***B:*** *1.5 x 10^5 cells/well RD-ES,* ***C:*** *1 x 10^5 cells/well SK-N-MC or* ***D:*** *2.5 x 10^5 cells/well MSC-2014-7 were sown out into 6-well plates. After 24 h cells were treated with A673: 5 nM, 30 nM or 50 nM doxorubicin; RD-ES: 5 nM, 10 nM, 30 nM or 50 nM doxorubicin; SK-N-MC: 10 nM, 30 nM or 50 nM doxorubicin and MSC-2014-7: 30 nM or 50 nM doxorubicin or the inhibitor solvent for 72 h. Cells were then stained with eFluor® 450 and analysed by flow cytometry. Negative controls were set to 0 % cell death and the rate of cell death upon treatment using doxorubicin was calculated. Mean values were plotted from three independent replicates. Standard deviations are represented by black error bars. Data presented in this figure was also published (Boehme et al., 2016 (1)).*

Effect of drug combinations on cell death induction in A673, RD-ES, SK-N-MC and MSC

Etoposide, Doxorubicin and Arsenic trioxide

For further enhancement of cell death two triple combinations consisting of etoposide, doxorubicin and ATO as well as the respective double combinations of etoposide and ATO and doxorubicin and ATO were applied to A673, RD-ES and SK-N-MC. The results are presented in **Figure 39**.

As A673 (**Figure 39A**) were rather sensitive to low concentrations of 0.1 µM and 0.3 µM ATO in the MTS assay, these doses were combined with 1 µM etoposide or/and 5 nM doxorubicin. The death rate reached 56 ± 3 % upon combination of 1 µM etoposide and

0.1 µM ATO. However, 1 µM etoposide in single application also led to 55 ± 2 % dead cells. The same result was obtained with the higher ATO dose of 0.3 µM combined with 1 µM etoposide, inducing 58 ± 3 % cell death. The uptake of eFluor® 450 seemed to be mostly dependent of the dose of etoposide applied. Regarding the combination of doxorubicin and ATO, 5 nM doxorubicin and 0.1 µM ATO presented a slightly higher level of eFluor® 450 positive cells in combination (9 ± 2 %) than in single treatment (5 nM doxorubicin: 2 ± 3 %; 0.1 µM ATO: 2 ± 1 %). In single application, increasing the ATO concentration to 0.3 µM 7 ± 1 % cells lost their membrane integrity. In combination with 5 nM doxorubicin however, an uptake of eFluor® 450 in 39 ± 3 % of the cells could be observed (**Figure 39A**). Unfortunately, in both triple combinations neither the combination of 1 µM etoposide and 5 nM doxorubicin with 0.1 µM ATO (53 ± 3 %) nor with 0.3 µM ATO (58 ± 2 %) produced death rates significantly above those of etoposide only or the double combination of etoposide and ATO.

In RD-ES cells (**Figure 39B**) a significant rise of eFluor® 450 positive cells to 49 ± 3 % was achieved with a combination of 0.5 µM etoposide and 2 µM ATO, whereas single treatment led to 14 ± 1 % dead cells (0.5 µM etoposide) or 32 ± 5 % dead cells (2 µM ATO). Neither the combination of 5 nM doxorubicin with 2 µM ATO nor the combination of 10 nM doxorubicin with 2 µM AO did significantly elevate the amount of dead cells (5 nM doxorubicin / 2 µM ATO: 33 ± 1 %; 10 nM doxorubicin / 2 µM ATO: 37 ± 3 %) above the percentage obtained with ATO alone (32 ± 5 %), whereas single treatment with 5 nM doxorubicin led to 2 ± 2 % and 10 nM doxorubicin to 8 ± 1 % dead cells. As A673 cells, RD-ES cells presented no higher levels of cell death (32 ± 5 %) upon triple treatment with 0.5 µM etoposide, 5 nM doxorubicin and 2 µM ATO than in the combination with equal concentrations of etoposide and ATO (0.5 µM etoposide / 2 µM ATO: 49 ± 3 %). Although the dose of doxorubicin was increased to 10 nM in the second triple combination with etoposide and ATO, no further increase in cell death (46 ± 2 %) was obtained.

In SK-N-MC cells (**Figure 39C**) combination of 0.5 µM etoposide and 3 µM ATO were required to increase the uptake of eFluor® 450 to 35 ± 8 % compared to single treatment with 0.5 µM etoposide (17 ± 1 %) or 3 µM ATO (21 ± 3 %). Doubling the dose of etoposide in combination to 1 µM etoposide showed no increase of the death rate (1 µM etoposide / 3 µM ATO: 34 ± 1 %) in comparison to single treatment (1 µM etoposide: 27 ± 3 %). The treatment with 10 nM doxorubicin and 3 µM ATO

(28 ± 5 %) led to a slightly higher uptake of eFluor® 450 compared to 10 nM doxorubicin (12 ± 2 %) or 3 µM ATO (21 ± 3 %) only. Similar to A673 and RD-ES cells, SK-N-MC cells achieving no higher ratio of eFluor® 450 positive cells under triple treatment (0.5 µM etoposide / 30 nM doxorubicin and 3 µM ATO: 28 ± 3 %) than under combined treatment with either 0.5 µM etoposide and 3 µM ATO or 20 nM doxorubicin and 3 µM ATO. Even doubling the dose of etoposide to 1 µM did not increase the rate of cell death in triple treatment (1 µM etoposide / 30 nM doxorubicin / 3 µM ATO: 31 ± 0 %).

For control, the highest etoposide, doxorubicin and ATO concentrations used in EWS cell lines were applied to MSC-2014-7 (**Figure 39D**). MSC did not reach a ratio of eFluor® 450 positive cells greater than 3 % neither in the double applications nor the triple combination of 1 µM etoposide, 30 nM doxorubicin and 3 µM ATO (**Figure 39D**).

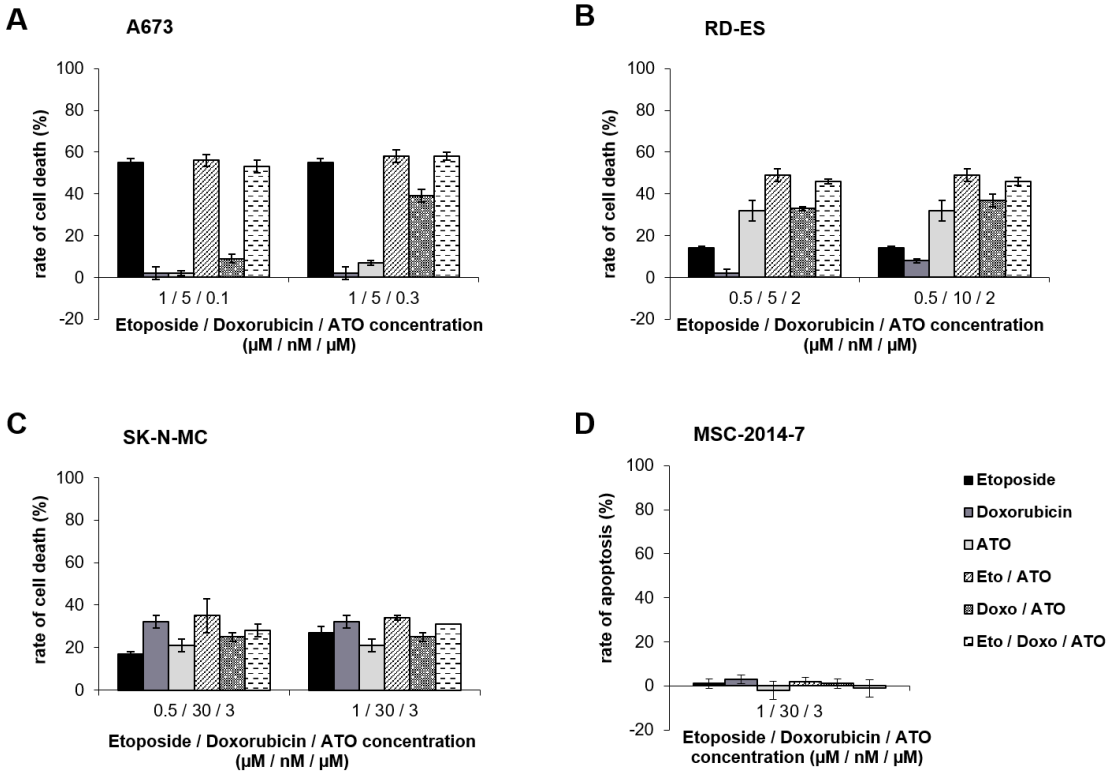

Figure 39: Effect of combined treatment with etoposide, doxorubicin and ATO on cell death induction in the EWS cell lines A673, RD-ES and SK-N-MC in comparison to MSC-2014-7. A: *2.5 x 10^5 cells/well A673,* ***B:*** *1.5 x 10^5 cells/well RD-ES,* ***C:*** *1 x 10^5 cells/well SK-N-MC or* ***D:*** *2.5 x 10^5 cells/well MSC-2014-7 were sown out into 6-well plates. After 24 h cells were treated with single doses or double and triple combinations of etoposide, doxorubicin and ATO or the inhibitor solvents for 72 h as indicated. Cells were then stained with eFluor® 450 and analysed by flow cytometry. Negative controls were set to 0 % cell death and the rate of cell death upon treatment was calculated. Mean values were plotted from three independent replicates. Standard deviations are represented by black error bars. Data presented in this figure was also published (Boehme et al., 2016 (1)).*

Summary

All EWS cell lines were resistant to doses up to 15 µM GANT61, with cell death not exceeding 9 % obtained in A673. Upon treatment with ATO, etoposide and doxorubicin A673 cells were the most sensitive of the three EWS cell lines. Maximum apoptosis rates received with single treatments ranged from 44 % (3 µM ATO) in RD-ES to 71 % (5 µM etoposide) in A673 and 70 % (5 µM ATO) in SK-N-MC. Combined treatment of A673 or SK-N-MC cells with etoposide and ATO did not significantly exceed the death rate obtained with etoposide alone. Only in RD-ES cells the combined treatment of etoposide ATO was clearly superior compared to the single doses. Using doxorubicin and ATO in the combined treatment of RD-ES cells as well as SK-N-MC cells the death rate was clearly dependent on the ATO dose applied and did not exceed single application. Only in A673 cells combination of 5 nM doxorubicin and 0.3 µM ATO was more efficient compared to the single treatment. A triple treatment with both cytostatics and ATO could not clearly enhance cell death compared to the combination of etoposide and ATO in any of the EWS cell lines, whereas cell death upon combination of doxorubicin with ATO was below that of triple treatment with equal doses in A673 and SK-N-MC cells. Fortunately, the control cells MSC-2014-7 were resistant to all single concentrations of GANT61, ATO, etoposide and doxorubicin as well as the combinations of etoposide, doxorubicin and ATO applied.

3.5.2 Detection of apoptosis induction by caspase 3 and PARP cleavage in Ewing sarcoma cell lines

As the FACS dye eFluor® 450 passes into all cells with a non-intact membrane, a distinction between apoptotic and necrotic cells cannot be made. However, cleaved PARP and caspase 3 are specific for apoptosis. Therefore, levels of both cleaved proteins where measured by western blot.

Effect of ATO and GANT61 on apoptosis induction in A673, RD-ES, SK-N-MC and MSC

GANT61

Both cleaved PARP (89 kDa) and cleaved caspase 3 (17 kDa) bands were found in GANT61 treated A673 cells (**Figure 40**; lanes 5 - 6). The cleavage increasing in a dose dependant manner after treatment with 10 µM and 15 µM GANT61 compared to the negative control. Neither cleaved caspase 3 nor cleaved PARP could be detected in RD-ES cells using the same GANT61 concentrations (**Figure 40**; lanes 11 - 12), whereas in SK-N-MC cells very faint caspase 3 bands appeared (**Figure 40**; lanes 16 - 18). A cleaved PARP band was barely visible in SK-N-MC after incubation with 15 µM GANT61. However, quantification revealed no significant increase of either caspase 3 or PARP cleavage normalised to tubulin in both RD-ES and SK-N-MC cells after GANT61 treatment in comparison to the negative control, whereas quantification verified the dose dependent increase of caspase 3 and PARP cleavage in A673 cells. After longer exposition of the RD-ES and SK-N-MC membranes also in MSC control cells two faint higher molecular weight bands were detected with the PARP antibody. A very slight caspase 3 (17 kDa) signal could be seen in **Figure 40** lanes 13 - 14 after long exposition. Quantification showed low levels of caspase 3 and PARP cleavage in MSC after treatment with both GANT61 concentrations.

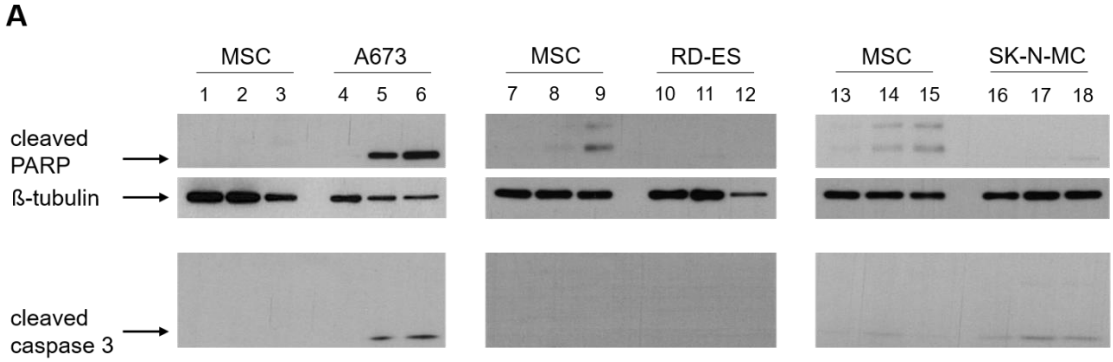

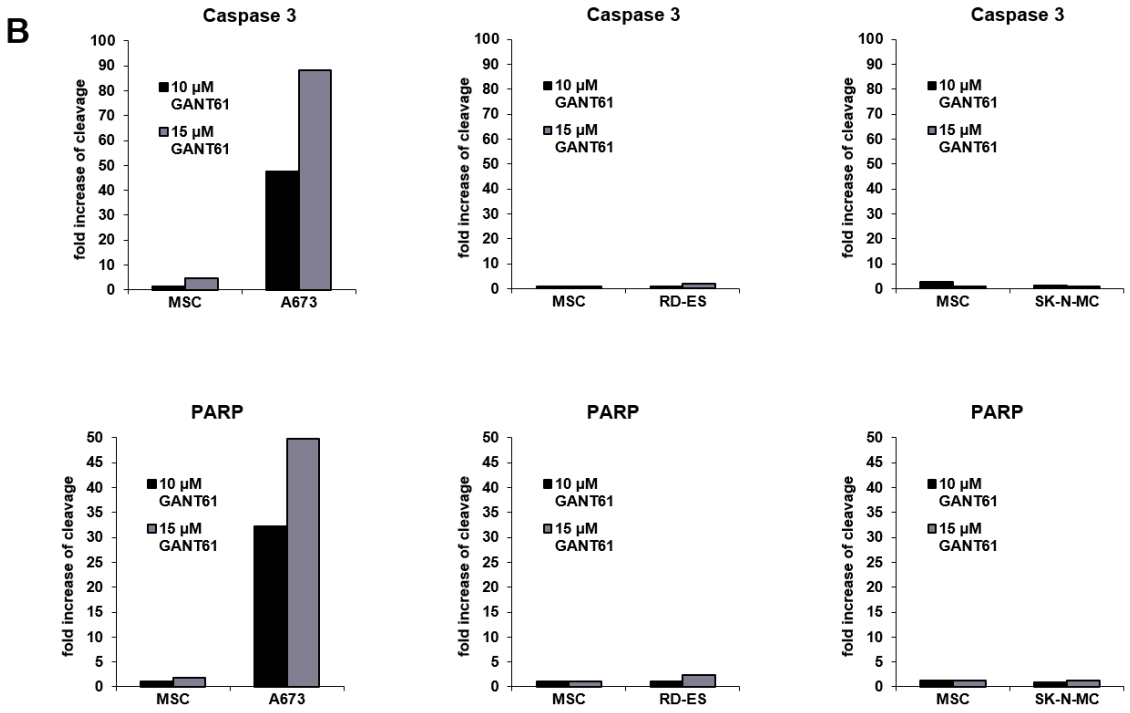

Figure 40: PARP and caspase 3 cleavage after GANT61 treatment of the EWS cell lines A673, RD-ES and SK-N-MC in comparison to MSC-2014-7. *1.5 x 10^4 cells/well of A673, RD-ES, SK-N-MC or MSC-2014-7 were sown into 12-well plates. After 24 h cells were treated with 10 µM GANT61, 15 µM GANT61 or the inhibitors solvent for 48 h. Proteins were isolated and their concentration was determined with Bradford assay. For the Western blot protein samples were loaded as follows: lane 1, 7, 13: MSC-2014-7 negative control; lane 2, 8, 14: MSC-2014-7 10 µM GANT61; lane 3, 9, 15: MSC-2014-7 15 µM GANT61; lane 4, 10, 16: EWS cell line negative control; lane 5, 11, 17: EWS cell line 10 µM GANT61; lane 6, 12, 18: EWS cell line 15 µM GANT61, with lanes 4 - 6: A673, lanes 10 - 12: RD-ES and lanes 16 - 18: SK-N-MC cells. Proteins were separated by SDS-PAGE and blotted onto a PVDF membrane. Membranes were incubated with primary antibodies against ß-tubulin, cleaved PARP and cleaved caspase 3 overnight. A horseradish peroxidase-conjugated secondary antibody was used. ECL substrate was added to the membranes and chemiluminescence signals were recorded on a film. ImageJ was utilised for western blot quantification. Data presented in this figure was also published (Boehme et al., 2016 (1)).*

Arsenic trioxide

ATO led to a dose dependent PARP and caspase 3 cleavage in A673 cells (**Figure 41**; lanes 5 - 6). Furthermore, A673 cells also exhibited cleaved PARP at low levels when treated with solvent only (**Figure 41**; lane 4). In RD-ES cells only after application of 5 µM ATO a very faint band of cleaved PARP was visible (**Figure 41**; lane 11). However, quantification showed no increase in cleavage of PARP or caspase 3 in ATO treated RD-ES cells compared to the negative control. SK-N-MC cells presented both bands of cleaved PARP and caspase 3 upon treatment with 2 µM and 5 µM ATO. Quantification revealed that upon application of 5 µM ATO (**Figure 41**; lanes 17 - 18) cleavage of PARP was slightly enhanced, whereas caspase 3 cleavage was comparable to that of 2 µM ATO

treated cells. As shown in **Figure 41**, again two higher molecular weight bands appeared with the PARP antibody in MSC. Moreover, on the A673 blot MSC showed bands of cleaved caspase 3 in ATO treated samples.

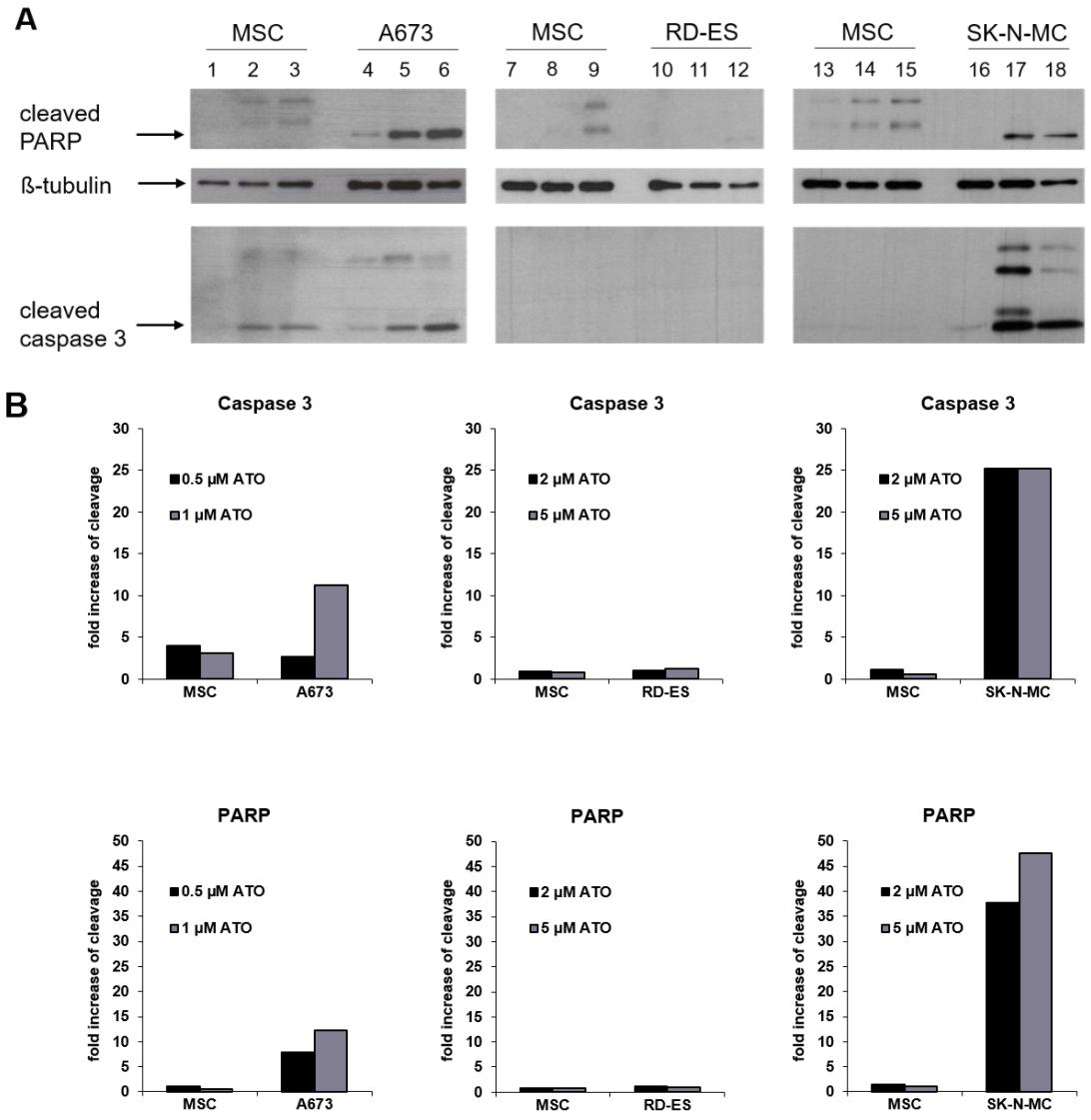

Figure 41: PARP and caspase 3 cleavage after ATO treatment of the EWS cell lines A673, RD-ES and SK-N-MC in comparison to MSC-2014-7. *1.5 x 10^4 cells/well of A673, RD-ES, SK-N-MC or MSC-2014-7 were sown into 12-well plates. After 24 h cells were treated with 2 µM ATO, 5 µM ATO or the inhibitors solvent for 48 h. Proteins were isolated and their concentration was determined with Bradford assay. For the Western blot protein samples were loaded as follows: lanes 1, 7, 13: MSC-2014-7 negative control; lanes 2, 8, 14: MSC-2014-7 2 µM ATO; lanes 3, 9, 15: MSC-2014-7 5 µM ATO; lanes 4, 10, 16: EWS cell line negative control; lanes 5, 11, 17: EWS cell line 2 µM ATO; lanes 6, 12, 18: EWS cell line 5 µM ATO with lanes 4 - 6: A673, lanes 10 - 12: RD-ES and lanes 16 - 18: SK-N-MC cells. Proteins were separated by SDS-PAGE and blotted onto a PVDF membrane. Membranes were incubated with primary antibodies against ß-tubulin, cleaved PARP and cleaved caspase 3 overnight. A horseradish peroxidase-conjugated secondary antibody was used. ECL substrate was added to the membranes and chemiluminescence signals were recorded on a film. ImageJ was utilised for western blot quantification. Data presented in this figure was also published (Boehme et al., 2016 (1)).*

Effect of the cytostatics etoposide and doxorubicin on apoptosis induction of A673, RD-ES, SK-N-MC and MSC

Etoposide

Etoposide induced both PARP and caspase 3 cleavage in all EWS cell lines (**Figure 42**). Already 2 µM etoposide were sufficient for apoptosis induction, whereas bands were weaker upon treatment with 5 µM, which however also corresponded to decreased ß-tubulin signals in all EWS cell lines. In A673 cells some cleaved PARP and caspase 3 was already present in the solvent treated sample (**Figure 42**; lane 4). A faint band of cleaved caspase 3 also appeared in solvent treated SK-N-MC cells (**Figure 42**; lane 16). Quantification data proved a significant increase of cleaved caspase 3 and PARP in all EWS cell lines treated with 2 µM etoposide. A further increase after treatment with 5 µM etoposide was only detectable for cleaved PARP in RD-ES cells (**Figure 42**; lanes 11 - 12). In A673 cells cleavage of caspase 3 decreased by half after treatment with 5 µM etoposide compared to 2 µM etoposide (**Figure 42**; lanes 5 - 6) and an even higher decline of cleaved PARP was present in SK-N-MC cells treated with 5 µM etoposide compared to the lower dose (**Figure 42**; lanes 17 - 18). Under treatment with etoposide cleaved caspase 3 was barely detectable in any of the MSC-2014-7 samples, whereas again weak bands with higher molecular weight compared to PARP in the EWS cell lines were present in treated and non-treated MSC-2014-7 samples. However, no increase in PARP cleavage compared to the solvent treated MSC was found, as well as only a slight increase in cleaved caspase 3 in one blot with 5 µM etoposide.

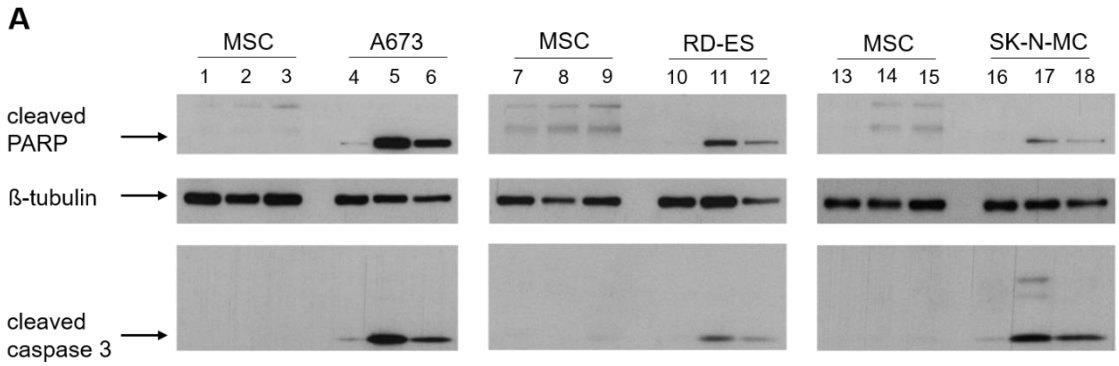

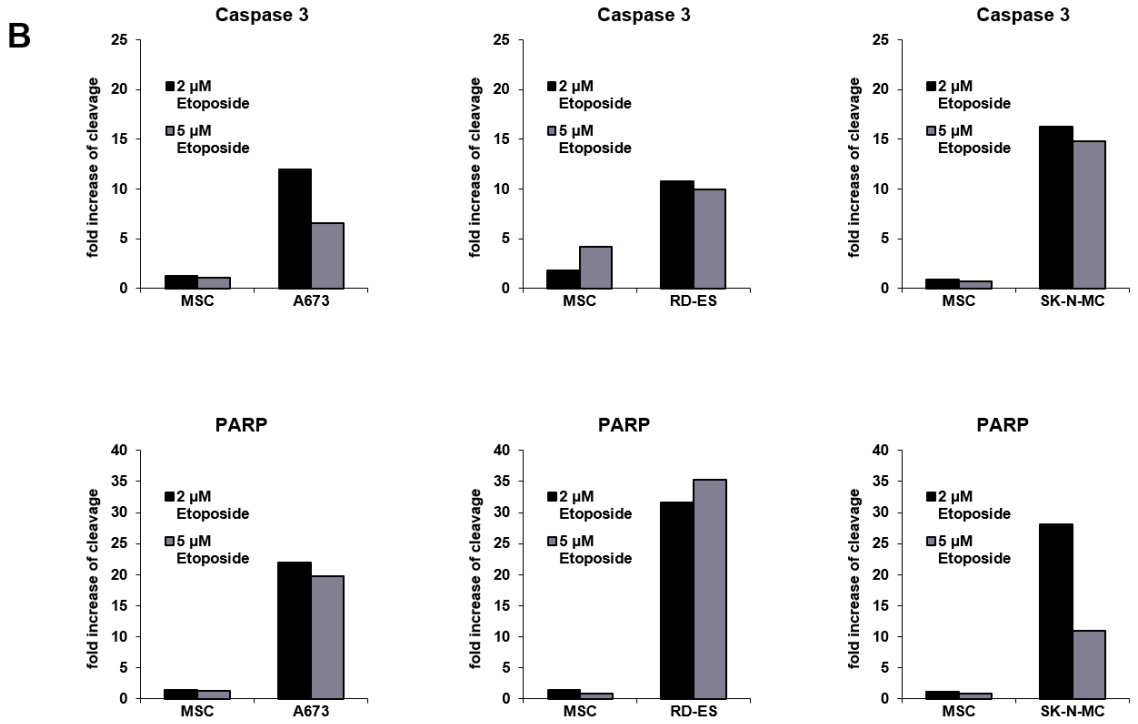

Figure 42: PARP and caspase 3 cleavage after etoposide treatment of the EWS cell lines A673, RD-ES and SK-N-MC in comparison to MSC-2014-7. *1.5 x 10^4 cells/well of A673, RD-ES, SK-N-MC or MSC-2014-7 were sown into 12-well plates. After 24 h cells were treated with 2 µM etoposide, 5 µM etoposide or the inhibitors solvent for 48 h. Proteins were isolated and their concentration was determined with Bradford assay. For the Western blot protein samples were loaded as follows: lanes 1, 7, 13: MSC-2014-7 negative control; lanes 2, 8, 14: MSC-2014-7 2 µM etoposide; lanes 3, 9, 15: MSC-2014-7 5 µM etoposide; lanes 4, 10, 16: EWS cell line negative control; lanes 5, 11, 17: EWS cell line 2 µM etoposide; lanes 6, 12, 18: EWS cell line 5 µM etoposide with lanes 4 - 6: A673, lanes 10 - 12: RD-ES and lanes 16 - 18: SK-N-MC cells. Proteins were separated by SDS-PAGE and blotted onto a PVDF membrane. Membranes were incubated with primary antibodies against ß-tubulin, cleaved PARP and cleaved caspase 3 overnight. A horseradish peroxidase-conjugated secondary antibody was used. ECL substrate was added to the membranes and chemiluminescence signals were recorded on a film. ImageJ was utilised for western blot quantification. Data presented in this figure was also published (Boehme et al., 2016 (1)).*

Doxorubicin

RD-ES and SK-N-MC cells showed very low amounts of cleaved caspase 3 (17 kDa) in doxorubicin treated samples (**Figure 43**). In A673 cells bands of the tubulin loading control were also intensified upon etoposide treatment (**Figure 43**; lanes 4 - 6). A pale band could additionally be seen in the negative control of SK-N-MC cells. Quantification showed a dose dependent increase of caspase 3 as well as PARP cleavage in all three EWS cells lines. However, the response was weak compared to etoposide. Especially 30 nM doxorubicin had comparable effects in MSC. Only after treatment with 50 nM doxorubicin the increase in both cleaved PARP and caspase 3 in EWS cells exceeded the

increase in MSC samples. In MSC-2014-7 again higher molecular weight bands were detected with the PARP antibody, but no cleaved caspase 3 (**Figure 43**). ß-tubulin was expressed in all samples with no distinct decline upon doxorubicin treatment.

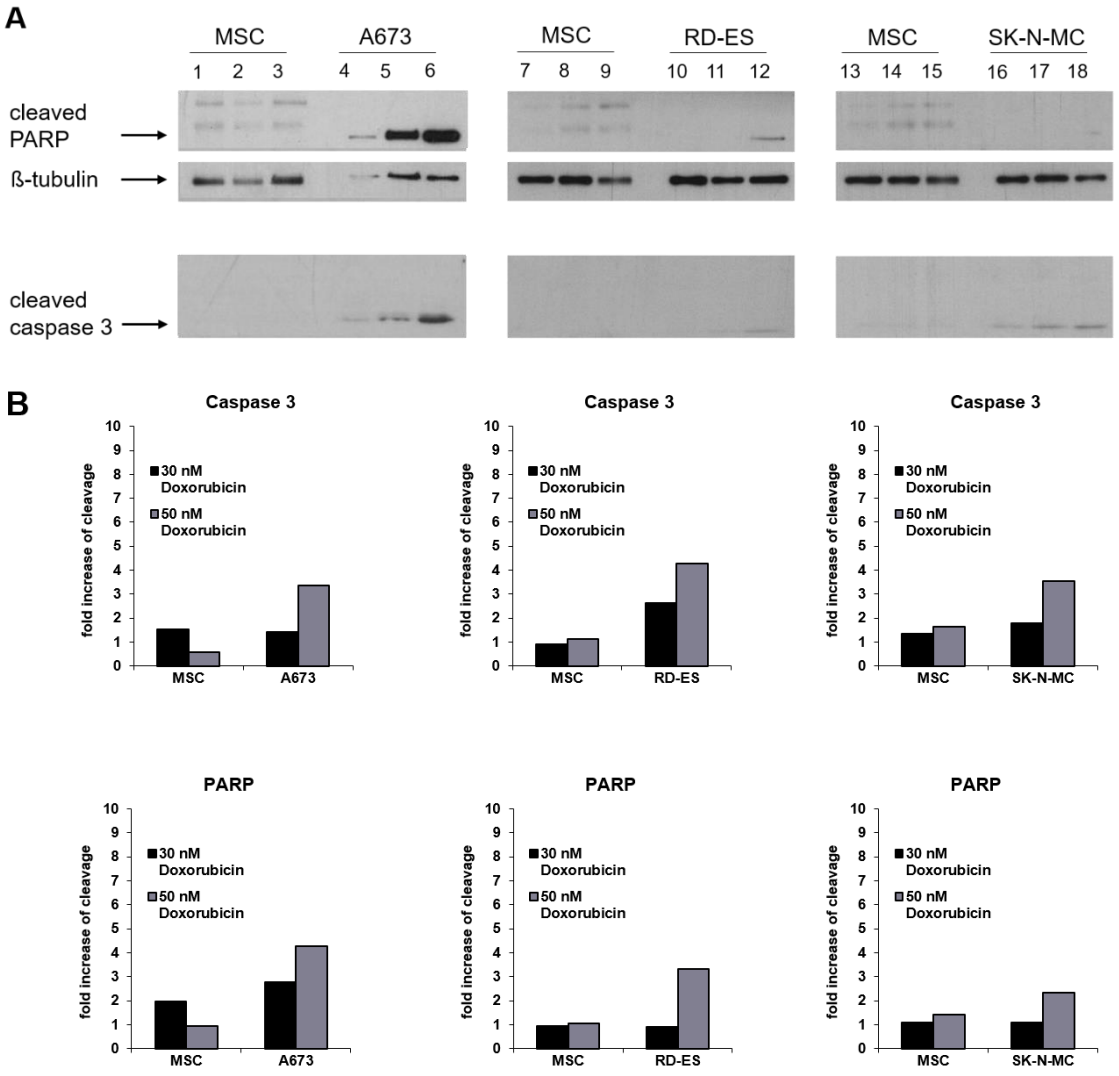

Figure 43: PARP and caspase 3 cleavage after doxorubicin treatment of the EWS cell lines A673, RD-ES and SK-N-MC in comparison to MSC-2014-7. *1.5 x 10^4 cells/well of A673, RD-ES, SK-N-MC or MSC-2014-7 were sown into 12-well plates. After 24 h cells were treated with 30 nM doxorubicin, 50 nM doxorubicin or the inhibitors solvent for 48 h. Proteins were isolated and their concentration was determined with Bradford assay. For the Western blot protein samples were loaded as follows: lanes 1, 7, 13: MSC-2014-7 negative control; lanes 2, 8, 14: MSC-2014-7 30 nM doxorubicin; lanes 3, 9, 15: MSC-2014-7 50 nM doxorubicin; lanes 4, 10, 16: EWS cell line negative control; lanes 5, 11, 17: EWS cell line 30 nM doxorubicin; lanes 6, 12, 18: EWS cell line 50 nM doxorubicin with lanes 4 - 6: A673, lanes 10 - 12: RD-ES and lanes 16 - 18: SK-N-MC cells. Proteins were separated by SDS-PAGE and blotted onto a PVDF membrane. Membranes were incubated with primary antibodies against ß-tubulin, cleaved PARP and cleaved caspase 3 overnight. A horseradish peroxidase-conjugated secondary antibody was used. ECL substrate was added to the membranes and chemiluminescence signals were recorded on a film. ImageJ was utilised for western blot quantification. Data presented in this figure was also published (Boehme et al., 2016 (1)).*

Summary

GANT61 treatment induced PARP and caspase 3 cleavage in A673 cells, whereas RD-ES and SK-N-MC were almost not compromised. ATO induced caspase 3 and PARP dependent apoptosis both in A673 and SK-N-MC cells. Neither cleaved PARP nor cleaved caspase 3 was detected in ATO treated RD-ES cells, which were however dying upon ATO treatment as determined by loss of membrane integrity (**Figure 36**). Under treatment with etoposide both cleaved PARP and caspase 3 were induced in all three EWS cell lines, whereas the effect with doxorubicin was less distinct.

3.6 Influence of ATO on GLI1 protein expression in A673, RD-ES and SK-N-MC cells in comparison to MSC

ATO has been reported to influence GLI expression in several papers. As the drug has presented a high specificity to the EWS cell lines in all experiments the influence ATO has on the GLI1 protein expression is of special interest.

Figure 44 shows GLI1 protein levels in the three EWS cell lines in comparison to MSC after treatment with two ATO concentrations. RD-ES and SK-N-MC were exposed to 2 µM and 5 µM ATO, whereas for A673, being more sensitive to ATO, 0.5 µM and 1 µM ATO were used. MSC-2014-7 cells were treated with equivalent concentrations for direct comparison. GLI1 protein levels of the negative controls were set to 100 %. Full length GLI1 protein (≥ 100 kDa) was detected in all MSC-2014-7 samples. Application of 0.5 µM (**Figure 44**; lane 2) and 1 µM ATO (**Figure 44**; lane 3) on MSC led to a slight increase of GLI1 protein abundance compared to solvent treated cells (0.5 µM ATO: 143 % and 1 µM ATO: 122 %) (**Figure 44**; lane 1). However, when treated with 2 µM (**Figure 44**; lanes 8 and 14) and 5 µM ATO (**Figure 44**; lanes 9 and 15) GLI1 abundance was reduced in MSC to 74 % or 49 % (with 2 µM ATO) and 64 % or 52 % (with 2 µM ATO). All EWS cell lines showed a significant increase in GLI1 protein under ATO treatment. In A673 cells 0.5 µM ATO induced GLI1 to 359 %, but 1 µM ATO (107 %) presented GLI1 protein levels compared to the negative control. In RD-ES and SK-N-MC both concentrations enhanced GLI1 protein levels. RD-ES cells showed more increased GLI1 abundance after treatment with the lower ATO dose of 2 µM (227 %), compared to 5 µM ATO (167 %), whereas GLI1 protein levels in SK-N-MC cells increased with rising ATO concentrations (2 µM ATO: 159 %; 5 µM ATO: 230 %).

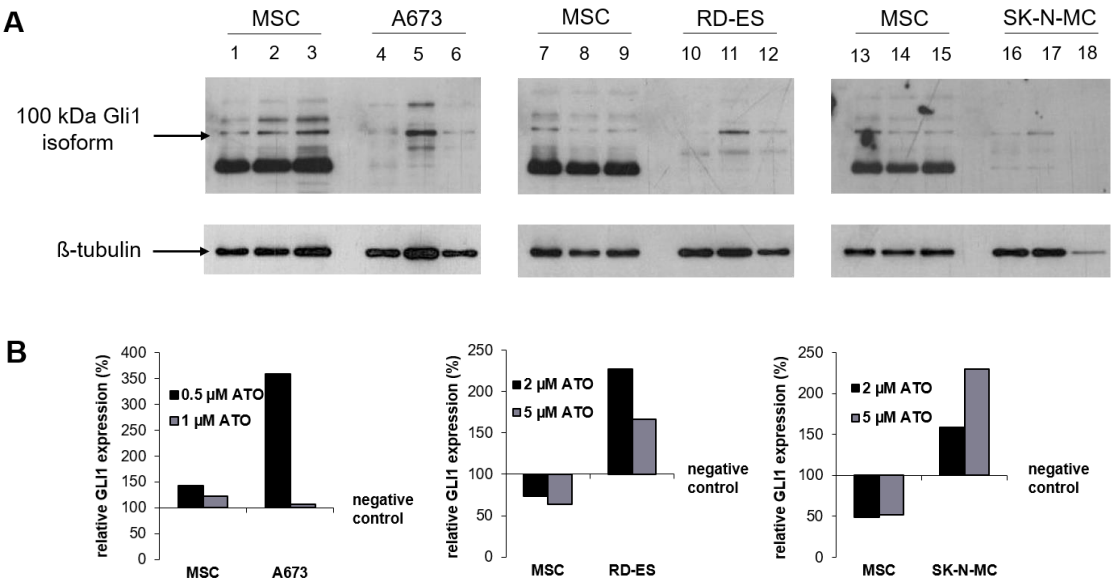

Figure 44: Expression of GLI1 protein after ATO treatment of the EWS cell lines A673, RD-ES and SK-N-MC as well as MSC-2014-7. *1.5 x 10^4 cells/well of A673, RD-ES, SK-N-MC or MSC-2014-7 were sown into 12-well plate and treated with 0.5 µM and 1 µM ATO (A673), 2 µM and 5 µM ATO (RD-ES and SK-N-MC) or the inhibitor solvent for control. After 48 h proteins were isolated and their concentration was measured with Bradford assay. For the western blot protein samples were loaded as follows: lanes 1, 7, 13: MSC-2014-7 negative control; lane 2: MSC-2014-7 0.5 µM ATO; lane 3: MSC-2014-7 1 µM ATO; lanes 8 and 14: MSC-2014-7 2 µM ATO; lanes 9 and 15: MSC-2014-7 5 µM ATO; lanes 4, 10, 16: EWS cell line negative control; lane 5: A673 0.5 µM ATO; lane 6: A673 1 µM ATO; lanes 11 and 17: RD-ES, respectively SK-N-MC 2 µM ATO; lanes 12 and 18: RD-ES, respectively SK-N-MC 5 µM ATO. Proteins were separated by SDS-PAGE and blotted onto a PVDF membrane. Membranes were incubated with the primary antibodies GLI1 rabbit mAb or tubulin rabbit mAb overnight. A horseradish peroxidase-conjugated anti-rabbit pAb was used as secondary antibody. ECL substrate was added to the membranes chemiluminescence signals were recorded on a film. ImageJ was utilised for western blot quantification.*

4 Discussion

Despite intensive therapy, mortality in patients with EWS is still very high. Even though 5-year survival rates after standard therapy of the local type of EWS are around 70 % (Esiashvili et al., 2008), patients with metastatic high-risk EWS treated with VIDE chemotherapy, which includes doxorubicin and etoposide, only show a 5-year survival of 20-30 % (Jiang et al., 2015a). Furthermore, drug resistance often occurs after first-line therapy, leading to a selection of more resistant tumour cells (May et al., 2013). Therefore, new therapeutic alternatives to the currently established chemotherapy, radiation and surgery are needed for overcoming the common drug resistance.

I focused on a new approach involving the inhibition of the Hh signalling pathway, as aberrant Hh activation has been observed in several cancers including EWS (Amakye et al., 2013; Joo et al., 2009; Kelleher et al., 2012). Aberrant Hh signalling correlates with cancer formation and progression and could lead to drug resistance by abundant expression of the ABC transporter MRP1 (Oda et al., 1997).

4.1 Hh signalling in Ewing sarcoma cell lines

The EWS-FLI1 fusion protein typically expressed in Ewing sarcoma is known to modulate the expression of genes involved in multiple signalling pathways including the Hh pathway (Taylor et al., 2011). Previous studies have identified the GLI1 protein as a direct transcriptional target of EWS-FLI1 (Beauchamp et al., 2009). As GLI1 can be specifically targeted by different inhibitors, the expression of GLI1 was of special interest in this work. Furthermore, GLI1 transcriptionally targets GLI2, which is also known to be inhibited by ATO (Raju, 2011). Therefore, GLI1 and GLI2 basal expression was analysed both at mRNA and protein levels. Moreover, the mRNA expression of additional pathway components such as GLI3, SMO and PTCH was examined.

Although Beauchamp et al. identified GLI1 as direct transcriptional target of the fusion protein EWS-FLI1 and showed its expression in several EWS cell lines including A673 (Beauchamp et al., 2009), in this work only A673 expressed significantly higher levels of GLI1 mRNA in comparison to MSC, whereas SK-N-MC presented lower levels than MSC. Moreover, the high levels of GLI1 mRNA in A673 could not be confirmed at

protein levels by western blot. However, mRNA levels are also influenced by other factors such as mRNA stability and protein expression underlies complex regulation (Payne, 2015). Therefore, differences between mRNA and protein levels are common. None of the three EWS cell lines presented higher levels of GLI1 protein compared to MSC although they are suspected to be the cells of EWS origin (Lin et al., 2011; Sand et al., 2015). Furthermore, other bands presenting lower molecular weights were found using the GLI1 antibody in all EWS cell lines and MSC, including a very dominant band running at 45 - 55 kDa in the MSC-2014-7 lane. These could represent degraded products of GLI1 with a lower molecular weight or unspecific bindings of the GLI1 antibody. However, further evaluation using antibodies binding other epitopes of GLI1 may reveal whether this band is GLI1 specific. GLI2 also initiating GLI1 transcription (Hanna and Shevde, 2016) was only slightly higher expressed at mRNA level in A673 compared to MSC whereas expression in RD-ES and SK-N-MC cells was similar to MSC. Furthermore, the elevated GLI2 mRNA levels in A673 could not be confirmed by protein expression using western blot, where all three EWS cell lines presented a significantly reduced amount of both full length GLI2 and the repressor form compared to MSC.

Even though all EWS cell lines presented lower levels of GLI1 and GLI2 protein compared to MSC this does not mean that survival and proliferation of EWS is not dependent on these proteins. The role GLI2 expression plays in EWS is currently undergoing analysis by Christensen et al., who have already found that GLI2 in EWS cells shows similar biologic effects than GLI1 and that knockdown of GLI2 compromises EWS cells (Christensen and May, 2016).

In EWS the EWS-FLI1 induced GLI1 expression appears to be independent of classical upstream stimulation of the Hh pathway. Therefore, Hh pathway inhibition upstream of GLI1 by means of SMO or PTCH1 has not been effective (Joo et al. 2009, Zwerner et al. 2008), although in this work SMO, GLI3 and PTCH1 mRNA could be found in all EWS cell lines, indicating presence of upstream pathway components.

The three EWS cell lines showed no common mRNA expression profiles of Hh pathway genes. Concerning GLI1 and GLI2 protein expression in comparison to MSC, however all EWS cell lines were comparable.

4.2 GANT61 and ATO - GLI inhibition in Ewing sarcoma

Aberrant activation of the Hh signalling pathway has been shown to correlate with the emergence of basal cell carcinoma (Bale and Yu, 2001; Johnson et al., 1996), medulloblastoma (Berman et al., 2002), RMS (Oue et al., 2013) and EWS (Beauchamp et al., 2011; Jung et al., 2006; Mathieu and Besancon, 2006; Smith et al., 2012). It has been described, that activation of the Hh pathway has influence on drug resistance mechanisms, due to the GLI-dependent regulation of ABC-transporter genes (Das et al., 2013; Singh et al., 2011). Furthermore, inhibition of the Hh pathway in cells of different cancer types has been proven to reduce proliferation and induce apoptosis in several studies (Agyeman et al., 2014; Hu et al., 2009; Rudin, 2012). As described in chapter 1.3.3 The Hedgehog pathway in Ewing sarcoma, the fusion protein EWS-FLI1 typically expressed in EWS interacts with the Hh pathway downstream of SMO and PTCH by direct transactivation of GLI1 (Beauchamp et al., 2009). Therefore, it is not surprising that the inhibition upstream of GLI1 has not been effective in EWS (Joo et al., 2009; Zwerner et al., 2008). As GLI1 and GLI2 expression could be confirmed with mRNA and on protein levels in all three EWS cell lines, direct targeting of GLI may be an option for future EWS treatment (Guo et al., 2006).

4.2.1 GANT61

GANT61 has been described to block both GLI1 and GLI2 mediated transcription (Agyeman et al., 2014; Lauth et al., 2007), thereby leading to cell cycle arrest, increased cell death as well as inhibition of DNA repair and cell migration (Gonnissen et al., 2015). These cytotoxic effects were apparent in cancer cell lines of various origin including RMS where first preclinical studies are being made (Agyeman et al., 2014; Boehme et al., 2016 (2)). With IC_{50} values of 12.01 µM (A673), 35.37 µM (RD-ES) and 59.56 µM (SK-N-MC), the EWS cell lines presented various responses to GANT61. Matsumoto et al. who also treated EWS cell lines with GANT61 achieved an IC_{50} value of 18.3 µM with SK-N-MC using MTS assays, which is significantly below the IC_{50} value for SK-N-MC in this work (Matsumoto et al., 2014). However, there were not many intermediate values in their growth curve, impeding precise results. Moreover, mutations can occur in cell lines during cultivation in vitro, by which sensitivity to drugs may differ

between laboratories and in time. Furthermore, cultivation and MTS assay procedure differed slightly from methods used in this work. In 3D spheroid culture both SK-N-MC and A673 were resistant to treatment up to 15 µM GANT61 and both RD-ES and SK-N-MC were barely compromised in their ability to form colonies. Neither EWS cell lines nor MSC presented significant levels of cell death in flow cytometry using 15 µM GANT61 and both RD-ES and SK-N-MC presented no PARP or caspase 3 cleavage.

Indeed, RD-ES and SK-N-MC to GANT61 have low protein levels of GLI1 and GLI2 compared to MSC as described in chapter 4.1. As GANT61 is a GLI1 and GLI2 inhibitor, high levels of these proteins may correlate with a higher sensitivity of cellular metabolism to this drug. This has already been shown in other studies with several tumours, including RMS (Srivastava et al., 2014), neuroblastoma (Wickström et al., 2013) and lung cancer (Huang et al., 2014).

Interestingly, only the EWS cell line A673 showed cleaved PARP and cleaved caspase 3 bands upon GANT61 treatment and was also the only cell line that was more sensitive in the MTS assay compared to the control cells MSC. Furthermore, A673 were significantly compromised using doses of GANT61 below 20 µM in colony growth. Equal results concerning A673 were made by Joo et al. with GANT58 which inhibited anchorage independent growth in A673 cells with doses of 5 µM GANT58 (Joo et al., 2009). As A673 showed GLI protein levels comparable to RD-ES and SK-N-MC, the higher sensitivity is not explained by this. For some reason A673 may be more dependent on availability of functional GLI1 and GLI2 proteins or off-target effects might play a significant role in this cell line. For instance, Geng et al. found GANT61 to down-regulate p-STAT3 and SOCS3 and thereby induce anti-tumour efficacy in T-cell lymphoma cells (Geng et al., 2016). Additionally, GANT61 induced apoptosis can also be dependent on an increased release of ROS from the mitochondria (Gonnissen et al., 2015; Lim et al., 2015). However, cell death was not observed in GANT61 treated A673 cells by flow cytometry, although PARP and caspase 3 cleavage was present.

As GANT61 did not selectively compromise the EWS cell lines in either viability, colony formation or apoptosis compared to MSC, the substance was not included in later analysis of combined treatment.

4.2.2 ATO

ATO has been described to interact with both GLI1 and GLI2, thereby mediating degradation of the GLI proteins which prevents the activation of GLI1 and GLI2 target genes (Beauchamp et al., 2011; Kim et al., 2013), leading to cell cycle arrest, increased death of cells and viability loss. These cytotoxic effects were apparent in various cancers including EWS. *In vitro* tests by Zhang et al. using ATO in A673 and RD-ES cells led to an inhibition of migration and invasion (Zhang et al., 2012) and even an EWS xenograft model was compromised by ATO (Beauchamp et al., 2011; Kim et al., 2010). However, other *in vivo* studies found no significant ATO effect on EWS xenografts (Smith et al., 2012). As both ATO and GANT61 are known to inhibit GLI1 and GLI2, the different results obtained using these two inhibitors were surprising.

Indeed, all EWS cell lines were significantly more sensitive to ATO in the MTS assay than MSC whose viability was barely compromised even using doses as high as 10 µM ATO. This indicates that ATO presents a high specificity for EWS cells. Both A673 and RD-ES acquired IC_{50} values blow 2 µM, whereas SK-N-MC cells were more resistant with a half maximal inhibitory concentration of 4.42 µM. Equal results concerning A673 and RD-ES were made by Beauchamp et al. with ATO in a WST-1 viability assay were both cell lines reached IC_{50} values below 1 µM (Beauchamp et al., 2011). Comparable results with ATO were also demonstrated previously with RMS cell lines in comparison to primary skeletal muscle cells (SKMC) in the laboratory of cell biology of the department of orthopaedic surgery (Boehme et al., 2016 (2)).

Concerning colony formation, doses of ATO required for significantly compromised colony formation were only slightly lower compared to the MTS assay. In 3D spheroid culture already the use of 2 µM ATO resulted in a sufficient growth inhibition and destabilisation of A673 and SK-N-MC cultures. To investigate the ability of ATO to induce cell death in EWS cell lines flow cytometry analysis was performed. Cell death was highly present in all EWS cell lines, whereas MSC presented no dying cells. However, SK-N-MCs needed 5 µM ATO for high rates of cell death which is the maximal achieved plasma level for ATO in leukaemia patients (Au et al., 2008). To confirm that cell death was actually caused by apoptosis, levels of cleaved PARP and cleaved caspase 3 were analysed and quantified. ATO induced caspase 3 dependent apoptosis

both in A673 and SK-N-MC cells. However, neither cleaved PARP nor cleaved caspase 3 was detected in ATO treated RD-ES cells, which were nevertheless dying as determined by loss of membrane integrity. This indicates that induction of apoptosis upon ATO in RD-ES could be dependent on other caspases or that RD-ES turn to necrosis instead. Furthermore, Kondo et al. provided evidence that the apoptosis-inducing factor (AIF), which is commonly known to be released from the mitochondria by PARP can also be induced PARP-independently in neuronal cells by α-eleostearic acid (α-ESA), a trienoic fatty acid and thereby induce apoptosis independently of PARP (Kondo et al., 2010). Further experiments are required for investigating this.

The high sensitivity of the EWS cell lines to ATO, whereas GANT61 was neither efficient nor selective, cannot be explained by GLI protein expression. It is possible that EWS are more dependent on GLI1 and GLI2 protein function compared to MSC. However, both inhibitors target GLI proteins. Therefore, off target effects of ATO might be involved the high sensitivity of the EWS cell lines and their individual reaction to ATO. So far MAPK inhibition, breakdown of mitochondrial membrane potential and subsequent ROS release leading to apoptosis, necrosis, autophagy or differentiation have been found to be influenced by ATO (Mathieu and Besancon, 2006; Zhao et al., 2015). Also discussed as potentially involved in differential ATO response is the expression of aquaporin 9 (AQP9), a water-selective membrane channel responsible for the uptake of ATO into the cell. Therefore, cells with high expression of AQP9 can be more sensitive to the drug (Iriyama et al., 2013; Leung et al., 2007). Additionally, p53 mutations detected in all of the EWS cell lines examined and loss of p16/p14 in A673 cells may interfere with drug sensitivities and the ability to undergo apoptosis (May et al., 2013). Differences in the degradation and secretion of ATO as well as further targets could also play a significant role. As shown by Mathieu and Besancon as well as Zhang et al. the EWS-FLI1 fusion protein abundance was not affected by ATO application (Mathieu and Besancon, 2006; Zhang et al., 2012). The wide range of possible causes for the contradictory sensitivity of the EWS cell lines to GANT61 and ATO and their correlation to GLI1 and GLI2 protein expression need to be further investigated.

4.3 Etoposide and doxorubicin sensitivity of Ewing sarcoma cells

4.3.1 Etoposide

As shown in previous studies etoposide treatment of HeLa cells and *in vivo* experiments with human tumour cells treated with etoposide, led to cell cycle arrest and therefore inhibition of proliferation (Loike and Horwitz, 1976a; Loike and Horwitz, 1976b; Stahelin, 1973). I treated three EWS cell lines (A673, RD-ES and SK-N-MC) as well as healthy MSC with a range of etoposide concentrations between 0.5 µM and 10 µM. The EWS cell lines all showed a significant decrease in viability with IC_{50} values ranging between 0.88 µM (A673) and 1.11 µM (SK-N-MC), with A673 cells being the most sensitive, whereas MSC seemed to be largely resistant to all etoposide doses applied. A study by May et al. also using A673 and SK-N-MC cells, shows similar results concerning the sensitivity of these two cell lines to etoposide. In a DIMSCAN cytotoxicity assay IC_{99} values of SK-N-MC (~6.8 µM etoposide) and A673 (<0.2 µM etoposide) showed that A673 cells are significantly more sensitive to etoposide than SK-N-MC (May et al., 2013). In this work the difference between A673 and SK-N-MC cells was not as significant, which could be due to the different assays used. However, all EWS cell lines were sensitive to etoposide in comparison to the slow growing MSC, which confirms that etoposide primarily targets fast growing cells.

Considering colony formation (chapter 3.3.2), A673 cells were less sensitive than RD-ES and SK-N-MC. However, all EWS cell lines already showed significantly reduced colony formation with lower doses of etoposide compared to MTS assays. These results are in agreement with previous studies using EWS (Fong et al., 2013) where it has been shown that the gene expression profile can vary with cell density. Therefore, lower cell densities as present in the clonogenic assay may increase sensitivity towards etoposide, whereas higher cell densities such as in the MTS assay may lead to lower drug sensitivity compared to colony formation. Moreover, MTS assays measure the activity of cellular metabolism in a collective of cells, whereas colony formation assays determine the ability of individual cells to proliferate and not only to survive.

Even higher etoposide concentrations up to 2 µM were needed for a significant suppression of growth in 3D spheroid culture of A673 and SK-N-MC. Here, SK-N-MCs presented themselves more sensitive to etoposide compared to A673. The increased drug

doses needed in 3D growth could be due to decreased drug penetration as well as an increase of cell-cell contacts in 3D structure, leading to mediation of pro-survival signals and less contact to the culture medium.

Proliferation and viability were reduced by etoposide in all EWS cell lines examined. Etoposide as a chemotherapeutic agent is interacting with topoisomerase II in proliferating cells. This leads to cell cycle arrest and an accumulation of DNA strand breaks which then activate the apoptotic pathway (Karpinich et al., 2002; Meresse et al., 2004). To examine the induction of cell death in etoposide-treated cells two methods were used. With flow cytometry the uptake of the fluorescent dye eFluor ® 450 was measured confirming the destabilisation of the cell membrane (compare chapter 3.5.1). Furthermore, to confirm that apoptosis was occurring, the amount of cleaved caspase 3 and cleaved PARP was analysed using western blot (compare chapter 3.5.2). With more than 50 % eFlour® 450 positive cells after treatment with 1 µM etoposide, A673 cells presented themselves as the most sensitive in flow cytometry. Both RD-ES and SK-N-MC also showed etoposide induced dye uptake, whereas the cell membrane in MSC appeared to be unaffected by any of the etoposide doses applied. Apoptosis could be confirmed in all three EWS cell lines, by both PARP and caspase 3 cleavage. In MSC cleaved caspase 3 was hardly detectable and only low amounts of higher molecular weight bands running above 116 kDa were found with the PARP antibody. As the molecular weight of full length PARP is 116 kDa these bands may represent binding of full length PARP or unspecific binding by the PARP antibody. Interestingly, these bands are only present in MSC samples, regardless of the substance used, which could indicate a modification in the antibody binding site of the full length PARP in MSC which permits binding in the absence of cleavage. Altogether, etoposide induced reduced proliferation and viability as well as apoptosis could be observed in all three EWS cell lines, whereas MSC seemed to be largely unaffected.

4.3.2 Doxorubicin

As shown in previous studies treatment of cells with doxorubicin inhibits nuclear DNA replication and RNA synthesis by binding of topoisomerase II, thus equally to etoposide leading to a cell cycle arrest and subsequent apoptosis (Minotti et al., 2004; Potmesil et al., 1984). The EWS cell lines and MSC were treated with a range of doxorubicin doses between 10 nM and 120 nM, resulting in a significant decrease of EWS cell viability with IC_{50} values ranging between 27.18 nM (A673) and 115 nM (RD-ES). Although, treatment with 150 nM doxorubicin also reduced the viability of MSC to 68.6 %, all EWS cell lines were more sensitive. A study by May et al. also using A673 and SK-N-MC cells, shows similar results concerning the range of doxorubicin applied in these two cell lines. In their cytotoxicity assay IC_{99} values of SK-N-MC (~12.0 nM doxorubicin) and A673 (~21.7 nM doxorubicin) showed that there SK-N-MC were slightly more sensitive than A673 (May et al., 2013), whereas in this work A673 were the most sensitive EWS cell line to doxorubicin. During colony formation doxorubicin affected all three EWS cell lines to the same extent with only 15 nM doxorubicin being sufficient to inhibit colony formation completely which is significantly below the IC_{50} values achieved in the MTS assay. As with etoposide (compare chapter 4.3.) the lower cell densities in the clonogenic assay may contribute to the increased sensitivity towards doxorubicin compared to the sensitivity in the MTS assay with higher cell densities. Similar again to etoposide, higher doxorubicin concentrations up to 50 nM were needed for a significant suppression of 3D spheroid culture growth of SK-N-MC and A673, as drug penetration of cells in 3D structure can be reduced due to a smaller outside-surface as well as different cell-cell contacts (Fong et al., 2013). Interestingly, A673 cell were significantly less sensitive to doxorubicin compared to SK-N-MC in 3D spheroid cultures in contrast to viability assays and colony formation assays. Both flow cytometry analysis and western blot were again used for confirmation of cell death and apoptosis. In accordance with the viability assay A673 cells presented themselves as most sensitive to doxorubicin in flow cytometry. Both RD-ES and SK-N-MC also showed dose dependent doxorubicin-induced dye uptake, whereas the cell membranes of MSC appeared to be unaffected by any doxorubicin doses applied. The restricted viability reduction of the SK-N-MC cell line compared to A673 might be explained by a previous doxorubicin treatment of the patient from whom SK-N-MCs were obtained (May et al., 2013). However, RD-ES cells showed an even

more limited response in the MTS assays, while previous doxorubicin treatment is not reported for the donor of RD-ES. Only A673 cells presented clear cleaved PARP and caspase 3 bands whereas traces of cleaved PARP and caspase 3 could be found in RD-ES and SK-N-MC. However, quantification normalised to tubulin expression showed low amounts of cleaved caspase 3 and PARP induction in all EWS cell lines especially using the higher dose of 50 nM doxorubicin. In MSC cleaved caspase 3 was barely detectable and only the previously described low amounts of a higher molecular weight band running with the PARP antibody were found. Altogether, reduced proliferation and viability as well as induced cell death could be observed in all three EWS cell lines. Apoptosis by means of cleaved PARP or cleaved caspase 3 was present in all three EWS cell lines. But also other mechanisms might contribute to cell death induction.

4.4 Effectiveness of ATO combinations with the cytostatics etoposide and doxorubicin

As multidrug resistance occurs in 30 % of patients with localised EWS after first line treatment further therapeutic options are required (May et al., 2013). Development of multidrug resistance is based on several cellular events such as enhanced repair of damage and thereby inhibition of apoptosis or failure to undergo cell cycle arrest, enhancing the efflux or exclusion of the applied cytostatic drug as well as their degradation, failure to activate prodrugs or alterations of the drug targets (Melguizo et al., 2011; Tan et al., 2000). One of the mechanism increasing the efflux of drugs overexpression of multidrug transporters such as MRP1 which is also known to be abundantly expressed in EWS (Oda et al., 1997) and also in all three EWS cell lines used in this work (Boehme et al., 2016 (1)). Furthermore, MRP1 can be transcriptionally targeted by GLI1 (Santisteban, 2010), which leads to the assumption that GLI1 inhibition could reduce MRP1 expression and therefore reverse resistance of EWS cells to MRP1 substrates such as etoposide or doxorubicin which were both used in this work.

Since GANT61 was not inducing cell death and additionally was not selective between MSC and the EWS cell lines tested concerning viability reduction, it was excluded from combination experiments. ATO significantly and specifically compromised viability, colony formation and growth in 3D culture as well as apoptosis induction. Additionally,

ATO has already been shown to reduce doxorubicin resistance in osteosarcoma by downregulation of stathmin expression (Feng et al., 2014) which is a regulatory protein in the assembly of the mitotic spindle (Rubin and Atweh, 2004). Furthermore, first potential additive effects were described after a combination with etoposide in EWS patients (Guo et al., 2006). Interestingly, the Arsenic-GSH conjugate is itself a substrate to MRP1 which means that MRP1 overexpression might also lead to resistance against ATO (Leslie et al., 2004). Therefore, ATO was combined with both etoposide and doxorubicin and potential additive effects were examined. Based on the individual drug sensitivities of each cell line the doses for combined treatment were selected and applied in different combinations.

Upon combination of etoposide with ATO the viability assay showed additive effects in all three EWS cell lines tested, whereas MSC were barely compromised. However, sensitivity to the individual drugs and combinatorial effects differed between the cell lines. In RD-ES and SK-N-MC cells 0.5 µM etoposide combined with ATO were sufficient to decrease viability significantly compared to single treatment and showed similar results in cell death analysis. A673 being extremely sensitive to ATO showed no significant cell death induction with 0.1 µM ATO combined with 1 µM etoposide. However, viability was significantly reduced. Furthermore, suppression of colony formation was reinforced in all three EWS cell lines with a combination of etoposide and ATO in comparison to single treatment. However, for an exact statement concerning significance, a quantification of colony growth would be necessary. Summarised, the combination of etoposide and ATO potentiated the effect of single treatments with etoposide or ATO in the EWS cell lines, only concerning cell death in A673 cell the effect of etoposide dominated.

Combined treatment of the EWS cell lines with doxorubicin and ATO significantly potentiated the suppression of colony formation achieved by single drug application. In addition, slightly additive effects on the inhibition of viability in all three EWS cell lines could be observed, whereas MSC again were barely compromised. Cell death was only efficiently increased compared to single treatment in A673 cells with the combination of 5 nM doxorubicin and 0.3 µM ATO, whereas RD-ES and SK-N-MC cells did not present any additive effects concerning loss of membrane integrity.

A triple treatment with both etoposide and doxorubicin as well as ATO could neither clearly enhance cell death nor compromise viability further compared to the combination of two drugs. However, later experiments in the laboratory achieved lowest number of colonies after application of the triple treatment in RD-ES and SK-N-MC (Boehme et al., 2016 (1)).

4.5 Conclusion and future outlook

In this work it could be shown that the EWS cell lines A673, RD-ES and SK-N-MC were highly sensitive to ATO which is known to inhibit GLI1 and GLI2. However, none of the EWS cell lines showed an over-expression of GLI1 or GLI2 protein compared to MSC, indicating that EWS are highly dependent on the small amount of residual GLI proteins or that off target effects of ATO may play a significant role. Moreover, the second GLI inhibitor GANT61 was inefficient, also indicating that GLI inhibition in these EWS cell lines might not be crucial, leading to the assumption that ATO might also work by other means. Off target effects of ATO may include interactions with different zinc finger proteins leading to an inhibition of tumour growth in APL (Nasr et al., 2008). Furthermore, ATO also inhibits MAPK and leads to ROS release from the mitochondria (Mathieu and Besancon, 2006; Zhao et al., 2015). For further investigation of the mechanism of action of ATO in EWS as well as the crosslink to etoposide and doxorubicin sensitivity, a wider spectrum of EWS cell lines would be of interest where also ROS release, MAPK inhibition and influence on drug transporter expression should be analysed. Especially, the application of ATO in combination with etoposide presented additive effects in RD-ES and A673 cell lines, so that this combination may be an option for chemo-resistant EWS *in vivo*, which should be tested in a mouse model. Negative side-effects could be reduced by combination as individual drug doses could be diminished. So far, the combination of etoposide and doxorubicin was not analysed in comparison. To rule out that effects seen upon triple treatment are mainly mediated by this combination it should be included in further analysis. In the meantime, combination treatment was also tested in 3D spheroid cultures showing that the impact of etoposide is dominating (Boehme et al., 2016 (1)). As the effect of applied drugs in the spheroid cultures was so far only evaluated by shape, size and surface integrity a quantitative analysis of the viability of all cells in the spheroids should be strived for. This could be obtained by measuring the acid phosphatase enzyme activity using 4-nitrophenyl

phosphate as described by Friedrich et al. (Friedrich et al., 2009; Ivanov et al., 2014). The spheroid assay has presented a first simulation of the conditions inside a tumour. Another aspect of 3D growth is hypoxia, which still has to be examined with the EWS cell lines and the drugs etoposide, doxorubicin and ATO as well as with *in vivo* experiments after that.

Furthermore, etoposide and doxorubicin are only two of several cytostatic drugs which are used in therapy for EWS. Vincristine also belonging to the standard first line therapy in Europe for localised EWS (Balamuth and Womer, 2010; Juergens et al., 2006) could be included in experiments with ATO combination as well as cyclophosphamide and ifosfamide, which may be investigated in *in vivo* experiments as they, being anticancer prodrug substances metabolised by several P450 enzymes, cannot be activated during *in vitro* culture (Chen et al., 2004). Furthermore, the mode of action connecting decreased chemo-resistance with ATO is of future interest. Therefore, chemo-resistant cell lines, for instance generated by gradually increasing drug doses over months should also undergo ATO treatment. Furthermore, the expression of ABC transporters in EWS cell lines compared to MSC should be tested after application of ATO both at mRNA and protein levels. Thereby, MRP1 is of special interest as it is known to be aberrantly expressed in EWS and is a target of GLI1 (Boehme et al., 2016 (1); Santisteban, 2010). Moreover, the ABC transporters ABCA6 and ABCA7 also play a role in EWS progression (Pasello, 2015) as well as MDR1 (Oda et al., 1997) and potential changes of expression upon ATO treatment are possible. Furthermore, cell lines with an inherent or experimentally induced over- or under-expression of these transporters could be selectively tested on any correlating resistances against etoposide and doxorubicin as well as the ability of ATO to reduce these in combined treatment. Therefore, knockdown experiments targeting these transporters in the EWS cell lines could be used. Possibly, also a combination with other substances tested for targeted therapy in EWS might show further additive effects. Currently, substances targeting the epidermal growth factor, vascular growth factor receptors, mammalian target of rapamycin, IGF1R, PARP1 and EWS-FLI1 are all in clinical or preclinical testing (Bagatell et al., 2014; Daw et al., 2005; Fox et al., 2010; Jiang et al., 2015b; Schwartz et al., 2013).

For more exact insights in the conditions inside the tumour and before potential clinical testing, drug combinations should be analysed *in vivo*. A mouse model has already been established by Beauchamp et al. (Beauchamp et al., 2011).

5 Abstract

Ewing sarcoma (EWS) are mesenchymal tumours usually occurring in children and adolescents. Currently, patients with non-metastatic EWS show 5-year survival rates above 70 % when treated radically with surgery, chemotherapy and radiotherapy, whereas relapsed or metastasised EWS are more difficult to treat. One of many reasons is the increasing drug resistance in relapsed EWS including the expression of ABC transporters such as PGP or MRP1 which transport cytostatic drugs back through the cell membrane into the extracellular matrix. Furthermore, EWS express the characteristic EWS-FLI1 fusion protein which also modulates the GLI proteins in the Hedgehog (Hh) pathway. Aberrant Hh-signalling has been observed in several malignancies including EWS and correlates with cancer formation and progression. As the Hh pathway directly targets expression of ABC transporter proteins, GLI inhibition as additional therapeutic option to overcome multi drug resistance was investigated. In the present study viability, colony formation, growth of 3D cultures and induction of cell death was analysed in three EWS cell lines treated with the GLI inhibitors GANT61 and ATO as well as the established cytostatics etoposide and doxorubicin using MTS assay, clonogenic assay, 3D spheroid assay, flow cytometry and western blot. ATO, etoposide and doxorubicin reduced viability significantly and selectively in all three EWS cell lines in comparison to mesenchymal stem cells (MSC). On the other hand, GANT61 was less efficient in two of three EWS cell lines and particularly not selective compared to MSC. Cell death was induced by ATO, etoposide and doxorubicin in all three EWS cell lines, but not MSC. The combination of ATO and etoposide potentiated this effect. The combined application of ATO and doxorubicin also significantly compromised viability compared to individual treatment. However, a triple combination of ATO with both cytostatics did not compromise cells more than the double combinations. The present results indicate that ATO is effective in EWS. Therefore, ATO may contribute to increased survival rates of patients with EWS and especially reduce resistance of aggressive EWS against chemotherapeutics. Furthermore, as doses for drugs can be reduced in combined treatment, adverse effects of chemotherapy may be diminished. However, further evaluation of the detailed inhibitory mechanisms in EWS is needed before transferring this approach to the clinic.

6 Zusammenfassung

Ewing Sarkome (EWS) zählen zu den mesenchymalen Tumoren und treten gehäuft bei Kindern und Jugendlichen auf. Patienten mit nicht-metastasiertem EWS, die sich einer radikalen chirurgischen Intervention, Radiotherapie und/oder Chemotherapie unterziehen, zeigen eine durchschnittliche 5-Jahres Überlebensrate von über 70 %, wohingegen metastasierte und rezidivierte EWS deutlich schwerer zu behandeln sind. Einer der vielen Gründe dafür ist die zunehmende Resistenz von rezidivierten EWS gegen Chemotherapeutika. Diese beruht unter anderem darauf, dass ABC Transporter wie PGP oder MRP1, welche die Chemotherapeutika wieder aus der Tumorzelle in den Extrazellularraum befördern, von diesen exprimiert werden. Darüber hinaus wird vom EWS das für den Tumor charakteristische Fusionsprotein EWS-FLI1 exprimiert, welches auch die GLI Proteine im Hedgehog (Hh) Signalweg moduliert. Veränderungen im Hh Signalweg wurden bereits in verschiedenen Tumoren beobachtet und korrelieren mit einer erhöhten Tumorbildung und Progression. Da der Hh Signalweg direkt die Expression von ABC Transportern beeinflusst, wurde in dieser Arbeit die Inhibition der GLI Proteine als mögliche zusätzliche Therapieoption zur Unterdrückung der Chemoresistenz getestet. Dafür wurden drei EWS Zelllinien mit den GLI Inhibitoren GANT61 und ATO, sowie den bereits etablierten Chemotherapeutika Etoposid und Doxorubicin behandelt und ihre Viabilität, Koloniebildungsfähigkeit, Wachstum in 3D Kulturen und Induktion von Zelltod mittels MTS Assay, Koloniebildungs-Assay, 3D Spheroid Assay, Durchflusszytometrie und Western Blot getestet. ATO, Etoposid und Doxorubicin reduzierten die Viabilität signifikant und selektiv in allen drei EWS Zelllinien im Vergleich zu mesenchymalen Stammzellen (MSC). Dahingegen war GANT61 weniger effizient in zwei der drei EWS Zelllinien und vor allem nicht selektiv gegenüber MSC. Zelltod konnte durch ATO, Etoposid und Doxorubicin in allen EWS Zelllinien, nicht aber in MSC induziert werden. Dieser Effekt wurde mit der Kombination von ATO und Etoposid noch einmal potenziert. Die Kombination von ATO und Doxorubicin reduzierte die Viabilität ebenfalls signifikant, verglichen mit der Einzelgabe. Eine dreifache Kombination aus ATO, Etoposid und Doxorubicin zeigte jedoch keinen zusätzlichen Nutzen im Vergleich zu den Zweifach-Kombinationen. Die bisherigen Ergebnisse deuten darauf hin, dass ATO zur Erhöhung der Überlebensraten von EWS

Patienten und zur Reduzierung von Resistenzen gegen Chemotherapeutika in aggressiven EWS beitragen kann. Durch die reduzierte Dosis der kombinierten Substanzen können Nebenwirkungen der Chemotherapeutika vermindert werden. Vor einem potenziellen klinischen Einsatz werden allerdings weitere Informationen über die detaillierten Wirkmechanismen in EWS benötigt.

7 List of Figures

1. Mechanism of the Hedhehog pathway 13
2. Molecular structure of GANT61 18
3. Molecular structure of Arsenic trioxide 19
4. Molecular structure of etoposide 21
5. Molecular structure of doxorubicin 23
6. Light micrographs of A673 cells during routine cell culture 24
7. Light micrographs of RD-ES cells during routine cell culture 25
8. Light micrographs of SK-N-MC cells during routine cell culture 26
9. Light micrographs of MSC-2014-7 cells during routine cell culture 26
10. SDS-PAGE band profile of the PageRuler Prestained Protein Ladder 38
11. Relative expression of Hedgehog pathway genes in EWS cell lines A673, RD-ES and SK-N-MC in comparison to MSC-2014-7 54
12. Expression of GLI1 protein in EWS cell lines A673, RD-ES and SK-N-MC as well as MSC-2014-7 55
13. Expression of GLI2 protein in the EWS cell lines A673, RD-ES and SK-N-MC as well as MSC-2014-7 56
14. Effect of GANT61 on the viability of EWS cell lines A673, RD-ES and SK-N-MC in comparison to MSC 57
15. Effect of ATO on the viability of the EWS cell lines A673, RD-ES and SK-N-MC in comparison to MSC 58
16. Effect of etoposide on the viability of the EWS cell lines A673, RD-ES and SK-N-MC in comparison to MSC 59
17. Effect of doxorubicin on the viability of the EWS cell lines A673, RD-ES and SK-N-MC in comparison to MSC 59
18. Effect of combined etoposide and ATO treatment on the viability of the EWS cell lines A673, RD-ES and SK-N-MC 62
19. Effect of combined etoposide and ATO treatment on the viability of MSC-2014-7 control cells 63

20. Effect of combined doxorubicin and ATO treatment on the viability of the EWS cell lines A673, RD-ES and SK-N-MC 66
21. Effect of combined doxorubicin and ATO treatment on the viability of MSC-2014-7 control cells 66
22. Effect of combined etoposide, doxorubicin and ATO treatment on the viability of the EWS cell lines A673, RD-ES and SK-N-MC 68
23. Effect of combined etoposide, doxorubicin and ATO treatment on the viability of MSC-2014-7 control cells 69
24. Clonogenic assay of the EWS cell lines A673, RD-ES and SK-N-MC treated with GANT61 70
25. Clonogenic assay of the EWS cell lines A673, RD-ES and SK-N-MC treated with ATO 71
26. Clonogenic assay of the EWS cell lines A673, RD-ES and SK-N-MC treated with etoposide 72
27. Clonogenic assay of the EWS cell lines A673, RD-ES and SK-N-MC treated with doxorubicin 73
28. Clonogenic assay of the EWS cell lines A673, RD-ES and SK-N-MC treated with a combination of etoposide and ATO 74
29. Clonogenic assay of the EWS cell lines A673, RD-ES and SK-N-MC treated with a combination of doxorubicin and ATO 75
30. 3D spheroid formation of the EWS cell lines A673, RD-ES and SK-N-MC 76
31. Effect of GANT61 on A673 and SK-N-MC cells growing in 3D spheroid cultures 77
32. Effect of ATO on A673 and SK-N-MC cells growing in 3D spheroid cultures 78
33. Effect of etoposide on A673 and SK-N-MC cells growing in 3D spheroid cultures 79
34. Effect of doxorubicin on A673 and SK-N-MC cells growing in 3D spheroid cultures 80

35. Effect of GANT61 on cell death induction in the EWS cell lines A673, RD-ES and SK-N-MC in comparison to MSC-2014-7 82
36. Effect of ATO on cell death induction in the EWS cell lines A673, RD-ES and SK-N-MC in comparison to MSC-2014-7 84
37. Effect of etoposide on cell death induction in the EWS cell lines A673, RD-ES and SK-N-MC in comparison to MSC-2014-7 85
38. Effect of doxorubicin on cell death induction in the EWS cell lines A673, RD-ES and SK-N-MC in comparison to MSC-2014-7 86
39. Effect of combined treatment with etoposide, doxorubicin and ATO on cell death induction in the EWS cell lines A673, RD-ES and SK-N-MC in comparison to MSC-2014-7 88
40. PARP and caspase 3 cleavage after GANT61 treatment of the EWS cell lines A673, RD-ES and SK-N-MC in comparison to MSC-2014-7 91
41. PARP and caspase 3 cleavage after ATO treatment of the EWS cell lines A673, RD-ES and SK-N-MC in comparison to MSC-2014-7 92
42. PARP and caspase 3 cleavage after etoposide treatment of the EWS cell lines A673, RD-ES and SK-N-MC in comparison to MSC-2014-7 94
43. PARP and caspase 3 cleavage after doxorubicin treatment of the EWS cell lines A673, RD-ES and SK-N-MC in comparison to MSC-2014-7 95
44. Expression of GLI1 protein after ATO treatment of the EWS cell lines A673, RD-ES and SK-N-MC as well as MSC-2014-7 97

8 List of Tables

1. Cell culture 27
2. Cytostatics and Inhibitors 28
3. Stock solutions 28
4. Devices 28
5. Disposables 30
6. Chemicals 32
7. Kits and enzymes 35
8. Oligonucleotides 35
9. Antibodies 37
10. Software 38
11. qRT-PCR program 43
12. Composition of SDS gels (sufficient for 4 gels) 49
13. IC_{50} values of the EWS cell lines A673, RD-ES and SK-N-MC compared to the control cells MSC-2014-7 after treatment with ATO, GANT61, etoposide or doxorubicin 60

9 Literature

Agyeman, A., B.K. Jha, T. Mazumdar, and J.A. Houghton. 2014. Mode and specificity of binding of the small molecule GANT61 to GLI determines inhibition of GLI-DNA binding. *Oncotarget* 5:4492-4503.

Aisner, J., and E.J. Lee. 1991. Etoposide. Current and future status. *Cancer* 67:215-219.

Amakye, D., Z. Jagani, and M. Dorsch. 2013. Unraveling the therapeutic potential of the Hedgehog pathway in cancer. *Nat Med* 19:1410-1422.

Arcamone, F., G. Cassinelli, G. Fantini, A. Grein, P. Orezzi, C. Pol, and C. Spalla. 1969. Adriamycin, 14-hydroxydaunomycin, a new antitumor antibiotic from S. peucetius var. caesius. *Biotechnol Bioeng* 11:1101-1110.

Arvand, A., and C.T. Denny. 2001. Biology of EWS/ETS fusions in Ewing's family tumors. *Oncogene* 20:5747-5754.

Athar, M., C. Li, X. Tang, S. Chi, X. Zhang, A.L. Kim, S.K. Tyring, L. Kopelovich, J. Hebert, E.H. Epstein, Jr., D.R. Bickers, and J. Xie. 2004. Inhibition of smoothened signaling prevents ultraviolet B-induced basal cell carcinomas through regulation of Fas expression and apoptosis. *Cancer Res* 64:7545-7552.

Au, W.Y., S. Tam, B.M. Fong, and Y.L. Kwong. 2008. Determinants of cerebrospinal fluid arsenic concentration in patients with acute promyelocytic leukemia on oral arsenic trioxide therapy. *Blood* 112:3587-3590.

Bacci, G., A. Longhi, S. Ferrari, M. Mercuri, M. Versari, and F. Bertoni. 2006. Prognostic factors in non-metastatic Ewing's sarcoma tumor of bone: an analysis of 579 patients treated at a single institution with adjuvant or neoadjuvant chemotherapy between 1972 and 1998. *Acta Oncol* 45:469-475.

Bagatell, R., R. Norris, A.M. Ingle, C. Ahern, S. Voss, E. Fox, A.R. Little, B.J. Weigel, P.C. Adamson, and S. Blaney. 2014. Phase 1 trial of temsirolimus in combination with irinotecan and temozolomide in children, adolescents and young adults with relapsed or refractory solid tumors: a Children's Oncology Group Study. *Pediatr Blood Cancer* 61:833-839.

Bai, C.B., W. Auerbach, J.S. Lee, D. Stephen, and A.L. Joyner. 2002. Gli2, but not Gli1, is required for initial Shh signaling and ectopic activation of the Shh pathway. *Development* 129:4753-4761.

Balamuth, N., and R.B. Womer. 2010. Ewing's sarcoma. *Lancet Oncol* 11:184-192.

Bale, A.E., and K.P. Yu. 2001. The hedgehog pathway and basal cell carcinomas. *Hum Mol Genet* 10:757-762.

Battula, V.L., S. Treml, P.M. Bareiss, F. Gieseke, H. Roelofs, P. de Zwart, I. Muller, B. Schewe, T. Skutella, W.E. Fibbe, L. Kanz, and H.J. Buhring. 2009. Isolation of functionally distinct mesenchymal stem cell subsets using antibodies against CD56, CD271, and mesenchymal stem cell antigen-1. *Haematologica* 94:173-184.

Beauchamp, E., G. Bulut, O. Abaan, K. Chen, A. Merchant, W. Matsul, Y. Endo, J.S. Rubin, J. Toretsky, and A. Üren. 2009. Gli1 is a direct transcriptional target of EWS-FLI1 oncoprotein. *The journal of biological chemistry* 284:9074-9082.

Beauchamp, E.M., L. Ringer, G. Bulut, K.P. Sajwan, M.D. Hall, Y.C. Lee, D. Peaceman, M. Ozdemirli, O. Rodriguez, T.J. Macdonald, C. Albanese, J.A. Toretsky, and A. Uren. 2011. Arsenic trioxide inhibits human cancer cell growth and tumor development in mice by blocking Hedgehog/GLI pathway. *J Clin Invest* 121:148-160.

Benjamin, R.S., L.H. Baker, R.M. O'Bryan, T.E. Moon, and J.A. Gottlieb. 1977. Advances in the chemotherapy of soft tissue sarcomas. *Med Clin North Am* 61:1039-1043.

Berman, D.M., S.S. Karhadkar, A.R. Hallahan, J.I. Pritchard, C.G. Eberhart, D.N. Watkins, J.K. Chen, M.K. Cooper, J. Taipale, J.M. Olson, and P.A. Beachy. 2002. Medulloblastoma growth inhibition by hedgehog pathway blockade. *Science* 297:1559-1561.

Biedler, J.L., L. Helson, and B.A. Spengler. 1973. Morphology and growth, tumorigenicity, and cytogenetics of human neuroblastoma cells in continuous culture. *Cancer Res* 33:2643-2652.

Boehme, K.A., J. Nitsch, R. Riester, R. Handgretinger, S.S. Schleicher, T. Kluba, and F. Traub. 2016. Arsenic trioxide potentiates the effectiveness of etoposide in Ewing sarcomas. *Int J Oncol* 49:2135-2146. (Boehme et al., 2016 (1))

Boehme, K.A., J.J. Zaborski, R. Riester, S.K. Schweiss, U. Hopp, F. Traub, T. Kluba, R. Handgretinger, and S.B. Schleicher. 2016. Targeting hedgehog signalling by arsenic trioxide reduces cell growth and induces apoptosis in rhabdomyosarcoma. *Int J Oncol* 48:801-812. (Boehme et al., 2016 (2))

Bonadonna, G., S. Monfardini, M. De Lena, and F. Fossati-Bellani. 1969. Clinical evaluation of adriamycin, a new antitumour antibiotic. *Br Med J* 3:503-506.

Bonadonna, G., S. Monfardini, M. De Lena, F. Fossati-Bellani, and G. Beretta. 1970. Phase I and preliminary phase II evaluation of adriamycin (NSC 123127). *Cancer Res* 30:2572-2582.

Bonadonna, G., R. Zucali, M. De Lena, and P. Valagussa. 1977. Combined chemotherapy (MOPP or ABVD)-radiotherapy approach in advanced Hodgkin's disease. *Cancer Treat Rep* 61:769-777.

Buller, N.V., S.L. Rosekrans, J. Westerlund, and G.R. van den Brink. 2012. Hedgehog signaling and maintenance of homeostasis in the intestinal epithelium. *Physiology (Bethesda)* 27:148-155.

Burdach, S., H. Jurgens, C. Peters, W. Nurnberger, C. Mauz-Korholz, D. Korholz, M. Paulussen, H. Pape, D. Dilloo, E. Koscielniak, and et al. 1993. Myeloablative radiochemotherapy and hematopoietic stem-cell rescue in poor-prognosis Ewing's sarcoma. *J Clin Oncol* 11:1482-1488.

Burdach, S., A. Meyer-Bahlburg, H.J. Laws, R. Haase, B. van Kaik, B. Metzner, A. Wawer, R. Finke, U. Gobel, J. Haerting, H. Pape, H. Gadner, J. Dunst, and H. Juergens. 2003. High-dose therapy for patients with primary multifocal and early relapsed Ewing's tumors: results of two consecutive regimens assessing the role of total-body irradiation. *J Clin Oncol* 21:3072-3078.

Burdach, S., B. van Kaick, H.J. Laws, S. Ahrens, R. Haase, D. Korholz, H. Pape, J. Dunst, T. Kahn, R. Willers, B. Engel, U. Dirksen, C. Kramm, W. Nurnberger, A. Heyll, R. Ladenstein, H. Gadner, H. Jurgens, and U. Go el. 2000. Allogeneic and autologous stem-cell transplantation in advanced Ewing tumors. An update after long-term follow-up from two centers of the European Intergroup study EICESS. Stem-Cell Transplant Programs at Dusseldorf University Medical Center, Germany and St. Anna Kinderspital, Vienna, Austria. *Ann Oncol* 11:1451-1462.

Burness, C.B. 2015. Sonidegib: First Global Approval. *Drugs* 75:1559-1566.

Burnette, W.N. 1981. "Western blotting": electrophoretic transfer of proteins from sodium dodecyl sulfate--polyacrylamide gels to unmodified nitrocellulose and radiographic detection with antibody and radioiodinated protein A. *Anal Biochem* 112:195-203.

Carpenter, D., D.M. Stone, J. Brush, A. Ryan, M. Armanini, G. Frantz, A. Rosenthal, and F.J. de Sauvage. 1998. Characterization of two patched receptors for the vertebrate hedgehog protein family. *Proc Natl Acad Sci U S A* 95:13630-13634.

Casazza, M., A. Di Marco, and G. Di Cuonzo. 1971. Interference of daunomycin and adriamycin on the growth and aggression of murine sarcoma virus (Moloney) tumors in mice. *Cancer Res* 31:1971-1976.

Castillero-Trejo, Y., S. Eliazer, L. Xiang, J.A. Richardson, and R.L. Ilaria, Jr. 2005. Expression of the EWS/FLI-1 oncogene in murine primary bone-derived cells Results in EWS/FLI-1-dependent, ewing sarcoma-like tumors. *Cancer Res* 65:8698-8705.

Cavazzana, A.O., J.S. Miser, J. Jefferson, and T.J. Triche. 1987. Experimental evidence for a neural origin of Ewing's sarcoma of bone. *Am J Pathol* 127:507-518.

Cavigelli, M., W.W. Li, A. Lin, B. Su, K. Yoshioka, and M. Karin. 1996. The tumor promoter arsenite stimulates AP-1 activity by inhibiting a JNK phosphatase. *EMBO J* 15:6269-6279.

Champeris Tsaniras, S., N. Kanellakis, I.E. Symeonidou, P. Nikolopoulou, Z. Lygerou, and S. Taraviras. 2014. Licensing of DNA replication, cancer, pluripotency and differentiation: an interlinked world? *Semin Cell Dev Biol* 30:174-180.

Chen, C.S., J.T. Lin, K.A. Goss, Y.A. He, J.R. Halpert, and D.J. Waxman. 2004. Activation of the anticancer prodrugs cyclophosphamide and ifosfamide: identification of cytochrome P450 2B enzymes and site-specific mutants with improved enzyme kinetics. *Mol Pharmacol* 65:1278-1285.

Christensen, L., and W.A. May. 2016. EWS/FLI1 activates GLI1 indirectly through GLI2 in Ewing Sarcoma. In AACR; Cancer Res 2016. P.o.t.t.A.M.o.t.A.A.f.C. Research, editor New Orleans, LA. Philadelphia (PA).

CLS. 2016. Product information: RD-ES. In.

Cullinane, C., and D.R. Phillips. 1990. Induction of stable transcriptional blockage sites by adriamycin: GpC specificity of apparent adriamycin-DNA adducts and dependence on iron(III) ions. *Biochemistry* 29:5638-5646.

Cutts, S.M., A. Rephaeli, A. Nudelman, I. Hmelnitsky, and D.R. Phillips. 2001. Molecular basis for the synergistic interaction of adriamycin with the formaldehyde-releasing prodrug pivaloyloxymethyl butyrate (AN-9). *Cancer Res* 61:8194-8202.

Cutts, S.M., A. Rephaeli, A. Nudelman, M. Ugarenko, and D.R. Phillips. 2015. Potential therapeutic advantages of doxorubicin when activated by formaldehyde to function as a DNA adduct-forming agent. *Curr Top Med Chem*

Das, S., R.S. Samant, and L.A. Shevde. 2013. Nonclassical activation of Hedgehog signaling enhances multidrug resistance and makes cancer cells refractory to Smoothened-targeting Hedgehog inhibition. *J Biol Chem* 288:11824-11833.

Davidson, N.E., and S. Sukumar. 2005. Of Snail, mice, and women. *Cancer Cell* 8:173-174.

Daw, N.C., W.L. Furman, C.F. Stewart, L.C. Iacono, M. Krailo, M.L. Bernstein, J.E. Dancey, R.A. Speights, S.M. Blaney, J.M. Croop, G.H. Reaman, P.C. Adamson, and G. Children's Oncology. 2005. Phase I and pharmacokinetic study of gefitinib in children with refractory solid tumors: a Children's Oncology Group Study. *J Clin Oncol* 23:6172-6180.

Dejean, L.M., S. Martinez-Caballero, S. Manon, and K.W. Kinnally. 2006. Regulation of the mitochondrial apoptosis-induced channel, MAC, by BCL-2 family proteins. *Biochim Biophys Acta* 1762:191-201.

Delattre, O., J. Zucman, T. Melot, X.S. Garau, J.M. Zucker, G.M. Lenoir, P.F. Ambros, D. Sheer, C. Turc-Carel, T.J. Triche, and et al. 1994. The Ewing family of tumors--a subgroup of small-round-cell tumors defined by specific chimeric transcripts. *N Engl J Med* 331:294-299.

Department of Chemistry & Biochemistry UCLA. 2015. Illustrated Glossary of Organic Chemistry. http://www.chem.ucla.edu/~harding/IGOC/D/doxorubicin01.png. access: 20.09.2016

Desai, S.S., and N.A. Jambhekar. 2010. Pathology of Ewing's sarcoma/PNET: Current opinion and emerging concepts. *Indian J Orthop* 44:363-368.

Di Marco, A., M. Gaetani, and B. Scarpinato. 1969. Adriamycin (NSC-123,127): a new antibiotic with antitumor activity. *Cancer Chemother Rep* 53:33-37.

Eggenschwiler, J.T., and K.V. Anderson. 2007. Cilia and developmental signaling. *Annu Rev Cell Dev Biol* 23:345-373.

Elledge, S.J. 1996. Cell cycle checkpoints: preventing an identity crisis. *Science* 274:1664-1672.

Elmore, S. 2007. Apoptosis: a review of programmed cell death. *Toxicol Pathol* 35:495-516.

Esiashvili, N., M. Goodmann, and R. Marcus. 2008. Changes in incidence and survival of Ewing's sarcoma patients over the past 3 decades: Surveillance Epidemiology and End Results data. *J Pediatr Hematol Oncol* 30:425-430.

Fan, H.X., S. Wang, H. Zhao, N. Liu, D. Chen, M. Sun, and J.H. Zheng. 2014. Sonic hedgehog signaling may promote invasion and metastasis of oral squamous cell carcinoma by activating MMP-9 and E-cadherin expression. *Med Oncol* 31:41.

Farooqi, A.A., S. Mukhtar, A.M. Riaz, S. Waseem, S. Minhaj, B.A. Dilawar, B.A. Malik, A. Nawaz, and S. Bhatti. 2011. Wnt and SHH in prostate cancer: trouble mongers occupy the TRAIL towards apoptosis. *Cell Prolif* 44:508-515.

Feng, T., G. Qiao, L. Feng, W. Qi, Y. Huang, Y. Yao, and Z. Shen. 2014. Stathmin is key in reversion of doxorubicin resistance by arsenic trioxide in osteosarcoma cells. *Mol Med Rep* 10:2985-2992.

Fesik, S.W., and Y. Shi. 2001. Structural biology. Controlling the caspases. *Science* 294:1477-1478.

Fisher Scientific. 2015. Product information: Arsenic(III) oxide, 99.5 %, ACROS Organics™. https://beta-static.fishersci.com/images/F156118~wl.jpg. access: 20.09.2016

Fong, E.L., S.E. Lamhamedi-Cherradi, E. Burdett, V. Ramamoorthy, A.J. Lazar, F.K. Kasper, M.C. Farach-Carson, D. Vishwamitra, E.G. Demicco, B.A. Menegaz, H.M. Amin, A.G. Mikos, and J.A. Ludwig. 2013. Modeling Ewing sarcoma tumors in vitro with 3D scaffolds. *Proc Natl Acad Sci U S A* 110:6500-6505.

Fox, E., R. Aplenc, R. Bagatell, M.K. Chuk, E. Dombi, W. Goodspeed, A. Goodwin, M. Kromplewski, N. Jayaprakash, M. Marotti, K.H. Brown, B. Wenrich, P.C. Adamson, B.C. Widemann, and F.M. Balis. 2010. A phase 1 trial and pharmacokinetic study of cediranib, an orally bioavailable pan-vascular endothelial growth factor receptor inhibitor, in children and adolescents with refractory solid tumors. *J Clin Oncol* 28:5174-5181.

Friedrich, J., C. Seidel, R. Ebner, and L.A. Kunz-Schughart. 2009. Spheroid-based drug screen: considerations and practical approach. *Nat Protoc* 4:309-324.

Fu, J., M. Rodova, S.K. Roy, J. Sharma, K.P. Singh, R.K. Srivastava, and S. Shankar. 2013. GANT-61 inhibits pancreatic cancer stem cell growth in vitro and in NOD/SCID/IL2R gamma null mice xenograft. *Cancer Lett* 330:22-32.

Fulwyler, M.J. 1965. Electronic separation of biological cells by volume. *Science* 150:910-911.

Geng, L., K. Lu, P. Li, X. Li, X. Zhou, Y. Li, and X. Wang. 2016. GLI1 inhibitor GANT61 exhibits antitumor efficacy in T-cell lymphoma cells through down-regulation of p-STAT3 and SOCS3. *Oncotarget*

Gensler, W.J., and C.D. Gatsonis. 1966. Synthesis of podophyllotoxin. *J Org Chem* 31:4004-4008.

Giard, D.J., S.A. Aaronson, G.J. Todaro, P. Arnstein, J.H. Kersey, H. Dosik, and W.P. Parks. 1973. In vitro cultivation of human tumors: establishment of cell lines derived from a series of solid tumors. *J Natl Cancer Inst* 51:1417-1423.

Gillett, C.E., and D.M. Barnes. 1998. Demystified ... cell cycle. *Mol Pathol* 51:310-316.

Gonnissen, A., S. Isebaert, and K. Haustermans. 2015. Targeting the Hedgehog signaling pathway in cancer: beyond Smoothened. *Oncotarget* 6:13899-13913.

Green, D.R. 2011. The end and after: how dying cells impact the living organism. *Immunity* 35:441-444.

Grier, H., M. Krailo, and N. Tarbell. 2003. Addition of ifosfamide and etoposide to standard chemotherapy for Ewing's sarcoma and primitive neuroectodermal tumor of bone. *N Engl J Med* 348:694-701.

Guo, W., X.D. Tang, S. Tang, and Y. Yang. 2006. [Preliminary report of combination chemotherapy including Arsenic trioxide for stage III osteosarcoma and Ewing sarcoma]. *Zhonghua Wai Ke Za Zhi* 44:805-808.

Gupta, R.S. 1983. Podophyllotoxin-resistant mutants of Chinese hamster ovary cells: cross-resistance studies with various microtubule inhibitors and podophyllotoxin analogues. *Cancer Res* 43:505-512.

Haeusler, J., A. Ranft, T. Boelling, G. Gosheger, G. Braun-Munzinger, V. Vieth, S. Burdach, H. van den Berg, H. Juergens, and U. Dirksen. 2010. The value of local treatment in patients with primary, disseminated, multifocal Ewing sarcoma (PDMES). *Cancer* 116:443-450.

Hahn, H., L. Wojnowski, A.M. Zimmer, J. Hall, G. Miller, and A. Zimmer. 1998. Rhabdomyosarcomas and radiation hypersensitivity in a mouse model of Gorlin syndrome. *Nat Med* 4:619-622.

Hanna, A., and L.A. Shevde. 2016. Hedgehog signaling: modulation of cancer properies and tumor mircroenvironment. *Mol Cancer* 15:24.

Hasegawa, T., K. Isobe, I. Nakashima, and K. Shimokata. 1993. Higher expression of topoisomerase II in lung cancers than normal lung tissues: different expression pattern from topoisomerase I. *Biochem Biophys Res Commun* 195:409-414.

Hayashi, T., T. Hideshima, M. Akiyama, P. Richardson, R.L. Schlossman, D. Chauhan, N.C. Munshi, S. Waxman, and K.C. Anderson. 2002. Arsenic trioxide inhibits growth of human multiple myeloma cells in the bone marrow microenvironment. *Mol Cancer Ther* 1:851-860.

Hooper, J.E., and M.P. Scott. 2005. Communicating with Hedgehogs. *Nat Rev Mol Cell Biol* 6:306-317.

Hosoya, T., M.A. Arai, T. Koyano, T. Kowithayakorn, and M. Ishibashi. 2008. Naturally occurring small-molecule inhibitors of hedgehog/GLI-mediated transcription. *Chembiochem* 9:1082-1092.

Hu, J., Y.F. Liu, C.F. Wu, F. Xu, Z.X. Shen, Y.M. Zhu, J.M. Li, W. Tang, W.L. Zhao, W. Wu, H.P. Sun, Q.S. Chen, B. Chen, G.B. Zhou, A. Zelent, S. Waxman, Z.Y. Wang, S.J. Chen, and Z. Chen. 2009. Long-term efficacy and safety of all-trans retinoic acid/arsenic trioxide-based therapy in newly diagnosed acute promyelocytic leukemia. *Proc Natl Acad Sci U S A* 106:3342-3347.

Huang, L., V. Walter, D.N. Hayes, and M. Onaitis. 2014. Hedgehog-GLI signaling inhibition suppresses tumor growth in squamous lung cancer. *Clin Cancer Res* 20:1566-1575.

Hui, C.C., and S. Angers. 2011. Gli proteins in development and disease. *Annu Rev Cell Dev Biol* 27:513-537.

Hunold, A., N. Weddeling, M. Paulussen, A. Ranft, C. Liebscher, and H. Jurgens. 2006. Topotecan and cyclophosphamide in patients with refractory or relapsed Ewing tumors. *Pediatr Blood Cancer* 47:795-800.

Igney, F.H., and P.H. Krammer. 2002. Death and anti-death: tumour resistance to apoptosis. *Nat Rev Cancer* 2:277-288.

Ikram, M.S., G.W. Neill, G. Regl, T. Eichberger, A.M. Frischauf, F. Aberger, A. Quinn, and M. Philpott. 2004. GLI2 is expressed in normal human epidermis and BCC and induces GLI1 expression by binding to its promoter. *J Invest Dermatol* 122:1503-1509.

Imbert, T.F. 1998. Discovery of podophyllotoxins. *Biochimie* 80:207-222.

Ingham, P.W., and A.P. McMahon. 2001. Hedgehog signaling in animal developement: paradigms and principles. *Genes Dev* 15:3059-3087.

Iriyama, N., B. Yuan, Y. Yoshino, Y. Hatta, A. Horikoshi, S. Aizawa, J. Takeuchi, and H. Toyoda. 2013. Aquaporin 9, a promising predictor for the cytocidal effects of arsenic trioxide in acute promyelocytic leukemia cell lines and primary blasts. *Oncol Rep* 29:2362-2368.

Ivanov, D.P., T.L. Parker, D.A. Walker, C. Alexander, M.B. Ashford, P.R. Gellert, and M.C. Garnett. 2014. Multiplexing spheroid volume, resazurin and acid phosphatase viability assays for high-throughput screening of tumour spheroids and stem cell neurospheres. *PLoS One* 9:e103817.

Jaffe, N., D. Paed, D. Traggis, S. Sallan, and R. Cassady. 1976. Improved outlook for Ewing's sarcoma with combination chemotherapy (vincristine, actinomycin D and cyclophosphamide) and radiation therapy. *Cancer* 38:1925-1930.

Jensen, P.B., H. Roed, T. Skovsgaard, E. Friche, L. Vindelov, H.H. Hansen, and M. Spang-Thomsen. 1990. Antitumor activity of the two epipodophyllotoxin derivatives VP-16 and VM-26 in preclinical systems: a comparison of in vitro and in vivo drug evaluation. *Cancer Chemother Pharmacol* 27:194-198.

Jiang, Y., W. Li, X. He, H. Zhang, F. Jiang, and Z. Chen. 2015a. Lgr5 expression is a valuable prognostic factor for colorectal cancer: evidence from a meta-analysis. *BMC Cancer* 15:948.

Jiang, Y., J. Ludwig, and F. Janku. 2015b. Targeted therapies for advanced Ewing sarcoma family of tumors. *Cancer Treat Rev* 41:391-400.

Johnson, D.H., J.D. Hainsworth, K.R. Hande, and F.A. Greco. 1991. Current status of etoposide in the management of small cell lung cancer. *Cancer* 67:231-244.

Johnson, R.L., A.L. Rothman, J. Xie, L.V. Goodrich, J.W. Bare, J.M. Bonifas, A.G. Quinn, R.M. Myers, D.R. Cox, E.H. Epstein, Jr., and M.P. Scott. 1996. Human homolog of patched, a candidate gene for the basal cell nevus syndrome. *Science* 272:1668-1671.

Joo, J., L. Christensen, K. Warner, L. States, H.G. Kang, K. Vo, E.R. Lawlor, and W.A. May. 2009. GLI1 is a central mediator of EWS/FLI1 signaling in Ewing tumors. *PLoS One* 4:e7608.

Juergens, C., C. Weston, I. Lewis, J. Whelan, M. Paulussen, O. Oberlin, J. Michon, A. Zoubek, H. Juergens, and A. Craft. 2006. Safety assessment of intensive induction with vincristine, ifosfamide, doxorubicin, and etoposide (VIDE) in the treatment of Ewing tumors in the EURO-E.W.I.N.G. 99 clinical trial. *Pediatr Blood Cancer* 47:22-29.

Julius, M.H., T. Masuda, and L.A. Herzenberg. 1972. Demonstration that antigen-binding cells are precursors of antibody-producing cells after purification with a fluorescence-activated cell sorter. *Proc Natl Acad Sci U S A* 69:1934-1938.

Jung, H.S., H.S. Kim, M.J. Lee, H.Y. Shin, H.S. Ahn, K.H. Ryu, J.Y. Seoh, C.J. Kim, and J.J. Jang. 2006. Arsenic trioxide concentration determines the fate of Ewing's sarcoma family tumors and neuroblastoma cells in vitro. *FEBS Lett* 580:4969-4975.

Kanda, S., T. Mitsuyasu, Y. Nakao, S. Kawano, Y. Goto, R. Matsubara, and S. Nakamura. 2013. Anti-apoptotic role of the sonic hedgehog signaling pathway in the proliferation of ameloblastoma. *Int J Oncol* 43:695-702.

Kapahi, P., T. Takahashi, G. Natoli, S.R. Adams, Y. Chen, R.Y. Tsien, and M. Karin. 2000. Inhibition of NF-kappa B activation by arsenite through reaction with a critical cysteine in the activation loop of Ikappa B kinase. *J Biol Chem* 275:36062-36066.

Kappler, R., J. Calzada-Wack, U. Schnitzbauer, M. Koleva, A. Herwig, G. Piontek, F. Graedler, J. Adamski, U. Heinzmann, J. Schlegel, B. Hemmerlein, L. Quintanilla-Martinez, and H. Hahn. 2003. Molecular characterization of Patched-associated rhabdomyosarcoma. *J Pathol* 200:348-356.

Karosas, A.O. 2010. Ewing's sarcoma. *Am J Health Syst Pharm* 67:1599-1605.

Karpinich, N.O., M. Tafani, R.J. Rothman, M.A. Russo, and J.L. Farber. 2002. The course of etoposide-induced apoptosis from damage to DNA and p53 activation to mitochondrial release of cytochrome c. *J Biol Chem* 277:16547-16552.

Kashima, T.G., N.G. Gamage, U. Dirksen, C.L. Gibbons, S.J. Ostlere, and N.A. Athanasou. 2013. Localized Ewing sarcoma of the tibia. *Clin Sarcoma Res* 3:2.

Kasper, M., G. Regl, A.M. Frischauf, and F. Aberger. 2006. GLI transcription factors: mediators of oncogenic Hedgehog signalling. *Eur J Cancer* 42:437-445.

Katoh, Y., and M. Katoh. 2009. Hedgehog target genes: mechanisms of carcinogenesis induced by aberrant hedgehog signaling activation. *Curr Mol Med* 9:873-886.

Kelleher, F.C., J.E. Cain, J.M. Healy, D.N. Watkins, and D.M. Thomas. 2012. Prevailing importance of the hedgehog signaling pathway and the potential for treatment advancement in sarcoma. *Pharmacol Ther* 136:153-168.

Kelly, M., and J.L. Hartwell. 1954. The biological effects and the chemical composition of podophyllin: a review. *J Natl Cancer Inst* 14:967-1010.

Kim, J., B.T. Aftab, J.Y. Tang, D. Kim, A.H. Lee, M. Rezaee, J. Kim, B. Chen, E.M. King, A. Borodovsky, G.J. Riggins, E.H. Epstein, Jr., P.A. Beachy, and C.M. Rudin. 2013. Itraconazole and arsenic trioxide inhibit Hedgehog pathway activation and tumor growth associated with acquired resistance to smoothened antagonists. *Cancer Cell* 23:23-34.

Kim, J., J.J. Lee, J. Kim, D. Gardner, and P.A. Beachy. 2010. Arsenic antagonizes the Hedgehog pathway by preventing ciliary accumulation and reducing stability of the Gli2 transcriptional effector. *Proc Natl Acad Sci U S A* 107:13432-13437.

Kimura, K., M. Saijo, M. Ui, and T. Enomoto. 1994. Growth state- and cell cycle-dependent fluctuation in the expression of two forms of DNA topoisomerase II and possible specific modification of the higher molecular weight form in the M phase. *J Biol Chem* 269:1173-1176.

Kinzler, K.W., S.H. Bigner, D.D. Bigner, J.M. Trent, M.L. Law, S.J. O'Brien, A.J. Wong, and B. Vogelstein. 1987. Identification of an amplified, highly expressed gene in a human glioma. *Science* 236:70-73.

Kinzler, K.W., J.M. Ruppert, S.H. Bigner, and B. Vogelstein. 1988. The GLI gene is a member of the Kruppel family of zinc finger proteins. *Nature* 332:371-374.

Kobayashi, K., and M.J. Ratain. 1994. Pharmacodynamics and long-term toxicity of etoposide. *Cancer Chemother Pharmacol* 34 Suppl:S64-68.

Kogerman, P., T. Grimm, L. Kogerman, D. Krause, A.B. Unden, B. Sandstedt, R. Toftgard, and P.G. Zaphiropoulos. 1999. Mammalian suppressor-of-fused modulates nuclear-cytoplasmic shuttling of Gli-1. *Nat Cell Biol* 1:312-319.

Kolf, C.M., E. Cho, and R.S. Tuan. 2007. Arthritis. *Res Ther* 9:204.

Kondo, K., S. Obitsu, S. Ohta, K. Matsunami, H. Otsuka, and R. Teshima. 2010. Poly(ADP-ribose) polymerase (PARP)-1-independent apoptosis-inducing factor (AIF) release and cell death are induced by eleostearic acid and blocked by alpha-tocopherol and MEK inhibition. *J Biol Chem* 285:13079-13091.

Koscielniak, E., U. Gross-Wieltsch, J. Treuner, P. Winkler, T. Klingebiel, P. Lang, P. Bader, D. Niethammer, and R. Handgretinger. 2005. Graft-versus-Ewing sarcoma effect and long-term remission induced by haploidentical stem-cell transplantation in a patient with relapse of metastatic disease. *J Clin Oncol* 23:242-244.

Kuhn, M., and A. von Wartburg. 1968. [The separation of acyl protection groups in alkali-sensitive glucosides. Synthesis of podophyllotoxin-beta-D-glucoside]. *Helv Chim Acta* 51:163-168.

Kumar, L. 1993. Epipodophyllotoxins and secondary leukaemia. *Lancet* 342:819-820.

Kurosaka, K., and Y. Kobayashi. 2003. [Macrophage responses during phagocytosis of apoptotic cells and their regulatory mechanism]. *Seikagaku* 75:59-62.

Lauth, M., A. Bergstrom, T. Shimokawa, and R. Toftgard. 2007. Inhibition of GLI-mediated transcription and tumor cell growth by small-molecule antagonists. *Proc Natl Acad Sci U S A* 104:8455-8460.

Le Deley, M.C., O. Delattre, K.L. Schaefer, S.A. Burchill, G. Koehler, P.C. Hogendoorn, T. Lion, C. Poremba, J. Marandet, S. Ballet, G. Pierron, S.C. Brownhill, M. Nesslbock, A. Ranft, U. Dirksen, O. Oberlin, I.J. Lewis, A.W. Craft, H. Jurgens, and H. Kovar. 2010. Impact of EWS-ETS fusion type on disease progression in Ewing's sarcoma/peripheral primitive neuroectodermal tumor: prospective results from the cooperative Euro-E.W.I.N.G. 99 trial. *J Clin Oncol* 28:1982-1988.

Le Deley, M.C., M. Paulussen, I. Lewis, B. Brennan, A. Ranft, J. Whelan, G. Le Teuff, J. Michon, R. Ladenstein, P. Marec-Berard, H. van den Berg, L. Hjorth, K. Wheatley, I. Judson, H. Juergens, A. Craft, O. Oberlin, and U. Dirksen. 2014. Cyclophosphamide compared with ifosfamide in consolidation treatment of standard-risk Ewing sarcoma: results of the randomized noninferiority Euro-EWING99-R1 trial. *J Clin Oncol* 32:2440-2448.

Lee, S.W., M.A. Moskowitz, and J.R. Sims. 2007. Sonic hedgehog inversely regulates the expression of angiopoietin-1 and angiopoietin-2 in fibroblasts. *Int J Mol Med* 19:445-451.

Leslie, E.M., A. Haimeur, and M.P. Waalkes. 2004. Arsenic transport by the human multidrug resistance protein 1 (MRP1/ABCC1). Evidence that a tri-glutathione conjugate is required. *J Biol Chem* 279:32700-32708.

Leung, J., A. Pang, W.H. Yuen, Y.L. Kwong, and E.W. Tse. 2007. Relationship of expression of aquaglyceroporin 9 with arsenic uptake and sensitivity in leukemia cells. *Blood* 109:740-746.

Li, X., W. Deng, C.D. Nail, S.K. Bailey, M.H. Kraus, J.M. Ruppert, and S.M. Lobo-Ruppert. 2006. Snail induction is an early response to Gli1 that determines the efficiency of epithelial transformation. *Oncogene* 25:609-621.

Lim, C.B., C.M. Prele, S. Baltic, P.G. Arthur, J. Creaney, D.N. Watkins, P.J. Thompson, and S.E. Mutsaers. 2015. Mitochondria-derived reactive oxygen species drive GANT61-induced mesothelioma cell apoptosis. *Oncotarget* 6:1519-1530.

Lin, P.P., R.I. Brody, A.C. Hamelin, J.E. Bradner, J.H. Healey, and M. Ladanyi. 1999. Differential transactivation by alternative EWS-FLI1 fusion proteins correlates with clinical heterogeneity in Ewing's sarcoma. *Cancer Res* 59:1428-1432.

Lin, P.P., Y. Wang, and G. Lozano. 2011. Mesenchymal Stem Cells and the Origin of Ewing's Sarcoma. *Sarcoma*

Loehrer, P.J., Sr. 1991. Etoposide therapy for testicular cancer. *Cancer* 67:220-224.

Loike, J.D., and S.B. Horwitz. 1976a. Effect of VP-16-213 on the intracellular degradation of DNA in HeLa cells. *Biochemistry* 15:5443-5448.

Loike, J.D., and S.B. Horwitz. 1976b. Effects of podophyllotoxin and VP-16-213 on microtubule assembly in vitro and nucleoside transport in HeLa cells. *Biochemistry* 15:5435-5443.

Lown, J.W. 1993. Anthracycline and anthraquinone anticancer agents: current status and recent developments. *Pharmacol Ther* 60:185-214.

Lu, J., E.H. Chew, and A. Holmgren. 2007. Targeting thioredoxin reductase is a basis for cancer therapy by arsenic trioxide. *Proc Natl Acad Sci U S A* 104:12288-12293.

Lu, N., Y. Chen, Z. Wang, G. Chen, Q. Lin, Z.Y. Chen, and H. Li. 2013. Sonic hedgehog initiates cochlear hair cell regeneration through downregulation of retinoblastoma protein. *Biochem Biophys Res Commun* 430:700-705.

Mackall, C.L., P.S. Meltzer, and L.J. Helman. 2002. Focus on sarcomas. *Cancer Cell* 2:

Malek, R., J. Matta, N. Taylor, M.E. Perry, and S.M. Mendrysa. 2011. The p53 inhibitor MDM2 facilitates Sonic Hedgehog-mediated tumorigenesis and influences cerebellar foliation. *PLoS One* 6:e17884.

Mann, K.K., K. Davison, M. Colombo, A.L. Colosimo, Z. Diaz, A.M. Padovani, Q. Guo, P.J. Scrivens, W. Gao, S. Mader, and W.H. Miller, Jr. 2006. Antimony trioxide-induced apoptosis is dependent on SEK1/JNK signaling. *Toxicol Lett* 160:158-170.

Martinez-Ramirez, A., S. Rodriguez-Perales, B. Melendez, B. Martinez-Delgado, M. Urioste, J.C. Cigudosa, and J. Benitez. 2003. Characterization of the A673 cell line (Ewing tumor) by molecular cytogenetic techniques. *Cancer Genet Cytogenet* 141:138-142.

Mathieu, J., and F. Besancon. 2006. Clinically tolerable concentrations of arsenic trioxide induce p53-independent cell death and repress NF-kappa B activation in Ewing sarcoma cells. *Int J Cancer* 119:1723-1727.

Matsumoto, T., K. Tabata, and T. Suzuki. 2014. The GANT61, a GLI inhibitor, induces caspase-independent apoptosis of SK-N-LO cells. *Biol Pharm Bull* 37:633-641.

Matsumoto, Y., K. Kunishio, and S. Nagao. 1999. Increased phosphorylation of DNA topoisomerase II in etoposide resistant mutants of human glioma cell line. *J Neurooncol* 45:37-46.

May, W.A., M.L. Gishizky, S.L. Lessnick, L.B. Lunsford, B.C. Lewis, O. Delattre, J. Zucman, G. Thomas, and C.T. Denny. 1993. Ewing sarcoma 11;22 translocation produces a chimeric transcription factor that requires the DNA-binding domain encoded by FLI1 for transformation. *Proc Natl Acad Sci U S A* 90:5752-5756.

May, W.A., R.S. Grigoryan, N. Keshelava, D.J. Cabral, L.L. Christensen, J. Jenabi, L. Ji, T.J. Triche, E.R. Lawlor, and C.P. Reynolds. 2013. Characterization and drug resistance patterns of Ewing's sarcoma family tumor cell lines. *PLoS One* 8:e80060.

Mazumdar, T., J. DeVecchio, A. Agyeman, T. Shi, and J.A. Houghton. 2011. The GLI genes as the molecular switch in disrupting Hedgehog signaling in colon cancer. *Oncotarget* 2:638-645.

McCall, T.D., C.A. Pedone, and D.W. Fults. 2007. Apoptosis suppression by somatic cell transfer of Bcl-2 promotes Sonic hedgehog-dependent medulloblastoma formation in mice. *Cancer Res* 67:5179-5185.

McMahon, A.P., P.W. Ingham, and C.J. Tabin. 2003. Developmental roles and clinical significance of hedgehog signaling. *Curr Top Dev Biol* 53:1-114.

Medicines Complete. 2016. Etoposide. https://www.medicinescomplete.com/mc/rem/2012/CLK0691C001.png. access: 20.09.2016

Melguizo, C., J. Prados, A.R. Rama, R. Ortiz, P.J. Alvarez, J.E. Fernandez, and A. Aranega. 2011. Multidrug resistance and rhabdomyosarcoma (Review). *Oncol Rep* 26:755-761.

Meresse, P., E. Dechaux, C. Monneret, and E. Bertounesque. 2004. Etoposide: Discovery and Medicinal Chemistry. *Current Medicinal Chemistry* 11:2443-2466.

Meyers, P., M. Krailo, and M. Ladany. 2001. High-dose melphalan, etoposide, total-body irradiation, and autologous stem-cell reconstitution as consolidation therapy for high-risk Ewing's sarcoma does not improve prognosis. *J Clin Oncol* 19:2812-2820.

Michaud, E.J., and B.K. Yoder. 2006. The primary cilium in cell signaling and cancer. *Cancer Res* 66:6463-6467.

Minotti, G., P. Menna, E. Salvatorelli, G. Cairo, and L. Gianni. 2004. Anthracyclines: molecular advances and pharmacologic developments in antitumor activity and cardiotoxicity. *Pharmacol Rev* 56:185-229.

Minow, R.A., and J.A. Gottlieb. 1975. Letter: Adriamycin cardiotoxicity. *Ann Intern Med* 82:855-856.

Mo, W., X. Xu, L. Xu, F. Wang, A. Ke, X. Wang, and C. Guo. 2011. Resveratrol inhibits proliferation and induces apoptosis through the hedgehog signaling pathway in pancreatic cancer cell. *Pancreatology* 11:601-609.

Molofsky, A.V., R. Pardal, and S.J. Morrison. 2004. Diverse mechanisms regulate stem cell self-renewal. *Curr Opin Cell Biol* 16:700-707.

Morrison, S.J., P.M. White, C. Zock, and D.J. Anderson. 1999. Prospective identification, isolation by flow cytometry, and in vivo self-renewal of multipotent mammalian neural crest stem cells. *Cell* 96:737-749.

Mosmann, T. 1983. Rapid colorimetric assay for cellular growth and survival: application to proliferation and cytotoxicity assays. *J Immunol Methods* 65:55-63.

Muggia, F.M., O.S. Selawry, and H.H. Hansen. 1971. Clinical studies with a new podophyllotoxin derivative, epipodophyllotoxin, 4'-demethyl-9-(4,6-O-2-thenylidine- -D-glucopyranoside) (NSC-122819). *Cancer Chemother Rep* 55:575-581.

Nasr, R., M.C. Guillemin, O. Ferhi, H. Soilihi, L. Peres, C. Berthier, P. Rousselot, M. Robledo-Sarmiento, V. Lallemand-Breitenbach, B. Gourmel, D. Vitoux, P.P. Pandolfi, C. Rochette-Egly, J. Zhu, and H. de The. 2008. Eradication of acute promyelocytic leukemia-initiating cells through PML-RARA degradation. *Nat Med* 14:1333-1342.

Ng, J.M., and T. Curran. 2011. The Hedgehog's tale: developing strategies for targeting cancer. *Nat Rev Cancer* 11:493-501.

Nichols, C.R. 1992. The role of etoposide therapy in germ cell cancer. *Semin Oncol* 19:72-77.

Nigg, E.A. 1995. Cyclin-dependent protein kinases: key regulators of the eukaryotic cell cycle. *Bioessays* 17:471-480.

Nissen, N.I., V. Larsen, H. Pedersen, and K. Thomsen. 1972. Phase I clinical trial of a new antitumor agent, 4'-demethylepipodophyllotoxin 9-(4,6-O-ethylidene- -D-glucopyranoside) (NSC-141540; VP-16-213). *Cancer Chemother Rep* 56:769-777.

Niu, C., H. Yan, T. Yu, H.P. Sun, J.X. Liu, X.S. Li, W. Wu, F.Q. Zhang, Y. Chen, L. Zhou, J.M. Li, X.Y. Zeng, R.R. Yang, M.M. Yuan, M.Y. Ren, F.Y. Gu, Q. Cao, B.W. Gu, X.Y. Su, G.Q. Chen, S.M. Xiong, T.D. Zhang, S. Waxman, Z.Y. Wang, Z. Chen, J. Hu, Z.X. Shen, and S.J. Chen. 1999. Studies on treatment of acute promyelocytic leukemia with arsenic trioxide: remission induction, follow-up, and molecular monitoring in 11 newly diagnosed and 47 relapsed acute promyelocytic leukemia patients. *Blood* 94:3315-3324.

Norbury, C.J., and I.D. Hickson. 2001. Cellular responses to DNA damage. *Annu Rev Pharmacol Toxicol* 41:367-401.

Nusslein-Volhard, C., and E. Wieschaus. 1980. Mutations affecting segment number and polarity in Drosophila. *Nature* 287:795-801.

Oberlin, O., M.C. Deley, B.N. Bui, J.C. Gentet, T. Philip, P. Terrier, C. Carrie, F. Mechinaud, C. Schmitt, A. Babin-Boillettot, J. Michon, and O. French Society of Paediatric. 2001. Prognostic factors in localized Ewing's tumours and peripheral neuroectodermal tumours: the third study of the French Society of Paediatric Oncology (EW88 study). *Br J Cancer* 85:1646-1654.

Oberlin, O., A. Rey, A.S. Desfachelles, T. Philip, D. Plantaz, C. Schmitt, E. Plouvier, O. Lejars, H. Rubie, P. Terrier, J. Michon, and l.E. Societe Francaise des Cancers de. 2006. Impact of high-dose busulfan plus melphalan as consolidation in metastatic Ewing tumors: a study by the Societe Francaise des Cancers de l'Enfant. *J Clin Oncol* 24:3997-4002.

Oda, Y., B. Dockhorn-Dworniczak, H. Jurgens, and A. Roessner. 1997. Expression of multidrug resistance-associated protein gene in Ewing's sarcoma and malignant peripheral neuroectodermal tumor of bone. *J Cancer Res Clin Oncol* 123:237-239.

Ohnishi, K., M. Takagi, Y. Kurokawa, S. Satomi, and Y.T. Konttinen. 1998. Matrix metalloproteinase-mediated extracellular matrix protein degradation in human pulmonary emphysema. *Lab Invest* 78:1077-1087.

Ouchida, M., T. Ohno, Y. Fujimura, V.N. Rao, and E.S. Reddy. 1995. Loss of tumorigenicity of Ewing's sarcoma cells expressing antisense RNA to EWS-fusion transcripts. *Oncogene* 11:1049-1054.

Oue, T., S. Uehara, H. Yamanaka, M. Nomura, and N. Usui. 2013. Hedgehog signal inhibitors suppress the invasion of human rhabdomyosarcoma cells. *Pediatr Surg Int* 29:1153-1158.

Parkin, D., and J. Nectoux. 1993. International variations in the incidence of childhood bone tumors. *Int. J. Cancer* 53:371-376.

Pasello, M.F., Marilù; Mularoni, Valentina; Ciotti, Sonia; Picci, Piero; Serra, Massimo; Scotlandi, Katia. 2015. Expression levels of ABCA6 or ABCA7 predict primary Ewing sarcoma progression at diagnosis. In 106th Annual Meeting of the American Association for Cancer Research. Philadelphia (PA).

Paulussen, M., S. Ahrens, and J. Dunst. 2001. Localized Ewing tumor of bone: final result of cooperative Ewing's Sarcoma Study CESS 86. *J Clin Oncol* 19:1818-1829.

Paulussen, M., A.W. Craft, I. Lewis, A. Hackshaw, C. Douglas, J. Dunst, A. Schuck, W. Winkelmann, G. Kohler, C. Poremba, A. Zoubek, R. Ladenstein, H. van den Berg, A. Hunold, A. Cassoni, D. Spooner, R. Grimer, J. Whelan, A. McTiernan, H. Jurgens, and S. European Intergroup Cooperative Ewing's Sarcoma. 2008. Results of the EICESS-92 Study: two randomized trials of Ewing's sarcoma treatment--cyclophosphamide compared with ifosfamide in standard-risk patients and assessment of benefit of etoposide added to standard treatment in high-risk patients. *J Clin Oncol* 26:4385-4393.

Payne, S.H. 2015. The utility of protein and mRNA correlation. *Trends Biochem Sci* 40:1-3.

Potmesil, M., M. Israel, and R. Silber. 1984. Two mechanisms of adriamycin-DNA interaction in L1210 cells. *Biochem Pharmacol* 33:3137-3142.

Potratz, J., U. Dirksen, H. Jurgens, and A. Craft. 2012. Ewing sarcoma: clinical state-of-the-art. *Pediatr Hematol Oncol* 29:1-11.

Pressey, J.G., J.R. Anderson, D.K. Crossman, J.C. Lynch, and F.G. Barr. 2011. Hedgehog pathway activity in pediatric embryonal rhabdomyosarcoma and undifferentiated sarcoma: a report from the Children's Oncology Group. *Pediatr Blood Cancer* 57:930-938.

Puck, T.T., and P.I. Marcus. 1955. A Rapid Method for Viable Cell Titration and Clone Production with Hela Cells in Tissue Culture: The Use of X-Irradiated Cells to Supply Conditioning Factors. *Proc Natl Acad Sci U S A* 41:432-437.

Rajeevan, M.S., D.G. Ranamukhaarachchi, S.D. Vernon, and E.R. Unger. 2001. Use of real-time quantitative PCR to validate the results of cDNA array and differential display PCR technologies. *Methods* 25:443-451.

Raju, G.P. 2011. Arsenic: a potentially useful poison for Hedgehog-driven cancers. *J Clin Invest* 121:14-16.

Ramaswamy, M., S.Y. Cleland, A.C. Cruz, and R.M. Siegel. 2009. Many checkpoints on the road to cell death: regulation of Fas-FasL interactions and Fas signaling in peripheral immune responses. *Results Probl Cell Differ* 49:17-47.

Raymond, S., and L. Weintraub. 1959. Acrylamide gel as a supporting medium for zone electrophoresis. *Science* 130:711.

Reagents Direct. 2010. Product information: GANT 61. http://www.reagentsdirect.com/media/catalog/product/cache/1/image/9df78eab33525d08d6e5fb8d27136e95/g/a/gant_61_image.gif. access: 20.09.2016

Riggi, N., L. Cironi, P. Provero, M.L. Suva, K. Kaloulis, C. Garcia-Echeverria, F. Hoffmann, A. Trumpp, and I. Stamenkovic. 2005. Development of Ewing's sarcoma from primary bone marrow-derived mesenchymal progenitor cells. *Cancer Res* 65:11459-11468.

Riggi, N., M.L. Suva, C. De Vito, P. Provero, J.C. Stehle, K. Baumer, L. Cironi, M. Janiszewska, T. Petricevic, D. Suva, S. Tercier, J.M. Joseph, L. Guillou, and I. Stamenkovic. 2010. EWS-FLI-1 modulates miRNA145 and SOX2 expression to initiate mesenchymal stem cell reprogramming toward Ewing sarcoma cancer stem cells. *Genes Dev* 24:916-932.

Riobo, N.A., and D.R. Manning. 2007. Pathways of signal transduction employed by vertebrate Hedgehogs. *Biochem J* 403:369-379.

Rodon, J., H.A. Tawbi, A.L. Thomas, R.G. Stoller, C.P. Turtschi, J. Baselga, J. Sarantopoulos, D. Mahalingam, Y. Shou, M.A. Moles, L. Yang, C. Granvil, E. Hurh, K.L. Rose, D.D. Amakye, R. Dummer, and A.C. Mita. 2014. A phase I, multicenter, open-label, first-in-human, dose-escalation study of the oral smoothened inhibitor Sonidegib (LDE225) in patients with advanced solid tumors. *Clin Cancer Res* 20:1900-1909.

Rosen, G., N. Wollner, C. Tan, S.J. Wu, S.I. Hajdu, W. Cham, G.J. D'Angio, and M.L. Murphy. 1974. Proceedings: Disease-free survival in children with Ewing's sarcoma treated with radiation therapy and adjuvant four-drug sequential chemotherapy. *Cancer* 33:384-393.

Rubin, C.I., and G.F. Atweh. 2004. The role of stathmin in the regulation of the cell cycle. *J Cell Biochem* 93:242-250.

Rudin, C.M. 2012. Vismodegib. *Clin Cancer Res* 18:3218-3222.

Sackett, D.L. 1993. Podophyllotoxin, steganacin and combretastatin: natural products that bind at the colchicine site of tubulin. *Pharmacol Ther* 59:163-228.

Sand, L.G., K. Szuhai, and P.C. Hogendoorn. 2015. Sequencing Overview of Ewing Sarcoma: A Journey across Genomic, Epigenomic and Transcriptomic Landscapes. *Int J Mol Sci* 16:16176-16215.

Santisteban, M. 2010. ABC transporters as molecular effectors of pancreatic oncogenic pathways: the Hedgehog-GLI model. *J Gastrointest Cancer* 41:153-158.

Savill, J., and V. Fadok. 2000. Corpse clearance defines the meaning of cell death. *Nature* 407:784-788.

Saylors, R.L., 3rd, K.C. Stine, J. Sullivan, J.L. Kepner, D.A. Wall, M.L. Bernstein, M.B. Harris, R. Hayashi, T.J. Vietti, and G. Pediatric Oncology. 2001. Cyclophosphamide plus topotecan in children with recurrent or refractory solid tumors: a Pediatric Oncology Group phase II study. *J Clin Oncol* 19:3463-3469.

Scales, S.J., and F.J. de Sauvage. 2009. Mechanisms of hedgehog pathway activation in cancer and implications for therapy. *Trends Pharmacol Sci* 30:303-312.

Schmittgen, T.D., B.A. Zakrajsek, A.G. Mills, V. Gorn, M.J. Singer, and M.W. Reed. 2000. Quantitative reverse transcription-polymerase chain reaction to study mRNA decay: comparison of endpoint and real-time methods. *Anal Biochem* 285:194-204.

Schwartsmann, G., E. Sprinz, M. Kromfield, L. Kalakun, E. Sander, G. Prolla, L. Di Leone, L. Gerhardt, and D.R. Mans. 1997. Clinical and pharmacokinetic study of oral etoposide in patients with AIDS-related Kaposi's sarcoma with no prior exposure to cytotoxic therapy. *J Clin Oncol* 15:2118-2124.

Schwartz, G.K., W.D. Tap, L.X. Qin, M.B. Livingston, S.D. Undevia, B. Chmielowski, M. Agulnik, S.M. Schuetze, D.R. Reed, S.H. Okuno, J.A. Ludwig, V. Keedy, P. Rietschel, A.S. Kraft, D. Adkins, B.A. Van Tine, B. Brockstein, V. Yim, C. Bitas, A. Abdullah, C.R. Antonescu, M. Condy, M.A. Dickson, S.D. Vasudeva, A.L. Ho, L.A. Doyle, H.X. Chen, and R.G. Maki. 2013. Cixutumumab and temsirolimus for patients with bone and soft-tissue sarcoma: a multicentre, open-label, phase 2 trial. *Lancet Oncol* 14:371-382.

Shapiro, A.L., E. Vinuela, and J.V. Maizel, Jr. 1967. Molecular weight estimation of polypeptide chains by electrophoresis in SDS-polyacrylamide gels. *Biochem Biophys Res Commun* 28:815-820.

Sherr, C.J., and J.M. Roberts. 1999. CDK inhibitors: positive and negative regulators of G1-phase progression. *Genes Dev* 13:1501-1512.

Siliciano, J.D., C.E. Canman, Y. Taya, K. Sakaguchi, E. Appella, and M.B. Kastan. 1997. DNA damage induces phosphorylation of the amino terminus of p53. *Genes Dev* 11:3471-3481.

Singh, R.R., K. Kunkalla, C. Qu, E. Schlette, S.S. Neelapu, F. Samaniego, and F. Vega. 2011. ABCG2 is a direct transcriptional target of hedgehog signaling and involved in stroma-induced drug tolerance in diffuse large B-cell lymphoma. *Oncogene* 30:4874-4886.

Sinha, B.K. 1995. Topoisomerase inhibitors. A review of their therapeutic potential in cancer. *Drugs* 49:11-19.

Smith, M.A., M.H. Kang, C.P. Reynolds, R.T. Kurmasheva, D. Alexander, C.A. Billups, J.A. Toretsky, and P.J. Houghton. 2012. Evaluation of arsenic trioxide by the pediatric preclinical testing program with a focus on Ewing sarcoma. *Pediatr Blood Cancer* 59:753-755.

Sordet, O., A. Goldman, and Y. Pommier. 2006. Topoisomerase II and tubulin inhibitors both induce the formation of apoptotic topoisomerase I cleavage complexes. *Mol Cancer Ther* 5:3139-3144.

Srivastava, R.K., S.Z. Kaylani, N. Edrees, C. Li, S.S. Talwelkar, J. Xu, K. Palle, J.G. Pressey, and M. Athar. 2014. GLI inhibitor GANT-61 diminishes embryonal and alveolar rhabdomyosarcoma growth by inhibiting Shh/AKT-mTOR axis. *Oncotarget* 5:12151-12165.

Stahelin, H. 1973. Activity of a new glycosidic lignan derivative (VP 16-213) related to podophyllotoxin in experimental tumors. *Eur J Cancer* 9:215-221.

Stahelin, H., and A. von Wartburg. 1989. From podophyllotoxin glucoside to etoposide. *Prog Drug Res* 33:169-266.

Stone, D.M., M. Murone, S. Luoh, W. Ye, M.P. Armanini, A. Gurney, H. Phillips, J. Brush, A. Goddard, F.J. de Sauvage, and A. Rosenthal. 1999. Characterization of the human suppressor of fused, a negative regulator of the zinc-finger transcription factor Gli. *J Cell Sci* 112 (Pt 23):4437-4448.

Sun, Y., W. Guo, T. Ren, W. Liang, W. Zhou, Q. Lu, G. Jiao, and T. Yan. 2014. Gli1 inhibition suppressed cell growth and cell cycle progression and induced apoptosis as well as autophagy depending on ERK1/2 activity in human chondrosarcoma cells. *Cell Death Dis* 5:e979.

Swift, L.P., A. Rephaeli, A. Nudelman, D.R. Phillips, and S.M. Cutts. 2006. Doxorubicin-DNA adducts induce a non-topoisomerase II-mediated form of cell death. *Cancer Res* 66:4863-4871.

Taatjes, D.J., G. Gaudiano, K. Resing, and T.H. Koch. 1996. Alkylation of DNA by the anthracycline, antitumor drugs adriamycin and daunomycin. *J Med Chem* 39:4135-4138.

Tan, B., D. Piwnica-Worms, and L. Ratner. 2000. Multidrug resistance transporters and modulation. *Curr Opin Oncol* 12:450-458.

Taylor, B.S., J. Barretina, R.G. Maki, C.R. Antonescu, S. Singer, and M. Ladanyi. 2011. Advances in sarcoma genomics and new therapeutic targets. *Nat Rev Cancer* 11:541-557.

Teglund, S., and R. Toftgard. 2010. Hedgehog beyond medulloblastoma and basal cell carcinoma. *Biochim Biophys Acta* 1805:181-208.

Teitell, M.A., A.D. Thompson, P.H. Sorensen, H. Shimada, T.J. Triche, and C.T. Denny. 1999. EWS/ETS fusion genes induce epithelial and neuroectodermal differentiation in NIH 3T3 fibroblasts. *Lab Invest* 79:1535-1543.

Tewey, K.M., T.C. Rowe, L. Yang, B.D. Halligan, and L.F. Liu. 1984. Adriamycin-induced DNA damage mediated by mammalian DNA topoisomerase II. *Science* 226:466-468.

Thermo Fisher Scientific. 2015. Product information: PageRuler^{TM} Prestained Protein Ladder, 10 to 180 kDa. In.

Thiyagarajan, S., N. Bhatia, S. Reagan-Shaw, D. Cozma, A. Thomas-Tikhonenko, N. Ahmad, and V.S. Spiegelman. 2007. Role of GLI2 transcription factor in growth and tumorigenicity of prostate cells. *Cancer Res* 67:10642-10646.

Tirode, F., K. Laud-Duval, A. Prieur, B. Delorme, P. Charbord, and O. Delattre. 2007. Mesenchymal stem cell features of Ewing tumors. *Cancer Cell* 11:421-429.

Torchia, E.C., S. Jaishankar, and S.J. Baker. 2003. Ewing tumor fusion proteins block the differentiation of pluripotent marrow stromal cells. *Cancer Res* 63:3464-3468.

Towbin, H., T. Staehelin, and J. Gordon. 1979. Electrophoretic transfer of proteins from polyacrylamide gels to nitrocellulose sheets: procedure and some applications. *Proc Natl Acad Sci U S A* 76:4350-4354.

Tsujimoto, Y. 1998. Role of Bcl-2 family proteins in apoptosis: apoptosomes or mitochondria? *Genes Cells* 3:697-707.

Varjosalo, M., and J. Taipale. 2008. Hedgehog: functions and mechanisms. *Genes Dev* 22:2454-2472.

Velcheti, V. 2007. Hedgehog signaling is a potent regulator of angiogenesis in small cell lung cancer. *Med Hypotheses* 69:948-949.

Vinci, M., S. Gowan, F. Boxall, L. Patterson, M. Zimmermann, W. Court, C. Lomas, M. Mendiola, D. Hardisson, and S.A. Eccles. 2012. Advances in establishment and analysis of three-dimensional tumor spheroid-based functional assays for target validation and drug evaluation. *BMC Biol* 10:29.

Wajant, H. 2002. The Fas signaling pathway: more than a paradigm. *Science* 296:1635-1636.

Wang, Y., C. Han, L. Lu, S. Magliato, and T. Wu. 2013. Hedgehog signaling pathway regulates autophagy in human hepatocellular carcinoma cells. *Hepatology* 58:995-1010.

Watt, P.M., and I.D. Hickson. 1994. Structure and function of type II DNA topoisomerases. *Biochem J* 303 (Pt 3):681-695.

Weiss, R.B. 1992. The anthracyclines: will we ever find a better doxorubicin? *Semin Oncol* 19:670-686.

White, D.E., and S.A. Burchill. 2008. BAY 11-7082 induces cell death through NF-kappaB-independent mechanisms in the Ewing's sarcoma family of tumours. *Cancer Lett* 268:212-224.

Wickström, M., C. Dyberg, T. Shimokawa, J. Milosevic, N. Baryawno, O.M. Fuskevag, R. Larsson, P. Kogner, P.G. Zaphiropoulos, and J.I. Johnsen. 2013. Targeting the hedgehog signal transduction pathway at the level of GLI inhibiits neuroblastoma cell growth in vitro and in vivo. *Int. J. Cancer* 132:1516-1524.

Womer, R.B., D.C. West, M.D. Krailo, P.S. Dickman, B.R. Pawel, H. Grier, K. Marcus, S. Sailer, J.H. Healey, J.P. Dormans, and A.R. Weiss. 2012. Randomized Controlled trial of interval-compressed chemotherapy for the treatment of localized Ewing sarcoma: A report from the children's oncology group. *J Clin Oncol* 30:4148-4154.

Yoo, Y.A., M.H. Kang, H.J. Lee, B.H. Kim, J.K. Park, H.K. Kim, J.S. Kim, and S.C. Oh. 2011. Sonic hedgehog pathway promotes metastasis and lymphangiogenesis via activation of Akt, EMT, and MMP-9 pathway in gastric cancer. *Cancer Res* 71:7061-7070.

Yu, M., J. Gipp, J.W. Yoon, P. Iannaccone, D. Walterhouse, and W. Bushman. 2009. Sonic hedgehog-responsive genes in the fetal prostate. *J Biol Chem* 284:5620-5629.

Zhang, D., L. Cao, Y. Li, H. Lu, X. Yang, and P. Xue. 2013. Expression of glioma-associated oncogene 2 (Gli 2) is correlated with poor prognosis in patients with hepatocellular carcinoma undergoing hepatectomy. *World J Surg Oncol* 11:25.

Zhang, S., W. Guo, T.T. Ren, X.C. Lu, G.Q. Tang, and F.L. Zhao. 2012. Arsenic trioxide inhibits Ewing's sarcoma cell invasiveness by targeting p38(MAPK) and c-Jun N-terminal kinase. *Anticancer Drugs* 23:108-118.

Zhao, Y.Y., L. Yu, B.L. Liu, X.J. He, and B.Y. Zhang. 2015. Downregulation of P-gp, Ras and p-ERK1/2 contributes to the arsenic trioxide-induced reduction in drug resistance towards doxorubicin in gastric cancer cell lines. *Mol Med Rep* 12:7335-7343.

Zwerner, J.P., J. Joo, K.L. Warner, L. Christensen, S. Hu-Lieskovan, T.J. Triche, and W.A. May. 2008. The EWS/FLI1 oncogenic transcription factor deregulates GLI1. *Oncogene* 27:3282-3291.

10 Personal contribution

This work was conducted in the laboratory of cell biology of the department of orthopaedic surgery at the university hospital Tübingen under support of my supervisor Prof. Dr. Torsten Kluba.

The study was designed by Dr. Karen A. Boehme, head of the laboratory of cell biology of orthopaedic surgery, who also wrote the article accepted for publication in the International Journal of Oncology.

I cultivated all cells used in this work and performed the quantitative real-time PCR analysis. MSC were established by Rosa Riester and Dr. K. A. Boehme. I also performed the MTS assays and the clonogenic assays. R. Riester helped with the cell culture in my absence during holidays. The cell death assay was performed by me with R. Riester analysing the samples at the flow cytometer and I also performed the western blot experiments including the preparation of the protein samples and the Bradford assay. R. Riester and I worked together on the establishment of the 3D spheroid assay with myself performing the experiment with A673 and SK-N-MC cells. The MTS assay, clonogenic assay, FACS analysis, qRT-PCR and western blot were established mainly by R. Riester and also by Dr. K. A. Boehme with other cell lines in the laboratory of cell biology of the department of orthopaedic surgery before I started my work and R. Riester did my initial training in the laboratory work and the methods used in this work.

I calculated all statistical analysis presented in figures 11, 14 - 23 and 35 - 39. The western blot quantification data presented in figures 12, 13 and 40 - 44 was obtained by Dr. K. A. Boehme and we were both involved in its statistical analysis. Dr. K. A. Boehme also calculated the IC_{50} values presented in table 3 using my data obtained from the MTS assays.

This work was written by myself and I made all figures presented in the results chapter.

Tübingen, 21.01.2020 Juliane Keller

11 Publications

Articles:

Parts of the present work (Data presented in figures 11 - 13; figures 18 - 23; figures 25 - 29; figures 32 - 43 and table 3) were published in the following paper:

- Boehme, Karen A.*; **Nitsch, Juliane***; Riester, Rosa; Handgretinger, Rupert; Schleicher, Sabine B.; Kluba, Torsten; Traub, Frank. Arsenic trioxide potentiates the effectiveness of etoposide in Ewing sarcomas. 2016. International Journal of Oncology 49:2135-2146.

* equal lead authors

Posters:

Parts of the present work (Data presented in figures 18 and 23; figures 28 and 29; figure 39; figures 41 - 44 and table 3) were presented as a poster at the following conference:

EACR-AACR-SIC Special Conference 2015:

Boehme, Karen A.; **Nitsch, Juliane**; Riester, Rosa; Handgretinger, Rupert; Schleicher, Sabine B.; Kluba, Torsten

Hedgehog signaling inhibition potentiates the effectiveness of cytostatic agents in Ewing sarcoma.

12 Acknowledgment

First of all, I want to thank Prof. Dr. Torsten Kluba for his continuing supervision of this doctoral thesis over the past two years even from some distance away and for the opportunity to work in the laboratory of cell biology of the department of orthopaedic surgery

I especially like to thank Dr. Karen Boehme for her constant mentoring and supervision in the laboratory and during my writing period. Her organisation of the project was great and I could always turn to her for guidance and help.

Huge thanks also go to Rosa Riester for her amazing support and tutoring. She always had an open ear as well as suggestions for any problems and created a great atmosphere in the laboratory.

Moreover, I like to thank my family and friends for their support and especially my parents Karsten Schulz and Heike Nitsch for always having been there for me.

I want to give special thanks to my partner Ronald Keller who always listened and shared his own experiences with me.

Furthermore, I thank my fellow students in the IZKF-Promotionskolleg for discussions, ideas and help. Here my special gratitude goes to Jan Schroeder.

Last but not least, I want to mention Prof. Dr. Marlies Knipper and Dr. Inka Montero without whose motivation the whole work would definitely have taken longer.

Tübingen, 21.01.2020 Juliane Keller